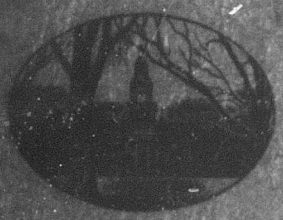

THE JOHNS HOPKINS UNIVERSITY

DEPARTMENT OF PHYSICS

Technical Report No. 1

RARE EARTH INFRARED LIFETIMES AND EXCITON MIGRATION RATES IN TRICHLORIDE CRYSTALS

by
William B. Gandrud

January, 1968

U. S. Army Research Office
Contract DA-31-124-ARO-D-339

Baltimore, Maryland 21218

Rare Earth Infrared Lifetimes and Exciton Migration Rates in Trichloride Crystals

by

William B. Gandrud

Technical Report No. 1

January, 1968

U. S. Army Research Office
Contract DA-31-124-ARO-D-339
DA Project 20014501B11B

Prepared by

The Johns Hopkins University
Department of Physics
Baltimore, Maryland 21218

ABSTRACT

Lifetimes of trivalent rare earth ion levels below 14,000 cm^{-1} have been measured in the $LaCl_3$, $GdCl_3$, and YCl_3 hosts, using the Infrared Quantum Counter and infrared fluorescence techniques. Because of their low radiative and multiphonon relaxation rates, these levels are well suited to concentration-quenching studies. Temperature dependences provide evidence that the ion pair decays of four levels in Pr^{3+} and Nd^{3+} occur resonantly (i.e., without phonon assistance) between excited Stark components. This enables the measured decay rates for these four levels to be used in estimating the rate for a single resonant transfer of all of the ion's energy to a neighboring ion. This latter process is the basic step of the excitation migration process. From the lifetimes of a number of levels which are quenched by migration of the excitation to "sinks", an estimate of 4×10^5 is obtained for the number of transfers that occur before a sink is reached. Levels quenched by migration to sinks are found to decay exponentially, with a lifetime which increases with increasing crystal purity. The roles of the various relaxation processes in determining the performance of the Infrared Quantum Counter as an infrared detector are discussed.

TABLE OF CONTENTS

LIST OF TABLES

BLANK PAGE

LIST OF ILLUSTRATIONS

1. INTRODUCTION

1.1 ENERGY LEVELS OF RE^{3+}: $LaCl_3$

The general theory of the energy levels of rare earth ions and rare earth salts has been summarized by Judd[1] and Wybourne.[2] The terminology and the relative sizes of the various perturbations for RE^{3+}:$LaCl_3$ (where RE represents any lanthanide rare earth) are illustrated by an example in Fig. 1.1.

The ground configuration of a neutral rare earth atom is typically $4f^n5s^25p^65d6s^2$. The atom usually enters crystalline hosts as a trivalent ion, giving up the 5d and 6s electrons. The RE^{3+} transitions in the visible and infrared are within the $4f^n$ configuration. The 4f eigenfunctions, generally having less spatial extent than the 5p's, are somewhat shielded from the environment by the 5p's, with the result that H_{xtal} is the smallest of the four terms in the Hamiltonian in Fig. 1.1.

The electrostatic (Coulomb) interaction between electrons and the spin-orbit interaction partially remove the degeneracy of the various configurations, leaving levels of a given J which are 2J + 1 degenerate. This degeneracy is then further reduced by the electrostatic crystal field, which splits each free ion level into components characterized by the crystal quantum number μ. Russell-Saunders coupling is closely approximated in the lower levels that will be

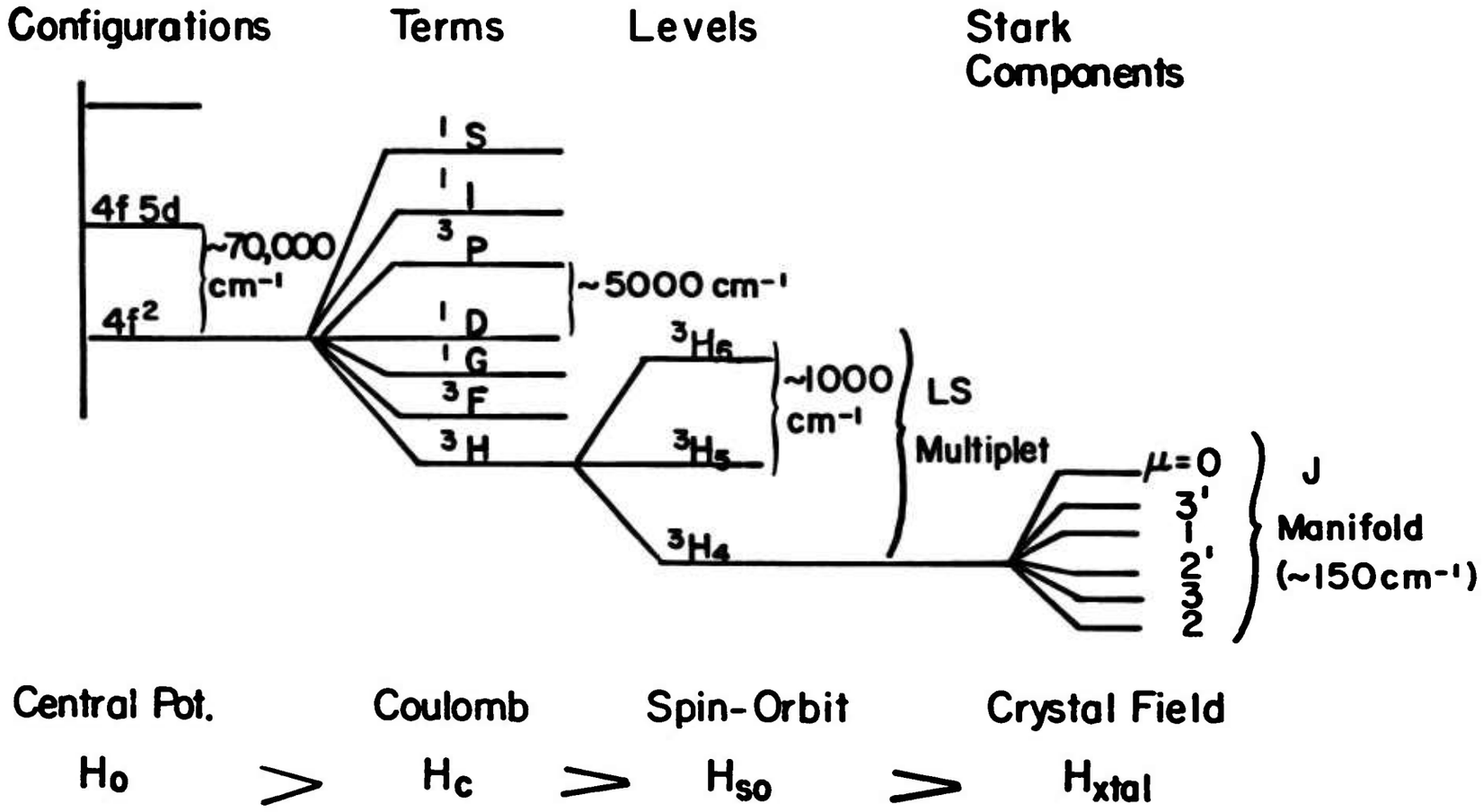

Fig. 1.1 Part of the Energy Level Scheme of Pr^{3+}:$LaCl_3$

studied here. This can be seen from determinations of free ion eigenfunctions, such as those in Ref. 8. Detailed discussions of the energy levels in $LaCl_3$ of the ions studied here (Pr^3, $Nd^{4,5}$, Tb^6, Dy^7, Ho^8, $Er^{9,10}$, Tm^{11}) are contained in the literature.

Since H_{xtal} is the smallest perturbation in Fig. 1.1, one expects that the free ion picture of electronic energy localized on individual ions may retain some of its validity, at least at low concentrations, in the solid state.

Mechanisms which enable an ion in a solid to transfer its energy to a neighboring ion, thus leading to a breakdown in the localized excitation picture, will be described in Sec. 1.2.3. Such processes may be detected through the reduction of the lifetime of excited states with increasing ion concentration. To extract rates for these processes, it is necessary to understand also the other de-excitation mechanisms, with which the ion-ion interactions must compete. Hence a brief summary of all of the important de-excitation processes will now be given.

1.2 DE-EXCITATION MECHANISMS

The mechanisms which depopulate excited states of ions in crystals may be arranged as follows:

I. Radiative

II. Nonradiative

A. Multiphonon Relaxation

B. Ion-Ion Interactions

1. Ion Pair Decay

2. Migration to Sinks

1.2.1 Radiative Decay

The theory of intra-configurational transitions by the forced electric dipole mechanism has been given by Judd[12] and Ofelt.[13] Since the RE^{3+} site in $LaCl_3$ lacks inversion symmetry, the crystal field contains odd components which can mix small amounts of states of the $4f^{n-1}5d$ configuration into states of the $4f^n$ configuration. This makes possible the change in parity required for electric dipole transitions. The intensities and polarizations of most of the RE^{3+}:$LaCl_3$ transitions reported in the literature are compatible with electric dipole selection rules, although a few appear to be magnetic dipole.[14]

The radiative rates follow roughly the familiar third power dependence on the emitted frequency, with radiative lifetimes being typically 100 μsec for levels ~ 20,000 cm^{-1} above the ground state, and 10 msec for ~ 4000 cm^{-1}.

1.2.2 Multiphonon Relaxation

Using a quantum efficiency measurement technique developed by Partlow and Moos,[15] multiphonon relaxation rates have been extracted from a number of excited state lifetimes in $RE^{3+}:LaCl_3$, and plotted against the energy gap below the decaying level[16] (Fig. 1.2). For rates which are of the order of the radiative rates, some five phonons are involved, thus making ab initio calculations impractical. The empirical relation (Fig. 1.2), however, enables one to predict the spontaneous multiphonon emission rate for a given gap with an accuracy of the order of a factor of three.

The exponential dependence of the multiphonon relaxation rate on gap has also been found to hold in $LaBr_3$,[17] LaF_3,[17,18] Y_2O_3,[19] and SrF_2.[19]

As the temperature rises to $\sim 100^{\circ}K$ in $LaCl_3$, the spontaneous multiphonon emission gives way to stimulated emission, whose rate at $300^{\circ}K$ is of the order of six times the spontaneous emission rate, when four to six phonons are involved. This is illustrated in Fig. 1.3.

1.2.3 Ion-Ion Interactions

Early work on the reduction in the luminescence yield of inorganic phosphors with increasing ion concentration was reviewed by Botden[20] and Klick and Schulman.[21] It was apparent

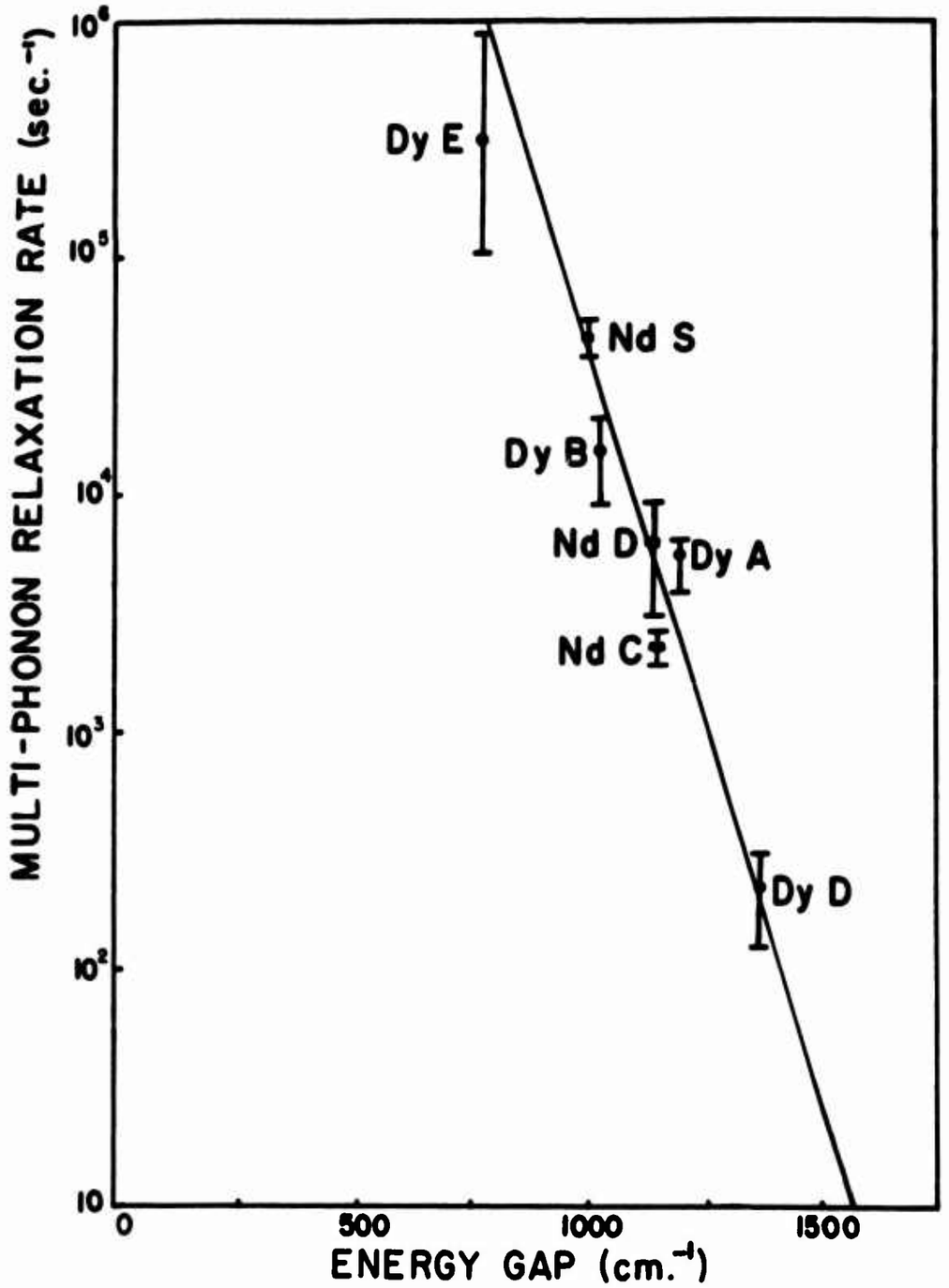

Fig. 1.2 Spontaneous Multiphonon Rate vs. Gap in $LaCl_3$ (Ref. 16)

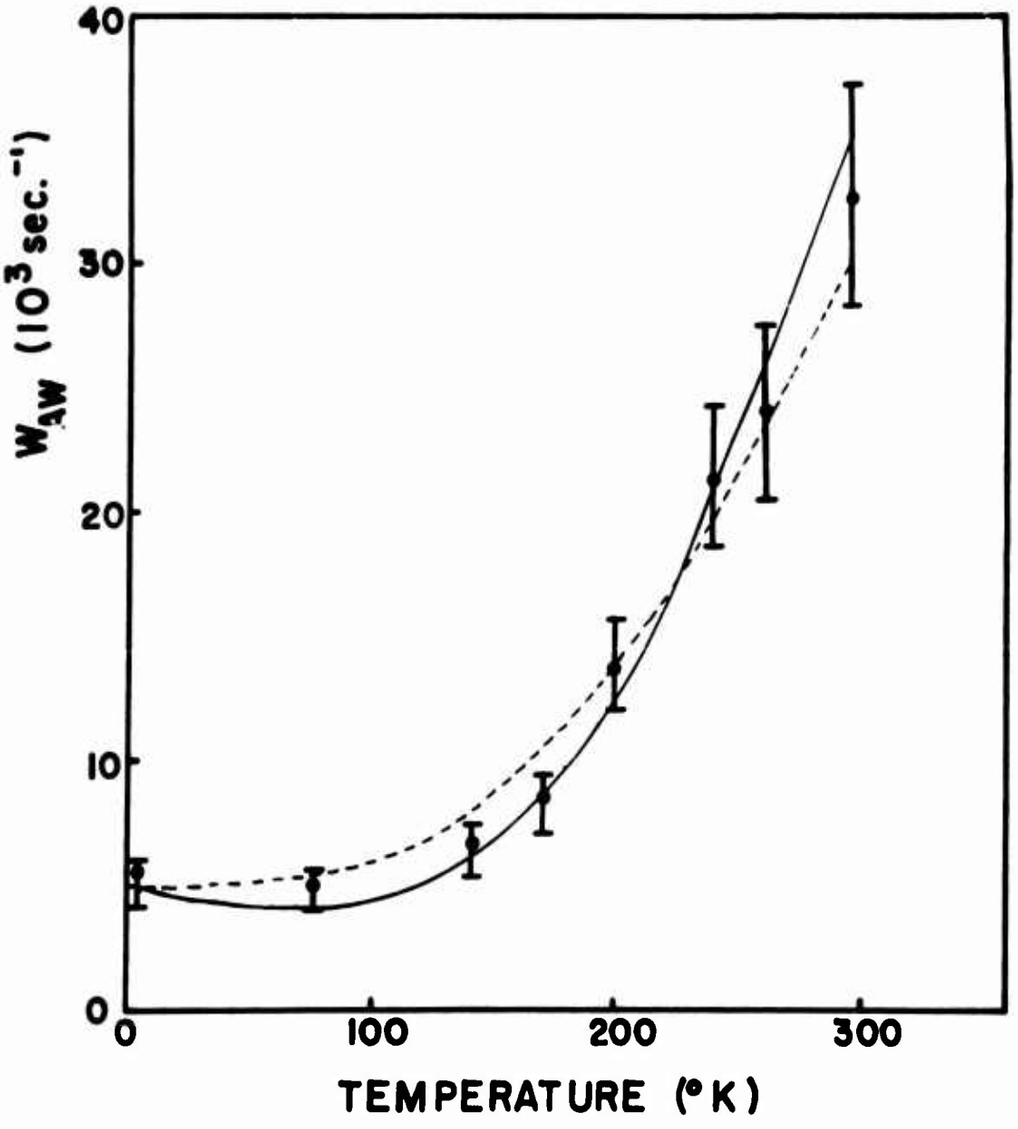

Fig. 1.3 Temperature dependence of the multiphonon relaxation rate between levels A and W in $Dy^{3+}:LaCl_3$ (from Ref. 16). The increase at higher temperatures is attributed to stimulated multiphonon emission.

in these experiments that energy transfer between ions was occurring over distances ~ 12 Å. A transfer mechanism involving the interaction of electrostatic multipole moments of the electron charge distribution was proposed by Dexter.[22] Such a mechanism would permit transfer over distances greater than the extent of the electronic wave functions. Dexter and Schulman[23] then suggested that many cases of concentration quenching might be explained by a series of transfers of this type which transport the energy to a sink (impurity, defect, coupled ion pair, etc.) where it is dissipated.

Demonstrations of simultaneous absorption by two similar ions,[24,25] as well as two dissimilar ions,[26] gave striking confirmation of the inadequacy of the independent-ion picture in rare earth salts. In an extension of his earlier theory, Dexter explained the two-ion absorption in terms of electrostatic multipolar coupling of the ions.[27]

A reduction of the $^5D_4$ lifetime in $TbCl_3 \cdot 6H_2O$ upon insertion of Ho^{3+}, Er^{3+}, or Nd^{3+} demonstrated the ability of rare earth ions of one species to transfer energy to ions of another species in a crystalline host.[28] Subsequent experiments in $LaCl_3$[29-31] and other hosts[32-40] amply confirmed the occurrence of energy transfer between both similar and dissimilar ions. Energy transfer has also been observed between rare earth ions and transition metal ions[41-46]

and organic complexes.[47-49] These latter two processes have been used to increase the pumping efficiency of rare earth lasers.

The electrostatic multipole transfer mechanism[22, 50] will now be described. Let us assume that an initially excited ion A^* undergoes a transition $A^* \rightarrow A$ which is described by a lineshape function $g_A(E)$, normalized so that $\int g_A(E)dE = 1$. Suppose that the energy yielded in this transition is taken up by a transition $B \rightarrow B^*$ in a nearby ion B whose absorption lineshape is $g_B(E)$. If V is the interaction Hamiltonian which produces the transfer of energy, the probability per unit time for the transfer will be[22, 50]

$$P = \frac{2\pi}{\hbar} |\langle AB^* | V | A^*B \rangle|^2 \int g_A(E)\, g_B(E)\, dE. \qquad (1.1)$$

Let $\vec{r}_{Ai}$ be a vector from the nucleus of A to the ith electron of A. Similarly, let $\vec{r}_{Bj}$ be a vector from the nucleus of B to the jth electron of B. If $\vec{R}$ extends from the nucleus of B to the nucleus of A, and K is the dielectric constant, then the electrostatic interaction between the electron charge clouds on A and B can be written as

$$H_{es} = \sum_{i,j} \frac{e^2}{K|\vec{r}_{Ai} + \vec{R} - \vec{r}_{Bj}|} . \qquad (1.2)$$

If the ions are separated by a distance greater than their dimensions, the usual multipole expansion can be performed:

$$H_{es} = H_{dd} + H_{dq} + H_{qq} + H_{qo} + H_{oo} + H_{oh} + H_{hh} + \cdots \qquad (1.3)$$

where, for example, H_{dq} is the interaction between the dipole moment of one ion's electronic charge distribution with the quadrupole moment of the other ion's electronic charge distribution. The simplest of these terms is the dipole-dipole interaction:

$$H_{dd} = \frac{e^2}{K R^3} \left\{ \vec{r}_A \cdot \vec{r}_B - \frac{3(\vec{r}_A \cdot \vec{R})(\vec{r}_B \cdot \vec{R})}{R^2} \right\} \qquad (1.4)$$

where $\vec{r}_A = \sum_i \vec{r}_{Ai}$ and $\vec{r}_B = \sum_j \vec{r}_{Bj}$.

We then ask: Does H_{dd} possess non-zero matrix elements between states $\langle AB^* |$ and $| A^* B \rangle$, and if so, are they large enough to account for observed energy transfer rates?

Averaging over all orientations of $\vec{R}$ yields

$$| \langle AB^* | H_{dd} | A^* B \rangle |^2 = \frac{2}{3} \frac{e^4}{K^2 R^6} | \langle A | \vec{r}_A | A^* \rangle |^2 | \langle B^* | \vec{r}_B | B \rangle |^2 \qquad (1.5)$$

$$\text{But} \quad | \langle A | \vec{r}_A | A^* \rangle |^2 = \frac{3\hbar\lambda}{4\pi mc} f_d (A^* \rightarrow A) \qquad (1.6)$$

where $f_d(A^* \rightarrow A)$ is the electric dipole oscillator strength for the transition $A^* \rightarrow A$. Putting (1.6) into (1.5), and (1.5) into (1.1), we obtain

a probability per unit time for transfer by the electric dipole-dipole interaction:

$$P_{dd} = \frac{3\hbar\lambda^2 e^4}{4\pi m^2 c^2 K^2 R^6} f_d(A^* \rightarrow A) f_d(B \rightarrow B^*) \int g_A(E) g_B(E) dE \qquad (1.7)$$

To see if this expression predicts reasonable transfer rates, we need typical values of R, f_d, λ, K and $\int g_A(E) g_B(E) dE$ for the $RE^{3+}:LaCl_3$ transitions studied here.

Each cation site in $LaCl_3$ has two neighbor cation sites at a distance of 4.3 Å, six at 5.0 Å, and six at 7.4 Å. The probability that in a 5% concentration crystal at least one of these 14 sites will contain a dopant ion is $1 - (.95)^{14} = .52$. Thus 7.5 Å is a reasonable "effective" R for 5% concentration.†

The average oscillator strength for a large number of $RE^{3+}:LaCl_3$ infrared transitions reported by Varsanyi and Dieke[14] is $\sim 10^{-7}$.

For perfect overlap, $\int g_A(E) g_B(E) dE$ is equal to the reciprocal of the linewidth. Assuming a 3 cm^{-1} linewidth,[51] the integral will have the value 0.3 cm.

†An experimentally determined effective R of 7.5 Å, resulting from assuming a square well interaction for a resonant transfer in 3.5% $Ho^{3+}:LaCl_3$, has been reported.[30]

The index of refraction is[30] ~ 1.6, so that $K = n^2 \sim 2.6$. Setting $\lambda = 1.5\ \mu$, (1.7) then gives† $P_{dd} = 6 \times 10^3\ \text{sec}^{-1}$. Experimentally determined transfer rates at 5% concentration will later be seen to be $\sim 10^6\ \text{sec}^{-1}$. It will now be shown that the expected values of P_{dq} and P_{qq} are even larger than the above estimate of P_{dd}.

Just as the electric dipole matrix element appeared in P_{dd}, Dexter[22, 23] has shown that the higher order terms P_{dq}, P_{qq}, etc. are proportional to the corresponding higher order radiative matrix elements. Thus, to estimate their importance relative to P_{dd}, it is necessary to know the relative magnitude of the electric quadrupole, octopole, hexadecapole, etc., radiative oscillator strengths (f_q, f_o, f_h, etc.). These quantities have never been measured, but using standard considerations,[32, 33, 50] we will estimate them, and, subsequently, the higher order P's.

If one always chooses initial and final states such that the transition will be allowed by parity considerations, one expects[52] the ratio of adjacent terms in the sequence f_d, f_q, f_o, f_h, ... to be $\sim \left(\frac{a}{\lambda}\right)^2 \sim 4 \times 10^{-9}$ where $a \sim 1$ Å is the radial extent of

†This is consistent with the estimate $P_{dd} = 10^3\ \text{sec}^{-1}$ obtained by Porter and Moos, using slightly different parameters (Ref. 30).

the 4f eigenfunction,† and $\lambda \sim 1.5\ \mu$ is a typical transition wavelength for this study. In this study we deal with transitions within the $4f^n$ configuration, however, so that transitions involving odd-parity operators (dipole, octopole, etc.) are forbidden to first order, while even-parity operators (quadrupole, hexadecapole, etc.) have allowed transitions. As pointed out in Sec. 1.2.1, non-centro-symmetric crystal fields are capable of making odd-parity transitions weakly allowed through configuration mixing. Thus we expect the odd-parity f's and even-parity f's to form two separate sequences, with adjacent terms within a sequence bearing the ratio $\left(\frac{a}{\lambda}\right)^4 \sim 10^{-17}$. The relative size of two terms from <u>different</u> sequences will depend on the degree of configuration mixing.

If we modify Broer et al.'s[53] estimate of f_q by using our values of $\lambda = 1.5\ \mu$ and $n = 1.6$, we obtain

$$f_q \sim 1.3 \times 10^{-10} .$$

Using this value of f_q, and our previous value of $f_d \sim 10^{-7}$, we expect the following orders of magnitude for the oscillator strengths:

Odd Multipoles: $f_d \sim 10^{-7}$, $f_o \sim 10^{-24}$, . . .

Even Multipoles: $f_q \sim 10^{-10}$, $f_h \sim 10^{-27}$ . . .

†See, e.g., Ref. 2, Fig. 2.10.

Deriving transfer rates[22,23] for the higher order terms in Eq. 1.3 and assuming $\int g_A(E)g_B(E)dE$ to be constant, we obtain the ratios in the middle column of Table 1.1. Using R = 7.5 Å (for 5% concentration), λ = 1.5 μ, and the above f estimates, we obtain the numerical values in Table 1.1.

Table 1.1. Relative magnitudes of energy transfer rates for the lowest order multipole terms.

$$\frac{P_{dq}}{P_{dd}} \sim \left(\frac{\lambda}{R}\right)^2 \left(\frac{f_q}{f_d}\right) \sim 4 \times 10^3$$

$$\frac{P_{qq}}{P_{dd}} \sim \left(\frac{\lambda}{R}\right)^4 \left(\frac{f_q}{f_d}\right)^2 \sim 2 \times 10^7$$

$$\frac{P_{qo}}{P_{dd}} \sim \left(\frac{\lambda}{R}\right)^6 \left(\frac{f_q}{f_d}\right)\left(\frac{f_o}{f_d}\right) \sim 6 \times 10^{-1}$$

$$\frac{P_{oo}}{P_{dd}} \sim \left(\frac{\lambda}{R}\right)^8 \left(\frac{f_o}{f_d}\right)^2 \sim 3 \times 10^{-8}$$

$$\frac{P_{oh}}{P_{dd}} \sim \left(\frac{\lambda}{R}\right)^{10} \left(\frac{f_o}{f_d}\right)\left(\frac{f_h}{f_d}\right) \sim 10^{-4}$$

$$\frac{P_{hh}}{P_{dd}} \sim \left(\frac{\lambda}{R}\right)^{12} \left(\frac{f_h}{f_d}\right)^2 \sim 4 \times 10^{-1}$$

It is seen in Table 1.1 that local maxima occur in the P_{dd}, P_{dq}, P_{qq}, . . . sequence whenever two even-parity f's are involved, i.e., at P_{qq}, P_{hh}, etc. Since each maximum is $\sim 10^8$ smaller than the preceding one, the series formed by summing the terms converges. It must be remembered, however, that only order of magnitude estimates have been used throughout, and some errors are cumulative. For example, an error of only a factor of two in the estimate of $\frac{\lambda}{R}$ introduces an error of $2^{12} \cong 4000$ in P_{hh}/P_{dd}.

If one multiplies the P_{qq}/P_{dd} value of 2×10^7 in Table 1.1 by the $P_{dd} = 6 \times 10^3$ sec^{-1} estimate, the result is

$$P_{qq} \sim 10^{11} \text{ sec}^{-1} .$$

The five orders of magnitude by which this exceeds the measured value of $\sim 10^6$ sec^{-1} at 5% concentration [Fig. 4.2(a)] is difficult to dismiss on grounds of uncertain estimates, even though P_{qq} is very sensitive to these estimates.

Other published estimates of the P's have predicted a faster convergence of the series, and these estimates are compared with the above estimates in Table 1.2. Because of shorter wavelengths and lower concentrations, all of these authors' $\left(\frac{\lambda}{R}\right)^2$ factor is about an order of magnitude smaller than the value used in Table 1.1. In addition, their f_q/f_d ratio is an order of magnitude smaller than the

Table 1.2. Published estimates of P_{dd}, P_{dq}, P_{qq}, using Dexter's[22,23] theory (see Table 1.1 for formulas).

	Values Used					Results			
Material	f_q	f_d	λ (μ)	R (Å)	$\int g_A g_B dE$	P_{dd} (sec^{-1})	$\frac{P_{dq}}{P_{dd}}$	$\frac{P_{qq}}{P_{dd}}$	Reference
$Cr^{3+}:Al_2O_3$	1.5×10^{-11}	3×10^{-7}	0.7	15	0.5 cm	200	7.5	60	Imbusch[30]
$Eu^{3+}:Y_2O_3$	10^{-9}	10^{-5}	1.0	a	10^{-4}	10^{4}	a	a	Axe and Weller[32]
$Pr^{3+}:LaF_3$	10^{-9}	10^{-5}	1.0	13	b	b	60	3500	Brown et al.[33]
$RE^{3+}:LaCl_3$	10^{-10}	10^{-7}	1.5	7.5	0.3	6×10^{3}	4000	2×10^{7}	Present Study

[a] These authors calculated the ratios of R^3's which give rise to the given transfer rate of $P = 10^4$ sec^{-1}.

[b] These authors did not calculate P_{dd}.

one used here. The $Cr^{3+}:Al_2O_3$ f's are not expected to be comparable to the $RE^{3+}:LaCl_3$ f's, because the transition dealt with in ruby is spin-forbidden, so it involves an additional matrix element for spin-orbit interaction. One might question, however, the $f_d \sim 10^{-5}$ value used by Axe and Weller[32] and by Brown et al.[33] for RE^{3+} in a non-centro-symmetric site. Published oscillator strengths[14,18,51] for $RE^{3+}:LaCl_3$ and $RE^{3+}:LaF_3$ indicate that this is an exceptionally large value. A more typical value for $\lambda = 1.0\ \mu$[†] would be $f_d \sim 2 \times 10^{-7}$. This would, of course, result in a much slower series convergence, and yield unreasonably large P_{qq} values.

The exact sources of the large difference between Imbusch's value of 60 for P_{qq}/P_{dd} in $Cr^{3+}:Al_2O_3$ and the present value of 2×10^7 in $RE^{3+}:LaCl_3$ can be seen by examining the expression

$$\frac{P_{qq}}{P_{dd}} \sim \left(\frac{\lambda}{R}\right)^4 \left(\frac{f_q}{f_d}\right)^2$$

from Table 1.1. The value of λ/R used by Imbusch is a factor of 4 smaller than the value appropriate to the present study, implying that his $(\lambda/R)^4$ is some 250 times smaller. Furthermore, his f_q/f_d is

[†]Whereas $f_q \propto 1/\lambda^3$, the facts that $f_d \tau \propto \lambda^2$ and $\tau \propto \lambda^3$ together imply that $f_d \propto 1/\lambda$.

5×10^{-5}, which is 20 times smaller than the present value of 10^{-3}, implying that $(f_q/f_d)^2$ is 400 times smaller. Thus the $\sim 10^5$ difference in the P_{qq}/P_{dd}'s is divided roughly evenly between the two factors.

Wolf and Birgeneau[54] have recently reappraised the practice of ignoring terms beyond P_{qq} for energy transfer in rare earth salts. They point out that electrostatic shielding of the 4f electrons by the 5s and 5p electrons, as well as any dipole moment induced in the ligands, can be expected to enhance the relative importance of higher terms in the multipole expansion. They also point out that the validity of an ionic electrostatic model is reduced by the existence of covalency, and that at present, it is unclear how close this model is to reality.

Transfer rates will simply be treated as empirical quantities in the present study, with no assumptions made regarding the mechanism by which resonant transfer occurs.

It should be emphasized that this discussion has been restricted to resonant transfer. Many of the examples of energy transfer presented in the literature involve assistance by the absorption or emission of phonons. This is a higher order process, and its rate should decrease as the number of phonons involved increases.

Selection rules may in some cases cause deviations from the mean transfer rates. Since Russell-Saunders coupling is closely approximated in many of the $RE^{3+}:LaCl_3$ levels, the selection rules $\Delta S = 0$, $|\Delta L| \leq 1$, $|\Delta J| \leq 1$ for electric dipole and $\Delta S = 0$, $|\Delta L| \leq 2$, $|\Delta J| \leq 2$ for electric quadrupole transitions may frequently affect energy transfer rates.

1.3 PURPOSE OF THE PRESENT STUDY

A survey of the lifetimes of $RE^{3+}:LaCl_3$ levels whose fluorescence could be detected with an S-20 photomultiplier (i.e., levels above 14,000 cm^{-1}) was performed by Barasch and Dieke.[55] Because of the generally small energy gaps (~ 1000 cm^{-1}) between these levels, multiphonon emission is an important relaxation mechanism for many of these levels. The resulting lifetimes produced semi-quantitative evidence that the rate for this process increased strongly as the gap decreased. The emission of radiation is also an important mechanism in the decay of many of these levels, and the measured lifetimes produced strong evidence of radiation trapping for the $^3P_0$-$^3H_4$ fluorescence in $Pr^{3+}:LaCl_3$. The information which a lifetime survey of these higher levels can yield about the third decay mechanism (ion-ion interactions) is more meager, however. The reason is that the large number of levels between the decaying level and the ground state

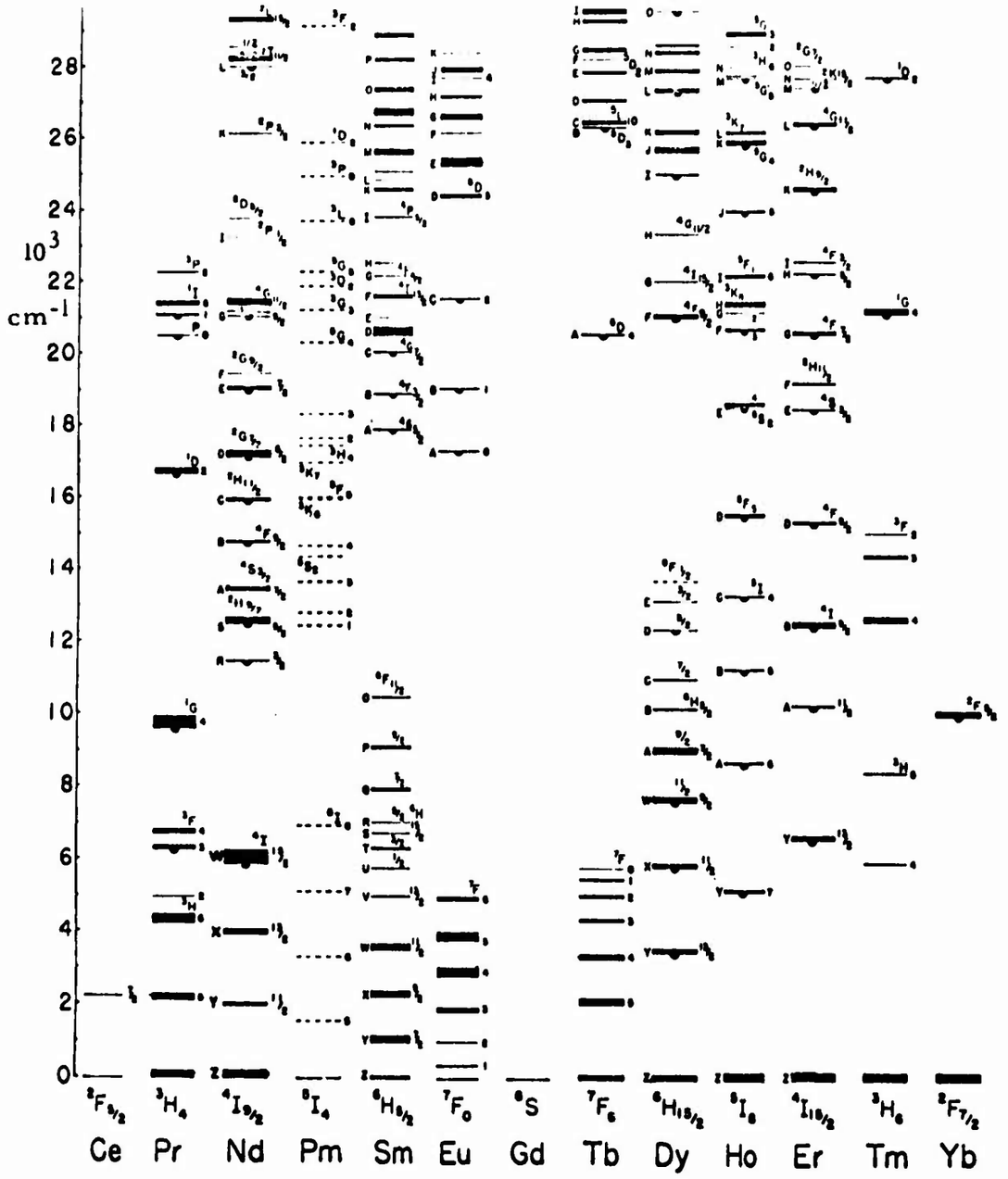

Fig. 1.4 $RE^{3+}:LaCl_3$ Energy Levels [reprinted from Optical Properties of Ions in Crystals (Interscience Publishers, 1967), ed. by Crosswhite and Moos, by permission of eds.].

introduces ambiguities in interpretation, because of the possibilities of three-ion decays and phonon-assisted pair decays involving several ($\sim$ 3) phonons. In addition, for these higher levels, whose lifetimes are $\sim$ 100 μsec, the relatively weak ion-ion decay mode[23] consisting of a series of transfers ("migration") to sinks can compete with the other decay modes only in concentrations close to 100%.

Levels below 14,000 cm^{-1} are more suitable for ion-ion decay studies because (1) the number of intervening levels can be reduced (even to zero in the study of the lowest excited level), (2) radiative lifetimes are $\sim$ 100 times longer because of the ν^3 dependence of the radiative rate, and (3) the larger gaps ($\sim$ 2000 cm^{-1}) make multiphonon relaxation negligible in many cases.

The purpose of this study is, then, (1) to measure the lifetimes and time dependences of the decays of RE^{3+}:$LaCl_3$ levels below 14,000 cm^{-1} as a function of concentration and temperature, and (2) from this data determine which levels decay by the ion pair and migration mechanisms, with the decay rates for these processes answering the question of how extensive energy migration is in these crystals. Since migration involves a series of resonant (no phonon assistance) ion pair interactions, the simple theory discussed in this chapter should be applicable to that process also.

2. EXPERIMENTAL TECHNIQUES

2.1 THE INFRARED QUANTUM COUNTER

2.1.1 Operation of the Device

The infrared quantum counter[56] (IRQC) is a two-step excitation device which permits one to measure the lifetime of infrared levels[57,58] with detectors which operate in the visible region of the spectrum.

The experimental arrangement is shown in Fig. 2.1. Radiation of frequency ν_{01} from the source on the left populates the infrared level whose lifetime is to be measured [1 in Fig. 2.2(a)]. Ions in level 1 are then raised to level 2 by the absorption of radiation at frequency ν_{12} from the source on the right in Fig. 2.1. Ions in level 2 then fluoresce, and that part of the fluorescence occurring at some convenient frequency, such as ν_{20}, is detected by a photomultiplier. Individual photoelectron spikes at the photomultiplier anode were amplified by CI Models 1405 and 1415 Preamplifier and RC Amplifier, and subjected to window discrimination by a CI Model 1430 Single Channel Analyzer. An integrating circuit prevented the pulses from overloading the P. A. R. Model HR-8 Lock-in Amplifier. A recorder was used for long integration times, as explained in Sec. 2.5.1.2.

A Sylvania "Sun Gun" 625 watt 3400°K tungsten-iodine filament lamp served as the infrared source. For visible pump

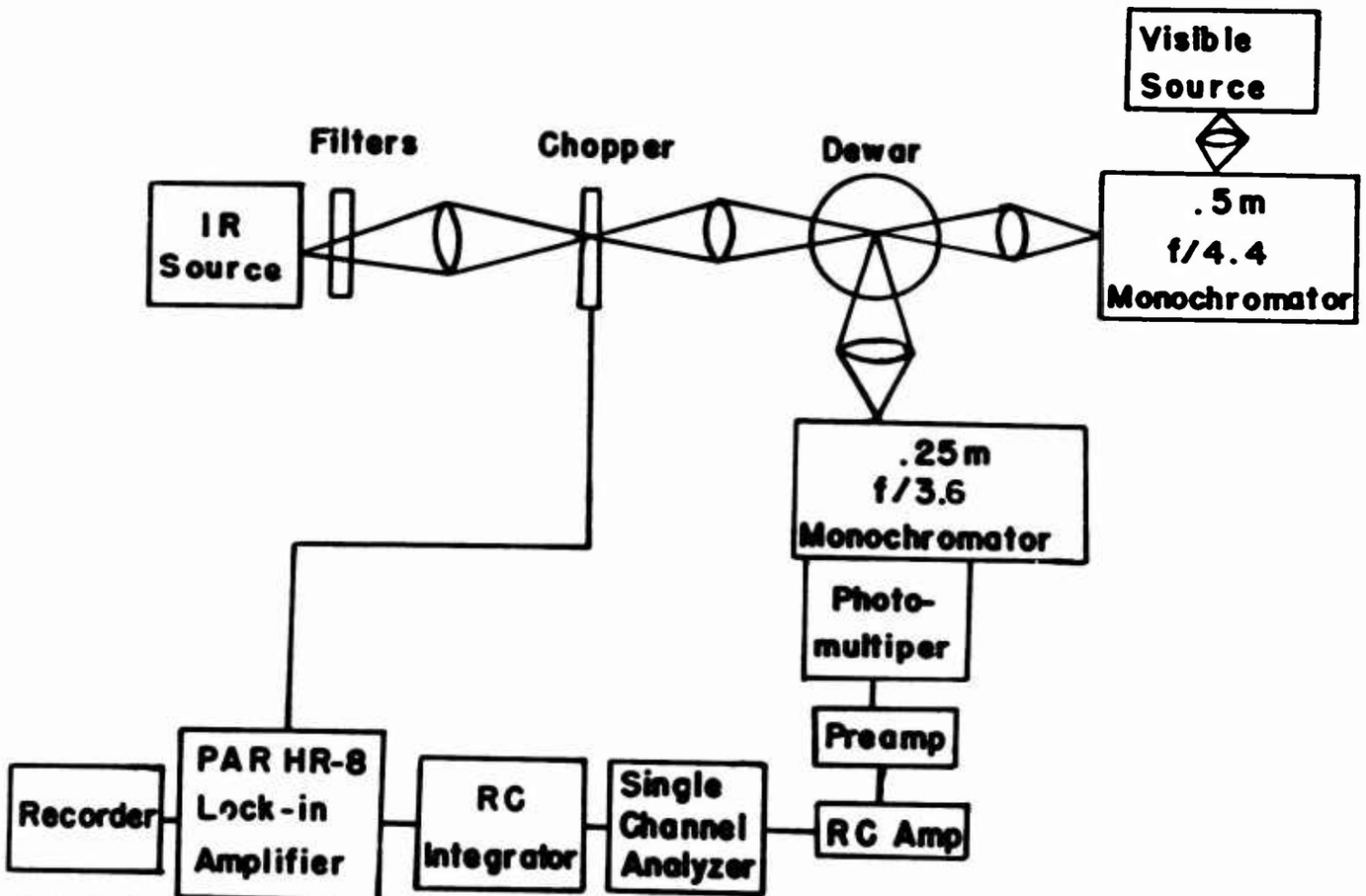

Fig. 2.1 Infrared Quantum Counter. Dewar, optics, and detector were enclosed in a light-tight box with a flat black interior.

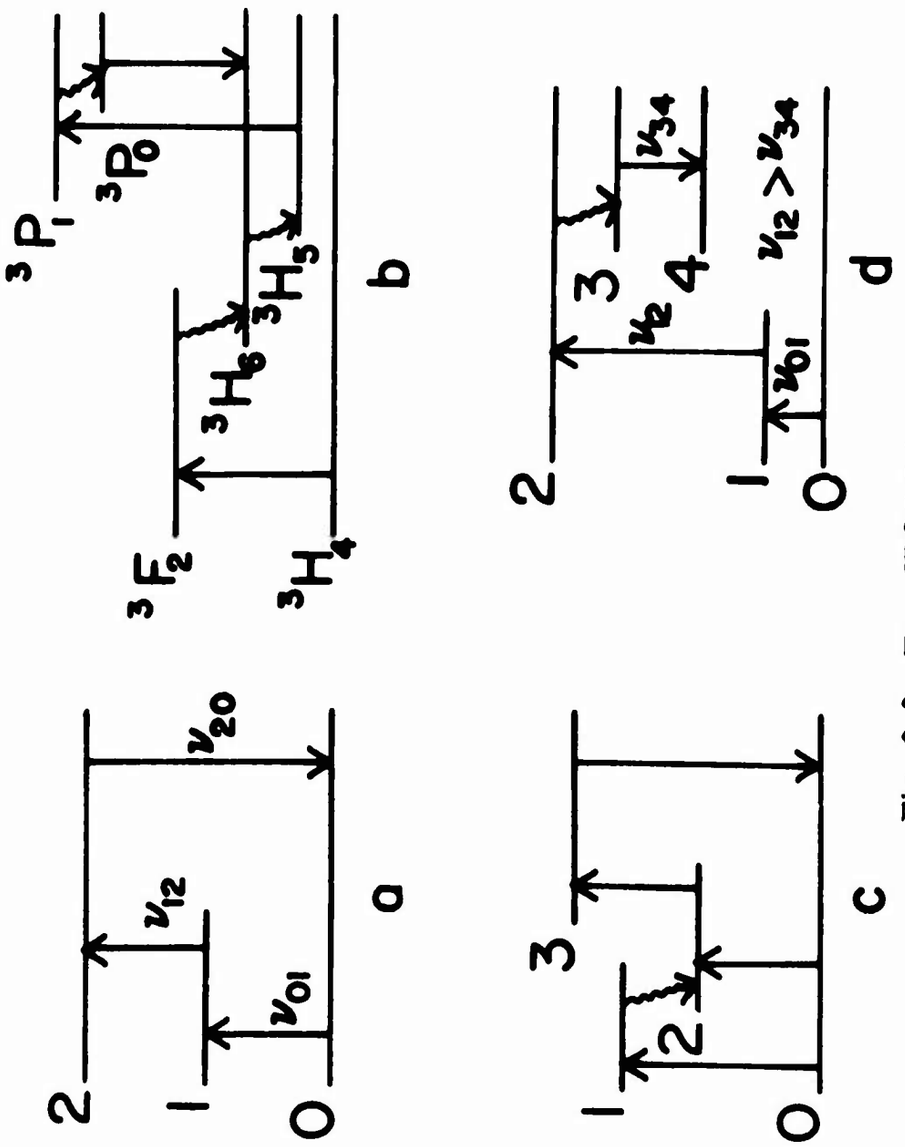

Fig. 2.2 Four IRQC Schemes

wavelengths < 6000 Å, an AH-6 mercury arc lamp was mounted on a Bausch and Lomb .5 m f/4.4 monochromator; for longer wavelengths, the AH-6 was replaced by a "Sun Gun." When possible, the f/3.6 monochromator was replaced by filters.

Several S-1 and S-20 surface photomultipliers were used, and were cooled to dry ice temperature in those instances when dark current noise limited the system's sensitivity.

2.1.2 Rate Equations; Lifetime Measurement

Lifetimes were measured with the Quantum Counter by modulating the infrared beam with a mechanical chopper (Sec. 2.4), and using the lock-in amplifier to measure the phase shift between the excitation and the fluorescence; the method is an extension (due to Porter[57]) of Bailey and Rollefson's method.[59]

The set of transitions involved in Quantum Counter action is called a "scheme." Whereas most lifetimes were measured with the simple scheme illustrated in Fig. 2.2(a), the rate equations will now be solved in sufficient generality to cover more complex schemes, such as the $LaCl_3:Pr^{3+}$ scheme illustrated in Fig. 2.2(b).

Let us assume that a given ion starts in the ground state (labelled 0), and progresses through levels 1, 2, 3, . . . before arriving at level n, which fluoresces and provides the signal to be detected. In Fig. 2.2(b), 0, 1, 2, 3, ... n are $^3H_4$, $^3F_2$, $^3H_6$,

$^3H_5$, $^3P_1$, and $^3P_0$, respectively. Let the transition probability per unit time for the $i \rightarrow (i+1)$ transition be $w_{i,i+1}$ (which will be a function of time if a modulated radiation source induces the transition), and the lifetime of level i be τ_i.

In order to obtain a simple solution to the rate equations, it is necessary to make three assumptions:

Assumption 1: Level i is populated only through the $(i-1) \rightarrow i$ transition.

This assumption places stringent requirements on the filtering. For example, the scheme in Fig. 2.2(c) is unacceptable, because level 2 is populated by two transitions, which may be of comparable importance.

Assumption 2: Absorption of radiation from the two sources may contribute to the population of levels (through the $w_{i,i+1}$), but its contribution to the depopulation (through the τ_i) is negligible; and the effect of stimulated emission must be negligible in both cases.

Calculations based on an approximate knowledge of the source intensities indicate that the rates for source-induced processes should be several orders of magnitude lower than the radiative decay rates in the crystal. If Assumption 2 were invalid, saturation effects would be evident as the intensities of the sources were varied (with Variacs and filters). No cases were found in which such effects could be seen.

Assumption 3: The lifetimes τ_i are the same for all ions in the sample, i.e., all decays are exponential.

This assumption is known to be violated in ion pair decays. Consequences of this violation will be considered in Sec. 3.1.

Under Assumptions 1, 2, and 3, the rate equations for the populations, N_i, of the various levels take the form

$$\begin{aligned} N_0 &= \text{const.} = \text{number of dopant ions per unit vol.} \\ \dot{N}_1 &= w_{01} N_0 - N_1/\tau_1 \\ \dot{N}_2 &= w_{12} N_1 - N_2/\tau_2 \\ &\cdots \\ \dot{N}_n &= w_{n-1,n} N_{n-1} - N_n/\tau_n \end{aligned} \tag{2.1}$$

Suppose that the $0 \rightarrow 1$ transition is induced by the infrared beam, which is chopped non-sinusoidally with an angular frequency ω; then

$$w_{01} = W_{01}^{(dc)} + W_{01}\left[\cos \omega t + \sum_{k=2}^{\infty} a_k e^{ik\omega t}\right] \tag{2.2}$$

where we have chosen the time origin so that there is no $\sin \omega t$ term.

Suppose further that the $j \rightarrow j+1$ transition is induced by the (unchopped) visible source; then

$$w_{j,j+1} = W_{j,j+1}\left[1 + \beta e^{i2\pi(120)t}\right] \qquad (2.3)$$

where $|\beta| \sim 1$ for an AH-6 lamp, and $|\beta| << 1$ for the tungsten-iodine lamp.

Since the IRQC signal (which is proportional to N_n) passes through a narrow-band amplifier in the P. A. R. HR-8 (Fig. 2.1), we need solve Eqs. (2.1) only for the ω component of N_n.

If all of the Eqs. (2.1) were linear, we could dispense with all terms in (2.2) except the cos ωt term, and throw away the 120 cps term in (2.3). The $w_{j,j+1}N_j$ term, however, is capable of generating new frequencies: in general, N_j will contain the same frequency components as (2.2), and for certain values of ω, a harmonic of ω in N_j can beat with the 120 cps term of $w_{j,j+1}$ to produce a spurious term at frequency ω. This is discussed further in Sec. 2.5.1.3; these chopping frequencies were avoided in making the measurements, hence it may be assumed for this discussion that the narrow band amplifier eliminates not only harmonics of ω, but sum and difference frequencies generated by the $w_{j,j+1}N_j$ term as well. Rewriting the constant $w_{i,i+1}$ coefficients as $W_{i,i+1}$ for uniformity, we may then write the ω components of Eqs. (2.1) as

$$\dot{N}_1^{(\omega)} = (W_{01} \cos \omega t)\, N_0 - N_1^{(\omega)}/\tau_1$$

$$\dot{N}_2^{(\omega)} = W_{12}\, N_1^{(\omega)} - N_2^{(\omega)}/\tau_2$$

. . .

$$\dot{N}_n^{(\omega)} = W_{n-1,n}\, N_{n-1}^{(\omega)} - N_n^{(\omega)}/\tau_n$$

By substituting into these the steady-state solution

$$N_i^{(\omega)} = a_i \cos \omega t + b_i \sin \omega t ,$$

we obtain for the recursion relations for the coefficients:

$$a_i = \frac{W_{i-1,\,i}\,(a_{i-1}/\tau_i - \omega b_{i-1})}{\omega^2 + 1/\tau_i^2}$$

$$b_i = \frac{W_{i-1,\,i}\,(\omega\, a_{i-1} + b_{i-1}/\tau_i)}{\omega^2 + 1/\tau_i^2} \qquad (2.4)$$

From these expressions, we can obtain Δ_n, the amount by which the phase of N_n is shifted relative to the excitation $W_{01} \cos \omega t$:

$$\Delta_n = \tan^{-1} \frac{b_n}{a_n} = \tan^{-1} \left[\frac{\omega a_{n-1} + b_{n-1}/\tau_n}{a_{n-1}/\tau_n - \omega b_{n-1}} \right]$$

$$= \tan^{-1} \left[\frac{\omega\tau_n + \dfrac{b_{n-1}}{a_{n-1}}}{1 - (\omega\tau_n)\left(\dfrac{b_{n-1}}{a_{n-1}}\right)} \right]$$

Using a well-known identity, this becomes

$$\Delta_n = \tan^{-1} \omega\tau_n + \tan^{-1} \frac{b_{n-1}}{a_{n-1}}$$

Applying the same procedure to the second term on the right, we get

$$\Delta_n = \tan^{-1} \omega\tau_n + \left[\tan^{-1} \omega\tau_{n-1} + \tan^{-1} \frac{b_{n-2}}{a_{n-2}} \right]$$

Repeating the procedure n-2 more times gives finally

$$\Delta_n = \tan^{-1} \omega\tau_n + \tan^{-1} \omega\tau_{n-1} + \cdots + \tan^{-1} \omega\tau_1 \qquad (2.5)$$

Thus the phase shifts $\tan^{-1} \omega\tau_i$ introduced by each of the lifetimes τ_i individually simply add to give the total phase shift between excitation and fluorescence, when Assumptions 1-3 are valid. Knowing the lifetimes $\tau_2, \tau_3, \cdots, \tau_n$, and measuring the phase shift Δ_n at some chopping frequency ω will then yield the lifetime τ_1 of the infrared-pumped level. The measurement of Δ_n is described in Sec. 2.5.1.2; the assorted means used in determining $\tau_2, \tau_3, \cdots, \tau_n$ are described in Sec. 3.2.

2.1.3 Scheme Selection

Since the spacing of absorptions to adjacent infrared levels of rare earth ions is typically ~ 5000 Å, infrared filters

(interference and semiconductor types) nearly always provide sufficient resolution for isolating the $0 \rightarrow 1$ transition in Fig. 2.2(a). On the other hand, the spacing of adjacent absorptions in the visible is typically ~ 500 Å, hence a monochromator is generally necessary to isolate the $1 \rightarrow 2$ transition.

Nearly all of the lifetime measurements performed with the quantum counter in this work utilized the type of scheme shown in Fig. 2.2(a). An alternative type is shown in Fig. 2.2(d); since $\nu_{12} > \nu_{34}$, red-pass filters must be used before the photomultiplier, and this means that photomultiplier noise induced by scattered light can almost never be reduced to the dark noise level in this type of scheme. The reason is that light of wavelength less than the cutoff wavelength of a Corning red-pass filter excites broad-band fluorescence in the filter at wavelengths greater than the cutoff wavelength.[60, 61] Most interference filters of the red-pass and narrow-band types are constructed with doped glass substrates which strongly absorb short wavelengths, and fluoresce at longer wavelengths with about the same efficiency as Corning red-pass filters. Even if the filter is oriented so that the light strikes the dielectric coating before striking the substrate, the 1% or so of the incident light which is passed by the coating can excite fluorescence in the substrate; further filtering can eliminate incident pump light which leaks through the filter, but

that part of the substrate fluorescence which is near the wavelength that one wishes to observe cannot be reduced by further filtering. Thus in the Fig. 2.2(d) scheme, scattered light cannot be reduced to an arbitrarily low level by filters alone, whereas it can in the Fig. 2.2(a) scheme.

Selection of an upper level [2 in Fig. 2.2(a)] must usually be done by trial and error. The lower (10,000-18,000 cm^{-1}) visible-fluorescing levels of rare earth ions are less likely to undergo concentration quenching, and provide a greater percentage separation of pump and fluorescence wavelengths, thus simplifying the filtering. On the other hand, the higher levels (18,000-28,000 cm^{-1}) fluoresce in a region of higher photocathode sensitivity, and are less likely to produce a spurious chopped fluorescence resulting from a two-step excitation induced by the infrared beam alone (see Sec. 2.5.1.2).

2.2 THE INFRARED FLUORESCENCE TECHNIQUE

Some 30% of the lifetimes reported here were measured on an infrared fluorescence apparatus (Fig. 2.3) assembled by L. A. Riseberg. The excitation source was a Sylvania "Sun Gun" 625 watt 3400°K filament lamp. The same chopper (Sec. 2.4) used with the Quantum Counter was used here. The infrared fluorescence was focussed by a spherical mirror onto the entrance slit of a MacPherson

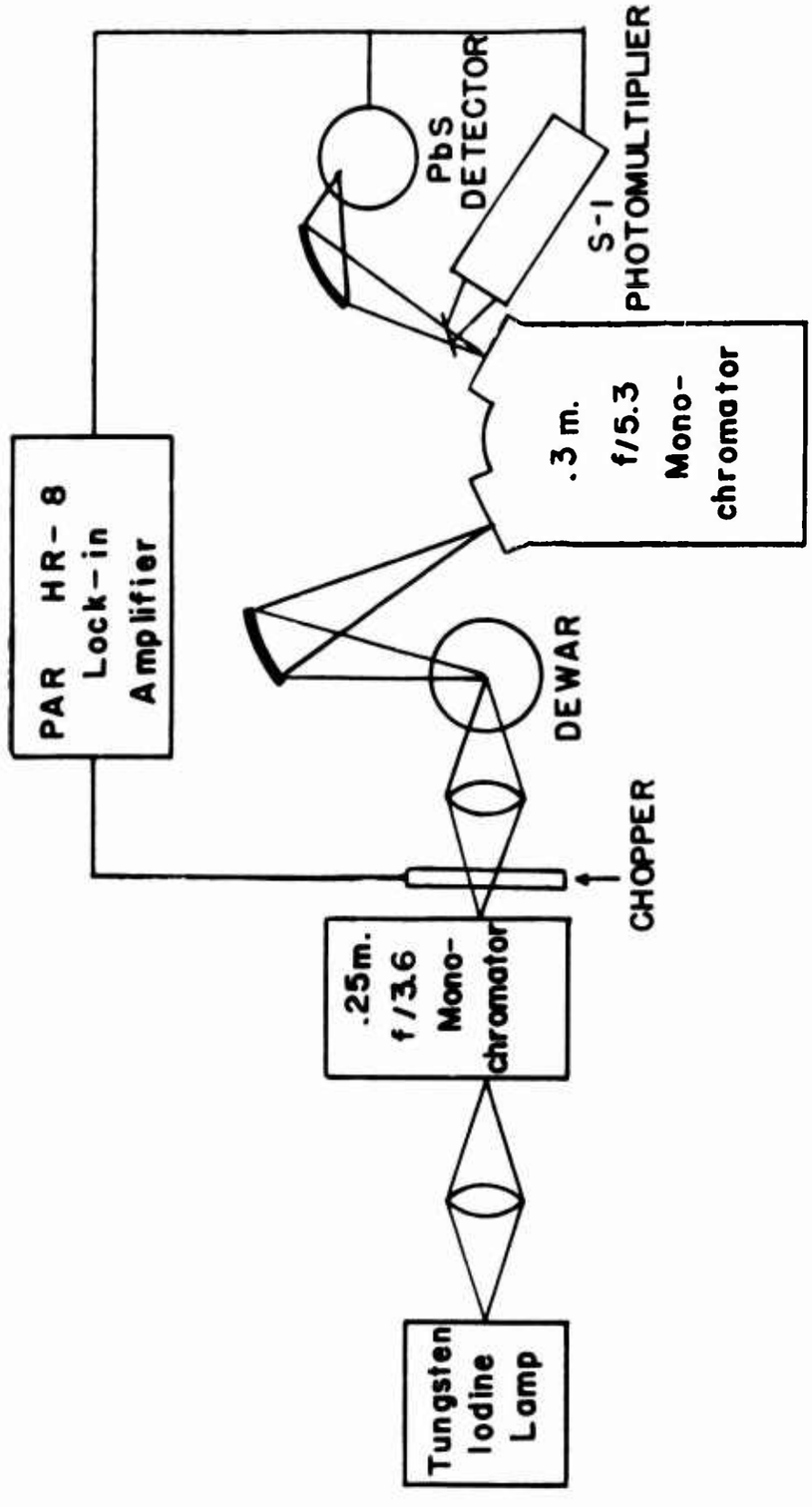

Fig. 2.3 Infrared Fluorescence Apparatus

Model 218 .3m Czerny-Turner spectrometer. Pump light and fluorescence were filtered by Corning, semiconductor, and interference filters, and the spectrometer output was focussed with a 6:1 reduction in image size by an off-axis elliptical mirror onto a Kodak Ektron PbS detector, cooled to dry ice temperature.

Since the visible pump term [Eq. (2.3)] in the IRQC rate equation analysis entered in the same way as all other unmodulated transitions, the same rate equation analysis may be carried over to the case of infrared fluorescence. For example, the fluorescence ν_{23} in Fig. 2.4 will be phase-shifted from the excitation ν_{01} by an amount $\Delta = \tan^{-1}\omega\tau_1 + \tan^{-1}\omega\tau_2$ according to Eq. (2.5). Thus a knowledge of τ_1 and a measurement of the phase shift Δ at some chopping frequency ω will yield τ_2.

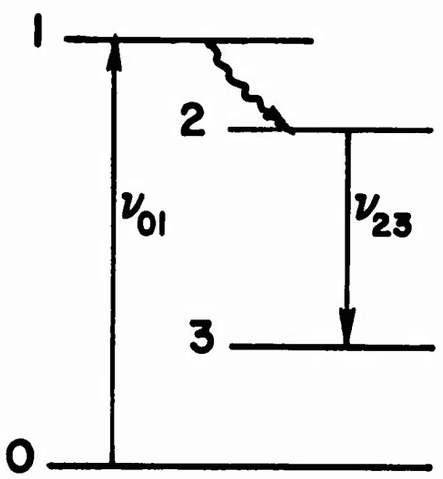

Fig. 2.4 One example of infrared fluorescence.

2.3 SAMPLES AND COOLING

All of the crystals used in this study were grown and mounted in this laboratory by E. F. Williams, according to the method of

Hutchison and Wong.[62] The purity of the starting materials varied from 99.9% to 99.999%. The $LaCl_3$ was obtained by the reduction of La_2O_3 whose total rare earth content was certified by the manufacturer, in most cases, to be at least 99.999% lanthanum. Spectrographic analyses of a lot of La_2O_3 and a sample prepared from La_2O_3 are given in Table 2.1. The La_2O_3 analysis was done by the manufacturer (American Potash and Chemical Corporation), while the .1% Nd^{3+}:$LaCl_3$ analysis was done by the Jarrell-Ash Company. The two analyses do not involve the same lot, but the manufacturer reports that analyses do not vary a great deal from lot to lot.

The crystals were encapsulated in quartz tubes, with varying amounts of helium (usually 1/2 atmosphere) for thermal contact with the bath.

Five of the samples were polycrystalline masses, two were powder samples, and the rest were single crystals, usually with polished faces, and typically .2 mm to 2 mm thick. Polycrystalline samples usually functioned in the quantum counter even with the two beams incident from opposite sides of the sample. After careful alignment, the signal observed was almost always within an order of magnitude of the signal observed from a single, polished crystal of the same composition. One case was found (.5% Ho^{3+} in $GdCl_3$)

Table 2.1. Spectrographic Analyses

Content	Analysis of one lot of La_2O_3 starting material, 99.999% pure with respect to all other rare earths	Analysis of a 0.1% Nd^{3+}:$LaCl_3$ sample prepared from 99.9% pure Nd_2O_3 and 99.999% pure La_2O_3
> 10%	La	La
.1 - 1%	--	Nd
.01 - .1%	--	Si
.001 - .01%	Ca, Si	Pr, Gd, Tb, Yb
.0001 - .001%	Al, Fe, Ag, Cu, K, Mg, Mn, and rare earths other than La	Ca, Cu, Mg
< .0001%	--	B, Al, Fe, Ag

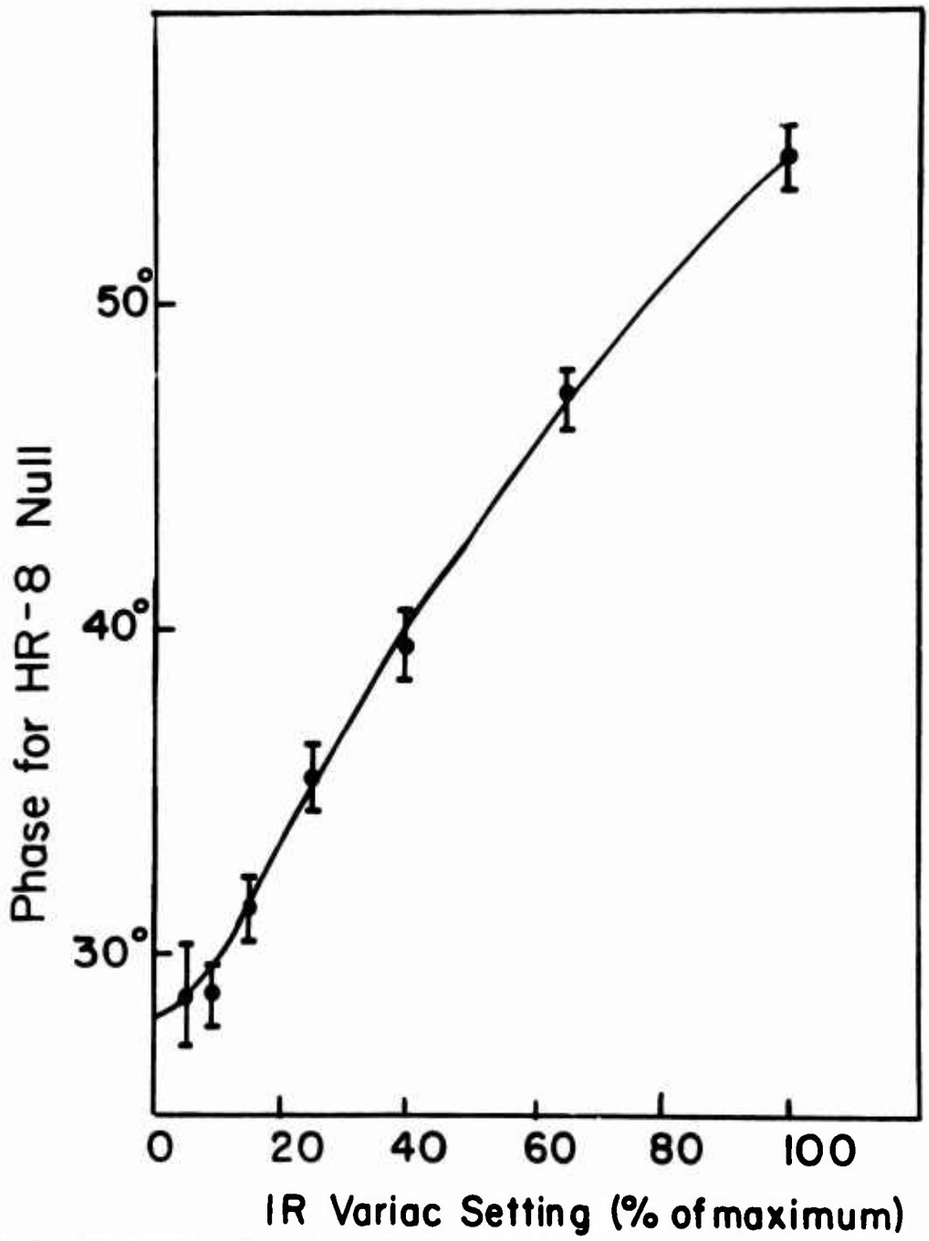

Fig. 2.5 Example of inadequate contact between sample and liquid helium bath. The lifetime being measured is $^3H_6$ in 2% Pr^{3+}:$LaCl_3$. As the IR intensity → 0, the phase yields a 21 ms lifetime; at full IR intensity, 7.9 ms.

in which the signal was a factor of 8.6 larger for the polycrystalline sample, presumably because of the increased path length resulting from scattering in the sample. Only one sample of each composition was used in obtaining the lifetimes, except where indicated otherwise.

For work at liquid nitrogen and liquid helium temperatures, an immersion type dewar with a double-walled Infrasil quartz tip, constructed by L. A. Riseberg, was used.

Several instances were found in which thermal contact of the sample with the bath was inadequate (i.e., the lifetime showed a dependence on the infrared source intensity). In this case, the life time was plotted as a function of the source intensity, and extrapolated to zero intensity (Fig. 2.5).

2.4 THE LIGHT CHOPPER

All of the phase shift measurements were performed with a light chopper built in this laboratory.[63] It is driven by a 10,000 rpm (maximum), 1/10 hp universal motor (Bodine Model B2208), whose speed is regulated by generating a square wave reference signal with a photocell looking through the chopper blades, and sending this signal into a frequency-to-voltage converter to control the D.C. current through the motor (Figs. 2.6, 2.7). After being amplified and clipped by a Schmitt Trigger, the photocell output starts a monostable

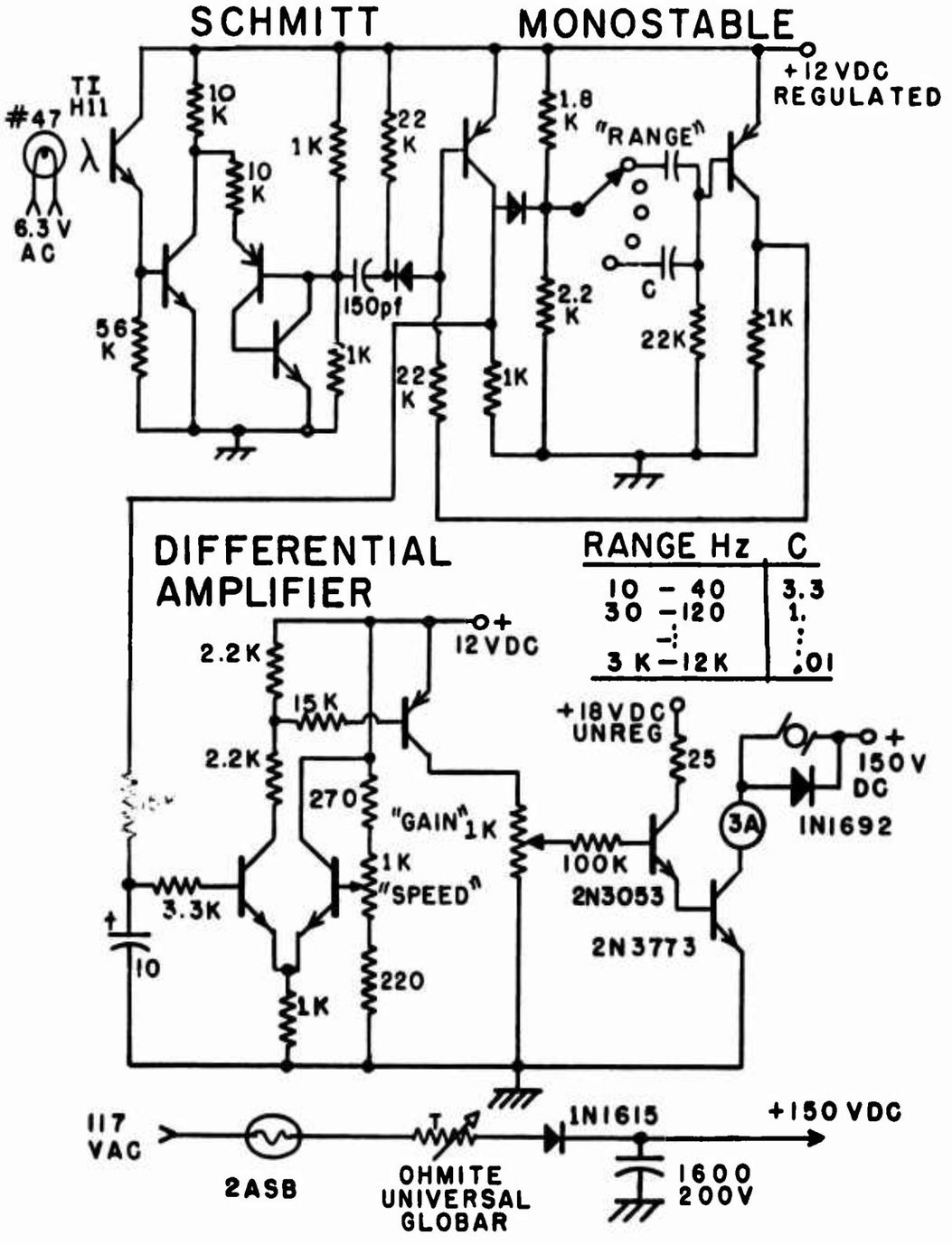

Fig. 2.6 Speed control electronics. Unmarked transistors are silicon types 2N3638 (PNP) or 2N3643 (NPN). Resistors are in ohms, capacitors in microfarads. Unmarked diodes are type 1N483.

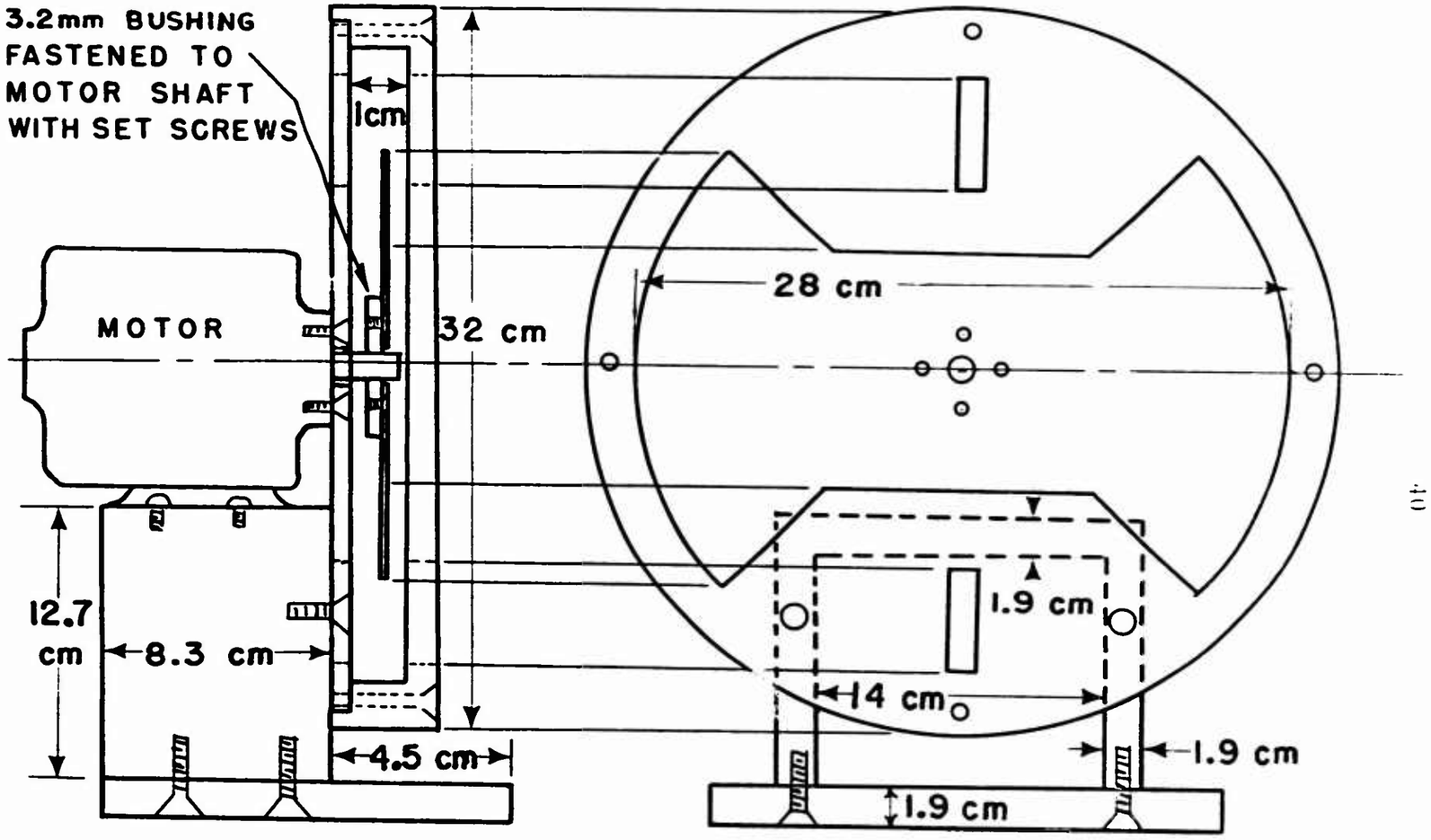

Fig. 2.7 Light chopper. The cover is removed in the front view to show the 2-blade wheel. The reference generator (#47 lamp plus small lens, and Tex. Instr. H-11 photo duo-diode) is not shown; those parts can be mounted in light-tight housings at the 3 or 9 o'clock positions of the wheel cover.

multivibrator. The D. C. component of the multivibrator's output is proportional to the frequency of the incoming signal; a differential amplifier compares this D. C. with a fixed D. C. voltage from a regulated supply, and generates an error signal which is fed into the base of a power transistor in series with the motor, thus regulating the motor current.

Three wheels were constructed, having 2, 8, and 30 blades respectively. In test periods of about four hours at a single frequency, it was found that the frequency stability was at least 1% for the range 8 to 100 Hz with the 2-blade wheel, 15 to 400 Hz with the 8-blade wheel, and 15 to 3000 Hz with the 30-blade wheel. The 3000 Hz frequency limit is set by the 1.3 amp current rating of the motor; because of motor loading, the maximum motor speed of 10,000 rpm was never reached.

The square wave generated by the photocell, amplifier, and shaper, was picked off and used as the reference signal for the phase-sensitive detector. At several thousand rpm a spurious lock-in signal was observed which originated in radiation from the motor leads; it was reduced to a low value (1 μv maximum) by making the motor leads coaxial, with the lead from the power supply as the outer conductor. When the chopper reference signal was used to trigger the signal averager sweep (Sec. 2.5.2), it was found that harmonics of

the line frequency at the signal averager input grew linearly with time in the memory. This effect was due to a 120 cps component in the reference signal, and was reduced to a negligible level by providing a D. C. voltage for the reference-generating light bulb.

2.5 EXPERIMENTAL PROCEDURE

2.5.1 Lifetime Measurements

2.5.1.1 IRQC vs Infrared Fluorescence

There are two categories of infrared levels in rare earth ions whose lifetime cannot be measured with infrared fluorescence by resonantly pumping the level and using quartz dewar tips: (1) the lowest excited level, and (2) the next to the lowest excited level if it is separated from the lowest by a transition of wavelength greater than the cutoff wavelength of quartz (about 4 microns). In both of these cases, the only detectable fluorescence occurs to the ground state, and thus resonant pumping of the level will saturate the detector with scattered pump light. In these cases, the IRQC may be used to advantage to obtain the lifetime; in nearly all other cases, infrared fluorescence is the more sensitive technique.

It is seen in Fig. 1.2 that a gap of less than 900 cm^{-1} between two levels produces a spontaneous multiphonon decay rate for the upper level of greater than 10^5 sec^{-1} in the $LaCl_3$ lattice.

Table 2.2. Measurement Methods

			Number of Levels	Pr^{3+}	Nd^{3+}	Eu^{3+}	Tb^{3+}	Dy^{3+}	Ho^{3+}	Er^{3+}	Tm^{3+}
Measured by Infrared Fluorescence			12					W, A B, D, E	A, B, C, D	A, B	$^3F_4$
Measured by IRQC	Could not be measured by IR fluorescence for this reason. →	Lowest excited level	7	$^3H_5$	Y		$^7F_5$	Y	Y	Y	$^3H_4$
		Next to lowest excited level, and transition to lowest occurs at $\lambda > 4\ \mu$.	4	$^3H_6$	X			X			$^3H_5$
	Gave strong IRQC action; could probably also be measured by IR fluorescence.		2	$^3F_3$	W						
Could not be measured by either method (in some cases a signal could be seen when level was thermally populated from a lower level).			14	$^3F_2$, $^3F_4$		$^7F_1$, $^7F_2$, $^7F_3$, $^7F_4$, $^7F_5$, $^7F_6$	$^7F_0$, $^7F_1$, $^7F_2$, $^7F_3$, $^7F_4$	C			

For an infrared level with a lifetime of 5 msec, this would result in a radiative quantum efficiency of $< .002$, which makes detection of fluorescence difficult. Also, a reduction in the lifetime of the infrared level will reduce the IRQC signal from that level, since the IRQC signal is proportional to $\tau [1 + (\omega\tau)^2]^{-\frac{1}{2}}$, where ω is the angular chopping frequency. These facts account for the inability of either apparatus to measure the lifetimes of the 14 levels in the bottom row of Table 2.2.

2.5.1.2 The Phase Shift Measurement

With both apparatuses (Figs. 2.1 and 2.3), the phase shift Δ_n (Eq. 2.5) was determined by finding the lock-in amplifier phase dial setting (ϕ) which gave a null† output with the detector viewing the signal fluorescence, and the setting (ϕ_0) which gave a null output with the detector viewing the chopped infrared excitation beam as scattered from the crystal with the infrared filters removed. The phase shift is then

$$\Delta_n = \phi - \phi_0$$

To obtain long integration times, the lock-in amplifier time constant was set ~ 10-100 sec, and the output was

† Porter[57] has pointed out that measuring nulls is a more sensitive method than measuring peaks.

traced out on a recorder for two different phase dial settings within a few degrees of ϕ. Lines were drawn by eye through the average value of each trace, the null position on the chart paper was determined by shorting the lock-in amplifier input, and a linear interpolation made to determine ϕ. Integration times of up to one hour were achieved this way.

An alternative method of achieving long integration times was to pass the detector signal only through the narrow band portion of the lock-in amplifier, and average the resulting sine wave-plus-narrow band noise with the multi-channel signal averager (Sec. 2.5.2) When an acceptable signal to noise was achieved, the contents of the memory could be read out on the recorder, the process repeated for the excitation signal, and the phase shift determined. This method was used sparingly, however, because of the demand it placed on chopper stability: the narrow band amplifier introduced a phase shift of about 11^{o} for each 1% change in the chopper frequency. This problem was much less severe in the first method described, because the chopper reference signal which drove the lock-in amplifier's mixer passed through a narrow band amplifier which was nearly identical to the one through which the fluorescence signal passed. Thus a frequency shift caused approximately equal phase shifts in the two, the difference in phase shifts being typically only 2.5^{o} for a 1% frequency change.

In some instances, the weakest signal from which a lifetime could be obtained was determined not by the length of time which one was willing to integrate, but by the level of spurious lock-in signals. Scattering of visible pump light off the chopper blade and leakage of visible light through the infrared filters were relatively simple to control, but two other sources of such spurious signals sometimes set the limit on the IRQC sensitivity:

(1) Fluorescence from either the active ion or an impurity in the crystal, induced by two and even three-step absorption from the infrared beam alone.

(2) Spurious electrical signals originating in the chopper motor.

Before measuring a lifetime, it was necessary to establish that lock-in signals from each of these sources were negligible; in some cases they were not, and the measurement attempt was abandoned.

2.5.1.3 Sources of Error

The primary sources of error in the lifetime measurements will now be discussed individually; the errors due to 120 cps source modulation and Single Channel Analyzer saturation apply only to the IRQC; all other errors apply to both apparatuses.

(1) Chopper Frequency Stability. As pointed out in Sec. 2.5.1.2, the simultaneous use of two nearly identical narrow-band amplifiers in the lock-in amplifier reduces the effective phase shift induced by frequency drift to about 2.5° per 1% frequency change. Tests were made of the chopper's stability, and during four-hour periods at a single frequency, maximum phase drifts were $\pm 1.5^{\circ}$.

(2) Source Intensity Drift. A recorder trace of the lock-in output at a fixed phase dial setting as described in Sec. 2.5.1.2 would be vulnerable to source intensity drift; however the phase dial settings were always within 10° of the value giving a null output, so that a 10% source drift would be required to introduce a 1° phase error. Stability of all sources used was better than 10%.

(3) Crystal Heating. As shown in Fig. 2.5, inadequate thermal contact of the crystal with the helium bath was capable of introducing very large lifetime errors in some instances. In these cases, the phase shift was extrapolated to zero source intensity by using plots such as Fig. 2.5, and a probable error consistent with the plot assigned.

(4) 120 cps Source Modulation. It was pointed out in Sec. 2.1.2 that for certain chopping frequencies ω, harmonics of ω can beat with the 120 cps component of the AH-6 excitation to produce an unwanted component at frequency ω in the

fluorescence. Since the chopping waveform approximates a square wave, the first few odd harmonics of ω will be the largest ones. Thus the values of $\frac{\omega}{2\pi}$ to be avoided are 60 cps (3 X 60 - 120 = 60), 30 cps (5 X 30 - 120 = 30, and 120 - 3 X 30 = 30), 20 cps (7 X 20 - 120 = 20, and 120 - 5 X 20 = 20), and 15 cps (9 X 15 - 120 = 15, and 120 - 7 X 15 = 15).

Since the chopper is not driven by a synchronous motor, the chopping frequency will never be precisely 30 cps (i.e., in the ratio 1:2 to the line frequency), or 20 cps, or 15 cps. Thus ω and the 120 cps AH-6 modulation will not be coherent in phase over a long period of time. In particular, if integration is performed for a time long compared to $[\, 4\,(\frac{\omega}{2\pi}) - 120 \text{ cps}\,]^{-1}$ for a chopping frequency $\frac{\omega}{2\pi} \cong 30$ cps, no error should be introduced in the lock-in signal. This was confirmed by the comparison of measurements of a lifetime obtained by alternately using the AH-6 and tungsten lamps as the visible source.

The chopping frequency was always kept at least 2 cps away from 15, 20, 30, and 60 cps when using the AH-6, so that integration times long compared to .5 sec would suffice.

(5) Displacement of Components in the Chopped Beam. If the infrared source, a lens, or the chopper is moved after ϕ (Sec. 2.5.1.2) is measured, but before ϕ_0 is measured,

an error is introduced in the quantity $(\phi - \phi_0)$, as a result of the fact that the excitation beam strikes the chopper wheel in different places in the two measurements, whereas the chopper reference signal is generated at the same position on the wheel for the two measurements.

The infrared source was imaged on the chopper aperture by a lens; with the 2-blade chopper wheel, a 1 mm displacement of this image would introduce a 1° phase error; with the 30-blade wheel, a 15° phase error would result. Because of this, lifetimes were always measured with the fewest number of blades possible, and the infrared source, chopper, and lenses were either mounted on heavy bases or bolted to the box containing the apparatus. Repeatability of measurements with the 30-blade wheel was $\sim 2^{\circ}$.

(6) Admixture of Unwanted Schemes. If a fluorescence originating from another IRQC scheme is present, it will introduce the largest phase error when it is 90° out of phase with the main fluorescence. In that case, the phase error in radians approximately equals the ratio of the spurious to the main fluorescence intensities; thus to insure 1° accuracy, spurious fluorescences must be kept to less than 2% of the main fluorescence.

(7) Presence of Fluorescence when Measuring ϕ_0. As was mentioned in Sec. 2.5.1.2, ϕ_0 was normally determined by scattering the unfiltered IR source light from the crystal.

In some cases, fluorescence from the crystal (which, of course, is phase-shifted from the excitation) was mixed with the scattered light with sufficient intensity to introduce errors in ϕ_0 of the order of 10°. In such cases the sample holder was moved vertically so that the crystal was not in the beam while measuring ϕ_0.

(8) Saturation Effects. To insure detector linearity, fluorescence and scattered light intensities were kept well below values recommended by the manufacturer. The HR-8 output was calibrated (Fig. 2.8) in terms of pulses per sec from the Single Channel Analyzer, and the latter's non-linearity was found† to become 10% around 10^5 pulses/sec; when scattered light produced a background level higher than this during lifetime measurements, the photomultiplier output was fed directly to a load resistor across the lock-in amplifier input, thus avoiding the Single Channel Analyzer.

(9) Harmonic Leakage through the Narrow Band Amplifier. The fact that both the signal and reference inputs to the lock-in amplifier are non-sinusoidal waveforms suggests the possibility of spurious lock-in signals being created by harmonics which leak through the narrow band amplifiers and reach the mixer. To

† This measurement was performed with pulses randomly distributed in time, except for a 100% low frequency modulation which produced the lock-in signal.

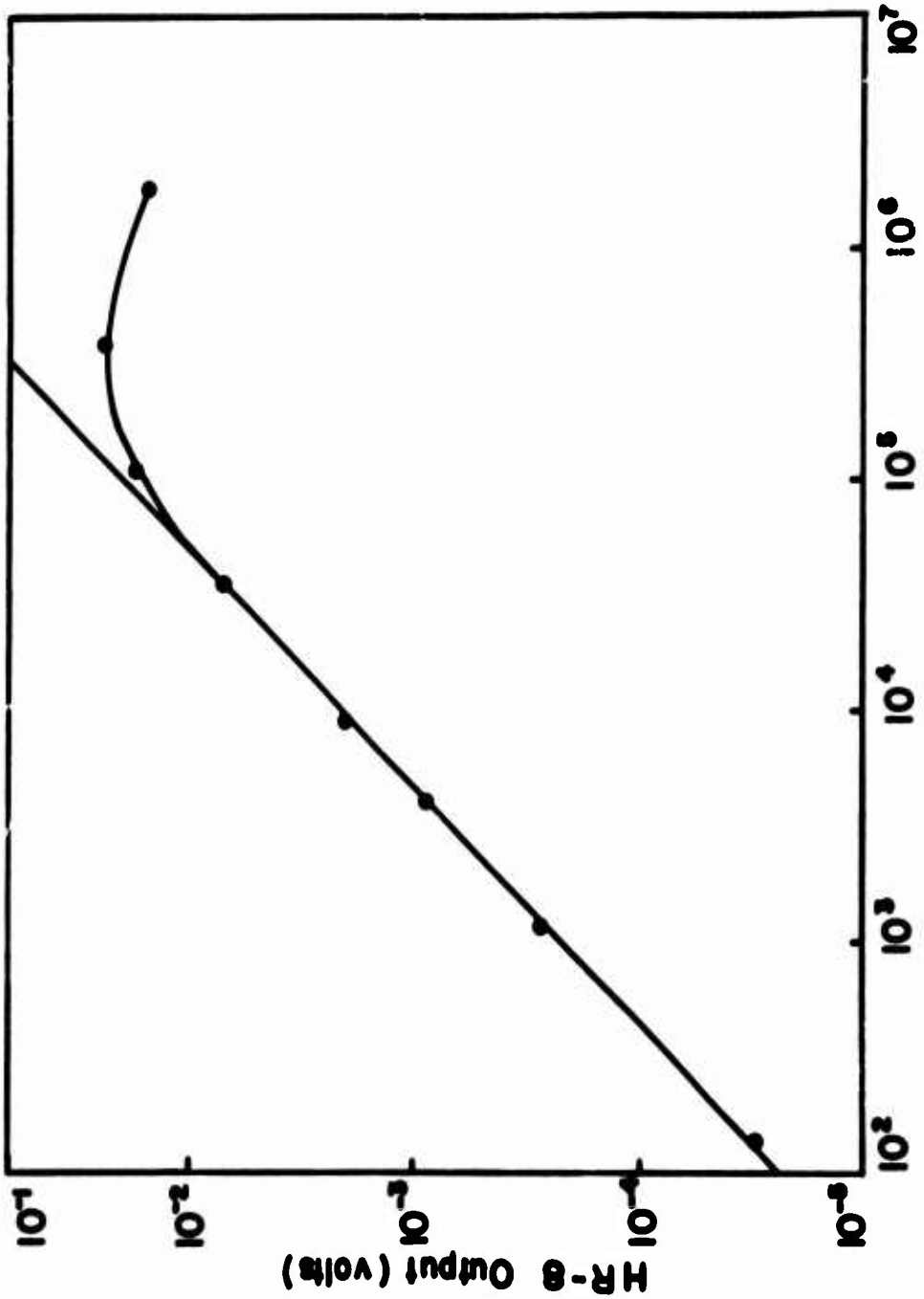

Fig. 2.8 Test of the Linearity of the Single Channel Analyzer's Response

investigate this possibility, the transfer function of the signal-tuned amplifier was measured for a center frequency of 10 cps with an audio oscillator, and the results entered in column 5 of Table 2.3.

The chopper was then set to 10 cps, and the waveforms of the chopper reference signal and chopped scattered light (as seen by the detector when measuring ϕ_0) were recorded. A numerical analysis was done on these waveforms, using Simpson's Rule to evaluate the first few Fourier coefficients; the results are entered in columns 4 and 6 of Table 2.3. An analysis of this type was also done on a typical IRQC fluorescence waveform, but because of the $\tau\,[1 + (\omega\tau)^2]^{-1/2}$ dependence of the IRQC signal intensity, higher harmonics in the excitation waveform are attenuated by the finite lifetime, τ, of the infrared level, and the resulting harmonic content is less rich than in the case of the chopped scattered light waveform. Hence errors due to the process being considered here are more likely to occur in the measurement of ϕ_0 than of ϕ.

From Table 2.3 it is seen that the largest spurious D. C. term generated in the mixer will come from the beating of the two third harmonic terms; its amplitude relative to that of the main D. C. term (which arises from the beating of the two first harmonics) is found by multiplying columns (4), (5), (6), (7) in Row 3.

Table 2.3. Effect of Harmonic Leakage

(1) Frequency (cps)	(2) Harmonic	(3) Relative Amplitude in Ideal Square Wave	(4) Relative Amplitude in Chopped Scattered Light	(5) Relative Transmission of Signal-Tuned Amplifier	(6) Relative Amplitude in Chopper Reference Signal	(7) Relative Transmission of Reference-Tuned Amplifier†
10	1st	1.000	1.000	1.000	1.000	1.000
20	2nd	.000	.005	.065	< .001	.065
30	3rd	.333	.52	.036	.54	.036
40	4th	.000	*	.025	*	.025
50	5th	.200	.22	.020	.14	.020

†Assuming, as claimed by the manufacturer, that the two narrow band amplifiers have the same transfer function.

*The amplitude of this harmonic was not computed, as it was expected to be small.

The result is:

$$(.52)\,(.036)\,(.54)\,(.036) = .00037$$

Thus the largest spurious term in the lock-in signal will be only .37% of the main term, and since the series involving the higher terms converges fairly rapidly, this source of error should be negligible.

(10) Non-exponential Decays. Violation of Assumption 3 (Sec. 2.1.2) by the non-exponentiality inherent in ion pair decays can introduce errors ~25% when the formula $\tau = \omega^{-1} \tan \Delta$ is used. This is discussed further in Sec. 3.1.

2.5.2 Measurement of the Time Dependence of Decays

The time dependences of a number of decays involving ion-ion interactions were obtained with the IRQC (see Sec. 3.1). This was done by choosing a fluorescing level whose lifetime was short compared to that of the infrared level being studied, and putting the Single Channel Analyzer (Fig. 2.1) output into a Fabritek Model 1052LSH Signal Averager.

The chopper was fitted with a wheel which provided an excitation whose duration was a few percent of the interval between excitations. The chopping speed was adjusted so that the excitation duration was about 12% of the e^{-1} lifetime of the decaying level. The

interval between excitations was then about 4 or 5 lifetimes, so that the zero-fluorescence baseline could be determined with reasonable accuracy.

The Signal Averager was operated in the frequency histogram mode, and triggered by the reference signal from the chopper. Averaging times were typically 30 minutes. The contents of the memory were analyzed after being read out on a Brush Mark 250 recorder.

3. RESULTS

3.1 TIME DEPENDENCE OF THE DECAYS

Using the technique described in Sec. 2.5.2, the time dependence of a number of decays involving ion-ion interactions were obtained. Decays involving only one ion pair were found to be non-exponential (Sec. 4.3.1). An example is shown in Fig. 3.1. In such case the term "lifetime" must be defined. Three common definitions, all of which reduce to the usual definition in the limit of exponentiality, are:

τ_i = reciprocal of the slope of the semi-log decay plot as $t \to 0$

τ_e = time for population to drop to e^{-1} of its initial value

τ_f = reciprocal of the slope of the semi-log decay plot as $t \to \infty$

The derivation of Eq. (2.5) in Sec. 2.1.2 assumed that all decays were exponential (Assumption 3). Empirically, it is found that the formula is still useful in the non-exponential cases encountered here, providing a scheme is chosen for which $\omega\tau_i \ll 1$ for all levels i in the IRQC scheme except the one under study. If that level decayed exponentially with lifetime τ, we would then expect to observe a phase shift Δ, where

$$\tau \cong \omega^{-1} \tan \Delta \qquad \text{(assumes exponentiality).} \qquad (3.1)$$

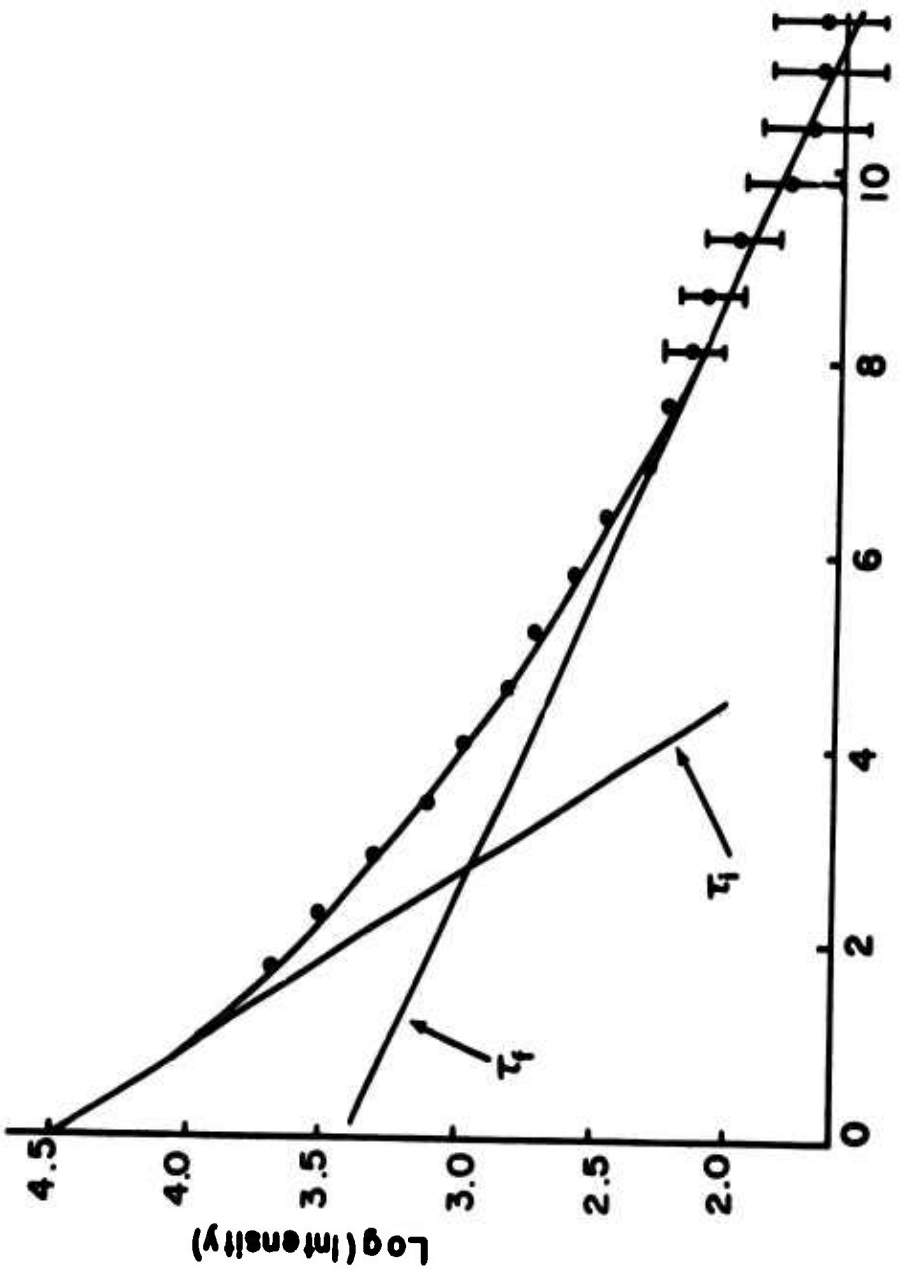

Fig. 3.1 Decay of the $^3H_6$ level in 0.25% Pr^{3+}:$LaCl_3$ at 300°K, obtained by the method described in Sec. 2.5.2. The fluorescing level was $^3P_0$, whose lifetime (12 μsec) is negligible on this time scale.

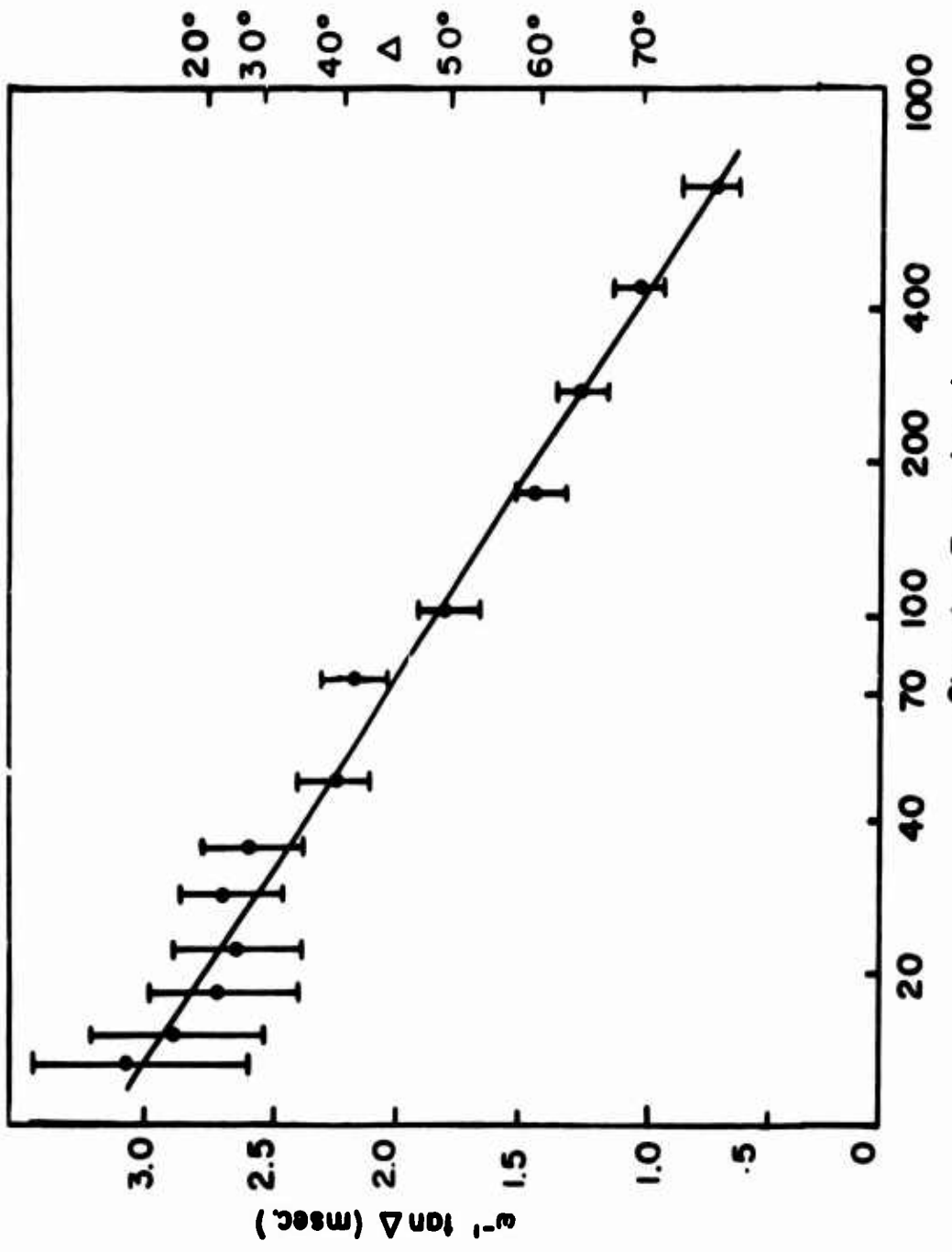

Fig. 3.2 Result of applying the phase shift method to the $^3H_6$ decay shown in Fig. 3.1.

In all non-exponential decays whose time dependence was studied (Table 3.1), it is seen that for $\Delta = 45^{o}$, the value of $\omega^{-1} \tan \Delta$ is within 25% of τ_e. Thus, in measuring the lifetime for a non-exponential decay by the phase shift method, the chopping frequency was chosen so as to produce a phase shift of approximately 45^{o}, and the resulting value of $\omega^{-1} \tan \Delta$ was called τ_e, with a 25% probable error assigned.

The increase in $\omega^{-1} \tan \Delta$ with decreasing Δ in Table 3.1 and Fig. 3.2 is reasonable, since the lower the chopping frequency, the more of the long-lifetime tail of the decay curve seen by the detector during the half-period in which the excitation is blocked by the chopper blade.

It should be realized that τ_i and τ_f are somewhat dependent on the particular experimental arrangement. The value of τ_i may be increased, for example, by inadequate time resolution, while the value of τ_f may be reduced by noise which limits the time after the flash that the decay curve can be followed.

Decays involving migration to sinks were found to be exponential (Sec. 4.3.2). These time-dependence measurements are listed in Table 3.2.

The quantum efficiencies listed in Tables 3.1 and 3.2 for the quenching processes are simply $\tau_o(\tau_e + \tau_o)^{-1}$, where τ_o is the

Table 3.1. Lifetimes for non-exponential decays

Level, Sample, Temperature	Percentage Decaying by Ion Pair Interaction	Lifetimes from Decay Curve (msec)	Lifetimes by Phase-Shift Method Δ	$\omega^{-1} \tan \Delta$
$^3H_6$,		$\tau_i = 1.60 \pm .20$	70°:	$1.00 \pm .10$
.25% Pr^{3+}:$LaCl_3$,	85%	$\tau_e = 1.79 \pm .07$	45°:	$1.95 \pm .14$
$300^\circ K$		$\tau_f = 5.50 \pm 1.0$	20°:	$2.72 \pm .19$
$^4I_{13/2}(X)$		$\tau_i = 4.92 \pm .90$	70°:	$5.44 \pm .67$
.1% Nd^{3+}:$LaCl_3$,	80%	$\tau_e = 5.90 \pm .50$	45°:	$7.30 \pm .55$
$77^\circ K$		$\tau_f = 8.12 \pm .93$	20°:	$8.60 \pm .50$
$^4I_{15/2}(W)$		$\tau_i = 1.16 \pm .12$	70°:	$0.70 \pm .20$
.3% Nd^{3+}:$LaCl_3$,	90%	$\tau_e = 1.65 \pm .18$	45°:	$2.06 \pm .16$
$77^\circ K$		$\tau_f = 3.54 \pm .35$	20°:	$3.40 \pm .41$

Table 3.2. Lifetimes for decays which were exponential to within the error of measurement (10%)

Level, Sample, Temperature	Percentage Decaying by Migration to Sinks	Lifetime from Decay Curve (msec)	Lifetime by Phase-Shift Method (msec)
$^3H_6$, 50% Pr^{3+}:$LaCl_3$, 4.2°K	70%	9.45 ± .47	9.15 ± .80
$^3H_6$, 85% Pr^{3+}:$LaCl_3$, 4.2°K	90%	1.97 ± .11	1.84 ± .12
$^3H_5$, 15% Pr^{3+}:$LaCl_3$, 77°K	70%	12.0 ± 1.1	11.1 ± 0.8
$^4I_{13/2}$(X), 10% Nd^{3+}:$LaCl_3$, 4.2°K	90%	4.74 ± .24	4.15 ± .32
$^4I_{13/2}$(Y), 25% Er^{3+}:YCl_3, 300°K	90%	2.99 ± .15	3.05 ± .18

radiative lifetime (obtained by extrapolating the lifetime-vs-concentration curve to zero concentration), and τ_e is the e^{-1} lifetime for the sample under consideration.

3.2 LIFETIMES

Lifetimes in samples of a given purity are listed in Table 3.3. Lifetimes for migration-quenched levels in samples of two different purities are compared in Table 3.4.

When the IRQC was used, the lifetimes of any intermediate levels involved in the scheme had to be determined before Eq. (2.5) could be used to obtain τ_1, the infrared level lifetime. Three methods were used:

(1) In some cases, the required lifetimes had been measured by Barasch and Dieke.[55]

(2) The lifetimes of some levels involved in IRQC action are expected† to be so shortened by multiphonon relaxation that they can be neglected in comparison with lifetimes reported here. Examples are $^3F_2$ and $^3F_4$ in Pr^{3+}:$LaCl_3$.

(3) When methods (1) and (2) were inapplicable, the required lifetimes were measured by either fluorescence or the IRQC techniques.

†See Fig. 1.2.

All lifetimes in Tables 3.1, 3.2, 3.3, and 3.4 have had these corrections for intermediate levels applied when necessary. Thus each of the values quoted represents only the lifetime of the infrared level referred to.

The weakness of some of the IRQC schemes provides evidence that the following fluorescing levels are appreciably quenched, probably by ion-pair decay, at the concentrations and temperatures indicated: Pr $^3P_1$, $c > 10\%$, $T \geq 4.2^\circ K$; Pr $^3P_0$, $c \sim 100\%$, $T = 300^\circ K$; Nd D $c > 10\%$, $T \geq 4.2^\circ K$; and Dy I, $c = 1\%$ $T = 300^\circ K$.

Table 3.3. Lifetimes (in msec) of infrared levels of rare earth trichlorides. The energy level notation of Refs. 3-11 is used (see Fig. 1.4). For purity-dependent lifetimes, samples were prepared from 99.9% purity dopant oxide and 99.999% purity host oxide. Radiationless transitions are omitted in specifying the scheme. For example, the scheme of Fig. 2.2(b) would be described in this Table as IR Pump: $^3H_4$-$^3F_2$, Visible Pump: $^3H_5$-$^3P_1$, Fluorescence: $^3P_0$-$^3H_6$.

Ion	Level	Lattice	Conc(%)	Lifetimes (milliseconds) 4.2°K	77°K	300°K	Infrared Pump	Visible Pump	Fluorescence
Pr^{3+}	$^3H_5$	$LaCl_3$	~.001[a]	b	22.0±3.1	16.8±5.5	$^3H_4$-$^3F_2$	$^3H_5$-$^3P_1$	$^3P_0$-$^3H_4$
			.25	b	26.6±1.8	20.2±1.5	"	"	"
			1	b	23.4±1.6	12.2±0.8	"	"	"
			2	b	26.3±2.5	15.8±1.0	"	$^3H_5$-$^3P_0$	$^3P_0$-$^3H_6$
			15	b	11.1±0.8	5.1±0.5	"	"	"
			25	b	1.98±.13	1.87±.18	"	"	"
			50	b	2.16±.16	1.85±.17	"	"	"
			85	b	0.94±.09	0.71±.09	"	"	"
			100	b	.190±.015	.157±.043	"	"	"
	$^3H_6$	$LaCl_3$	~.001[a]	20.0±1.2	15.9±1.5	10.7±2.0	"	$^3H_6$-$^3P_0$	$^3P_0$-$^3H_4$
			.25	19.5±1.9	2.42±.60[c]	2.00±.50[c]	"	$^3H_6$-$^3P_2$	"
			1	20.4±1.2	.014±.007[c]	.020±.007[c]	"	$^3H_6$-$^3P_0$	"
			2	21.0±1.9	.023±.010[c]	.022±.010[c]	"	"	"

Table 3.3 (cont'd).

Ion	Level	Lattice	Conc(%)	Lifetimes (milliseconds) 4.2°K	77°K	300°K	Infrared Pump	Visible Pump	Fluorescence
Pr^{3+}	$^3H_6$	$LaCl_3$	15	20.4±1.2	b	b	$^3H_4$-$^3F_2$	$^3H_6$-$^3P_0$	$^3P_0$-$^3H_4$
			25	5.90±.51	b	b	"	"	"
			50	.190±.017	b	b	"	"	"
			85	1.84±.12	b	b	"	"	"
			100	.016±.005	b	b	"	"	"
	$^3F_2$	$LaCl_3$	.25	b	b	1.99±.50[c,d]	"	$^3F_2$-$^3P_2$	"
	$^3F_3$	$LaCl_3$	.25	.348±.040	.565±.080	.216±.025	$^3H_4$-$^3F_3$	$^3F_3$-$^3P_2$	"
			1	.322±.035			"	"	"
			2	.340±.042	.014±.007[c]	.012±.005[c]	"	$^3F_3$-$^3P_1$	"
			15	.334±.048	b	b	"	$^3F_3$-$^3P_2$	"
			50	.172±.062	b	b	"	"	"
			85	.133±.023	b	b	"	"	"
			100	b	b	b	"	"	"
	$^3F_4$	$LaCl_3$	.25	b	b	.193±.050[d]	$^3H_4$-$^3F_4$	$^3F_4$-$^3P_0$	"

Table 3.3 (cont'd).

Ion	Level	Lattice	Conc(%)	Lifetimes (milliseconds) 4.2°K	77°K	300°K	Infrared Pump	Visible Pump	Fluorescence
Nd^{3+}	Y	$LaCl_3$	.01	100±30	49.2±6.0	b	Z-R[g]	Y-D	D-Z
			0.3	79±30	43.6±7.5		"	"	"
			1.0	89±21	56.5±7.8	12.4±2.0	"	"	"
			10	60±12	31.8±4.3		"	"	"
			100		b		"	"	"
	X	$LaCl_3$	.01	41.2±4.5	21.0±5.0	14.3±3.6	Z-X	X-L	L-Z
			0.1	30.8±3.7	7.55±2.0[c]	6.6±1.7[c]	"	"	"
			0.3	31.4±2.5	1.13±.30[c]	1.20±.40[c]	"	"	"
			1.0	22.3±1.6	0.26±.07[c]	0.46±.12[c]	"	"	"
			10	4.15±.32	b	b	"	"	"
			100	.122±.026	b	b	"	"	"
		$GdCl_3$	1.0	18.2±1.7	0.28±.07[c]	0.38±.10[c]	"	"	"
	W	$LaCl_3$	.01	12.4±1.0	12.1±1.1	8.4±1.0	Z-W	W-L	"
			0.1	13.2±1.2	7.8±1.5[c]	5.0±1.5[c]	"	"	"
			0.3	15.7±1.0	2.0±0.6[c]	1.6±0.5[c]	"	"	"
			1.0	15.7±1.1	.61±.25[c]	.36±.10[c]	"	"	"

Table 3.3 (cont'd).

Ion	Level	Lattice	Conc(%)	Lifetimes (milliseconds) 4.2°K	77°K	300°K	Infrared Pump	Visible Pump	Fluorescence
Nd^{3+}	W	$LaCl_3$	10	16.5±1.3	b	b	Z-W	W-L	L-Z
			100	4.7±1.0	b	b	"	"	"
		$GdCl_3$	1.0	12.8±0.9			"	"	"
Tb^{3+}	$^7F_5$	$LaCl_3$	2.0	31.3±3.6	40.7±3.7	27.4±2.8	$^7F_6$-$^7F_3$	$^7F_5$-$^5D_3$	$^5D_3$-$^7F_6$
		$GdCl_3$	0.5	12.5±1.0	30.8±2.4	15.2±1.2	"	"	"
	$^7F_4$	$LaCl_3$	2.0	b	b	14.9±1.1[d]	"	$^7F_4$-$^5D_3$	"
		$GdCl_3$	0.5	b	b	6.6±1.2[d]	"	"	"
Dy^{3+}	Y	$LaCl_3$	.25			12.8±1.0	Z-Y	Y-F	F-Z
			1.0	17.4±1.6		14.9±0.9	"	"	"
	X		.25			5.5±0.9	Z-X	X-F	"
			1.0	9.0±0.5	6.6±0.6	5.9±0.8	"	"	"
	W		.25	1.10±.10[e]		.67±.07[e]	Z-W	f	W-Y
			1.0	1.19±.08[e]		.72±.07[e]	"	f	"
	A		.25	.138±.013[e]		.028±.003[e]	Z-A	f	A-Y
			1.0	.164±.014[e]	.174±.015[e]	.030±.003[e]	"	f	"

Table 3.3 (cont'd).

Ion	Level	Lattice	Conc(%)	Lifetimes (milliseconds) 4.2°K	77°K	300°K	Infrared Pump	Visible Pump	Fluorescence
Dy^{3+}	B	$LaCl_3$	1.0	.068±.030[e]			Z-B	f	A-Y
	D		.25	.318±.030[e]		.270±.020	Z-D	f	D-X
			1.0	.364±.020[e]	.398±.032	.218±.022	"	f	"
	E		1.0	.0032±.0022[e]			Z-E	f	E-Y
Ho^{3+}	Y	$LaCl_3$	0.1	7.5±1.3		8.4±0.5	Z-Y	Y-D	D-Z
			1.0			8.9±0.6	"	"	"
			2.5	7.76±.54	9.10±.55	9.9±0.7	"	"	"
		$GdCl_3$	0.5			8.1±0.5	"	"	"
			2.5	8.04±.56	9.37±.63	10.1±0.7	"	"	"
		YCl_3	2.0	19.8±3.1	18.4±1.7	21.2±2.0	"	"	"
	A	$LaCl_3$	0.1			3.84±.32	Z-A	f	A-Y
			2.5	4.45±.41		4.76±.30	"	f	"
		$GdCl_3$	0.5	3.40±.52		3.52±.26	"	f	"
			2.5	3.00±.35		4.76±.30	"	f	"

Table 3.3 (cont'd).

Ion	Level	Lattice	Conc(%)	Lifetimes (milliseconds) 4.2°K	77°K	300°K	Infrared Pump	Visible Pump	Fluorescence
Ho^{3+}	B	$LaCl_3$	1.0			5.31±.35	Z-B	f	B-Y
			2.5	5.24±.32	5.50±.36	5.00±.39	"	f	"
		$GdCl_3$	0.5	4.55±.33		4.33±.27	"	f	"
			2.5			3.90±.23	"	f	"
		YCl_3	2.0			17.9±1.8	"	f	"
	C	$LaCl_3$	2.5	6.63±.47		6.57±.48	Z-C	f	C-Y
		$GdCl_3$	0.5	4.79±.35		5.06±.37	"	f	"
			2.5	4.85±.30		5.32±.38	"	f	"
	D	$LaCl_3$		(see Ref. 55)					
		YCl_3	2.0		1.91±.13	1.52±.11	Z-D	f	D-Y
Er^{3+}	Y	$LaCl_3$	5.0		4.96±.66	5.35±.52	Z-Y	Y-M	L-Z
		$GdCl_3$	1.0	6.04±.60	5.10±.47	4.72±.23	"	"	"
		YCl_3	2.0	40.1±4.8	30.7±3.1	22.5±1.3	"	"	"
			25	1.82±.34	1.85±.34	3.05±.18	"	"	"

Table 3. 3 (cont'd).

Ion	Level	Lattice	Conc(%)	Lifetimes (milliseconds) 4.2°K	77°K	300°K	Infrared Pump	Visible Pump	Fluorescence
Er^{3+}	A	$LaCl_3$	5	4.68±.34	4.12±.33	5.18±.43	Z-A	f	A-Y
		$GdCl_3$	1	4.82±.82	4.35±.24	4.25±.25	"	A-M	L-Z
		YCl_3	2	16.9±1.9	16.3±1.7	12.0±1.4	"	"	"
			25	1.49±.11	2.70±.16	4.33±.28	"	f	A-Y
			50	0.41±.10	.340±.028	1.34±.08	"	f	"
	B	$LaCl_3$	5	2.36±.18	1.73±.11	1.73±.20	Z-B	f	B-Y
		$GdCl_3$	1			1.73±.11	"	f	"
		YCl_3	2	20.3±1.5	18.1±1.1	10.5±0.6	"	f	"
			25	17.7±1.1	16.9±1.1	b	"	f	"
			50	9.8±0.9	6.06±.42	b	"	f	"
Tm^{3+}	$^3H_4$	$LaCl_3$	2	2.32±.14		2.74±.19	$^3H_6$-$^3H_4$	$^3H_4$-$^1D_2$	$^1D_2$-$^3H_6$
		YCl_3	2	8.95±.55		8.25±.67	"	"	"
	$^3H_5$	$LaCl_3$	2	1.59±.12		2.50±.18	$^3H_6$-$^3H_5$	$^3H_5$-$^1D_2$	"
		YCl_3	2	8.0±1.0		5.51±.72	"	"	"
	$^3F_4$	$LaCl_3$	2	.547±.036		.545±.037	$^3H_6$-$^3F_4$	f	$^3F_4$-$^3H_4$
		YCl_3	2	.547±.053		.588±.037	"	f	"

Table 3.3 (cont'd).

[a]This sample was nominally .01% Nd:$LaCl_3$, and Pr^{3+} was present only as an impurity, probably at a level of about .001%.

[b]A signal of sufficient strength for a lifetime measurement could not be obtained.

[c]The "1/e" lifetime (decay is non-exponential--see Sec. 3.1).

[d]This apparent lifetime results from thermal population from the level below; the true lifetime is expected to be much shorter(see Sec. 4.2).

[e]This measurement was performed by Mr. L. A. Riseberg.

[f]Infrared fluorescence was used, hence there was no visible pump.

[g]IR fluorescence measurements on Nd^{3+}:$LaCl_3$ indicate that the branching of the R fluorescence is ~10% R→Z, ~90% R→Y, ~1% R→X, and ~0.4% R→W. Hence population of Y by cascading through X and/or W (which would increase the observed phase shift) should be negligible.

Table 3.4. Lifetimes of migration-quenched levels in $Pr^{3+}:LaCl_3$ which illustrate the correlation between quenching rate and purity of the starting materials. The samples were prepared from host oxide of 99.999% purity, and dopant oxide of the purity indicated.

Conc. (%)	Sample Number	Dopant Purity (%)	Lifetimes (msec) $^3H_6$, 4.2°K	$^3H_5$, 77°K	$^3H_5$, 300°K
50	083	99.9	.190 ± .017	2.16 ± .16	1.85 ± .17
50	325	99.999	9.15 ± .80	2.25 ± .17	1.60 ± .18
85	077	99.9	1.84 ± .12	.944 ± .086	.713 ± .092
85	391	99.999	.481 ± .026	.854 ± .071	.610 ± .084
100	069	99.9	.045 ± .007	1.15 ± .07	.93 ± .10
100	084	99.9	.016 ± .005	.190 ± .015	.157 ± .043
100	217	99.999	.063 ± .006	4.81 ± .30	4.25 ± .31
100	239	99.999	.066 ± .005	5.65 ± .37	3.25 ± .30

4. ANALYSIS OF THE RESULTS

4.1 RADIATIVE DECAY

Those low concentration lifetimes in Table 3.3 which are expected to be predominantly radiative and from which a direct comparison of the $LaCl_3$, $GdCl_3$, and YCl_3 lattices can be made are compiled in Table 4.1. The lifetimes in $GdCl_3$ average 13% smaller than the corresponding lifetimes in $LaCl_3$, while the YCl_3 lifetimes are 4.9 times larger, on the average, than the corresponding $LaCl_3$ lifetimes. This is consistent with observations on the visible levels (see Table II in Barasch and Dieke[55]). The fact that the YCl_3 lifetimes are longer probably results from lower electric dipole oscillator strengths due to the fact that the RE^{3+} site symmetry in YCl_3 is very nearly octahedral.[64]

Changes of the order of 50% in radiative lifetimes in Table 3.3 are frequently seen to occur when the temperature goes from 4.2°K to 300°K. The change may be either an increase (e.g., Y in 2.5% Ho:$LaCl_3$) or a decrease (e.g., Y in 1% Er:$GdCl_3$) with temperature, and may be explained on the basis of thermal population of higher Stark components whose decay times differ. In some cases, radiation reabsorption[55] may also contribute to the change.

Table 4.1. Radiative lifetimes in chloride lattices.

Ion	Level	Temperature	Lifetimes (msec) $LaCl_3$	$GdCl_3$	YCl_3
Nd^{3+}	$^4I_{15/2}$(W)	4.2°K	15.7	12.8	
Ho^{3+}	$^5I_7$ (Y)	4.2°	7.76	8.04	19.8
	$^5I_6$ (A)	4.2°	4.45	3.00	
	$^5I_5$ (B)	300°	5.00	3.90	17.9
	$^5I_4$ (C)	4.2°	6.63	4.85	
	$^5F_5$ (D)	77°	0.32†		1.91
Er^{3+}	$^4I_{13/2}$(Y)	77°	5.0	5.10	30.7
	$^4I_{11/2}$(A)	4.2°	4.68	4.82	16.9
	$^4I_{9/2}$(P)	4.2°	2.36		20.3
Tm^{3+}	$^3H_4$	4.2°	2.32		8.95
	$^3H_5$	4.2°	1.59		8.0

† From Ref. 55

4.2 MULTIPHONON RELAXATION

For multiphonon relaxation to produce an observable effect on a 10 msec lifetime, its rate must be > 10 sec^{-1}. If its rate is greater than 10^4 sec^{-1}, however, a signal of sufficient strength for a lifetime measurement in most cases cannot be obtained. For the spontaneous multiphonon emission rate to fall between 10 and 10^4 sec^{-1} in $LaCl_3$ requires† 1080 cm^{-1} < (energy gap) < 1580 cm^{-1}. A number of such levels exist in Nd^{3+} and Dy^{3+}, and multiphonon relaxation rates have been extracted from the lifetimes of these levels.[15,16] The only level below 14,000 cm^{-1} in Pr^{3+}, Eu^{3+}, Tb^{3+}, Ho^{3+}, Er^{3+}, or Tm^{3+} which has a gap between 1080 cm^{-1} and 1580 cm^{-1} is $^3F_3$ in Pr^{3+}. The gap below this level is 1329 cm^{-1} in $LaCl_3$, so that from Fig. 1.2 one would expect a phonon decay rate ~ 300 sec^{-1}. Since the observed low-concentration-and-temperature total decay rate for this level (Table 3.3) is ~ 3000 sec^{-1}, the decay is probably about 10% by spontaneous multiphonon emission. One $^3F_3$ lifetime at 77°K will later be used in obtaining an energy transfer rate; from Fig. 1.3, it is seen that the multiphonon emission rate should not increase significantly in going from 4.2°K to 77°K.

†See Fig. 1.2.

When a level is appreciably thermally populated from a level below, care must be used in interpreting the measured lifetime. We consider the common case of a level, 1, which, in the absence of thermal population, would have a lifetime τ_1, determined by multiphonon emission to a level, 2, below, whose lifetime is τ_2. Suppose that $\frac{E_1 - E_2}{kT}$ is small enough that the number of ions raised thermally from 2 to 1 is sufficient to be detected by the apparatus measuring the lifetime of 1. The time, τ_m, for the exciting light source to drop from 90% to 10% intensity usually determines the time resolution of the measuring apparatus.

If $\tau_2 > \tau_1 \tilde{>} \tau_m$, the observed decay of 1 will be a sum of exponentials with time constants τ_1 and τ_2. In such case, the phase shift method yields a lifetime intermediate between τ_1 and τ_2. This is the case with $^7F_4$ in Tb^{3+} at 300°K in Table 3.3. In that case, $\tau_2 \equiv \tau\,(^7F_5) \sim 20$ ms $> \tau_1 \equiv \tau\,(^7F_4) \sim 20\ \mu s \sim \tau_m$. (The 20 μsec value at 300°K is obtained from Sec. 1.2.2, using the fact that the $^7F_4 - {}^7F_5$ gap is 1066 cm^{-1}.)

If $\tau_2 \tilde{>} \tau_m >> \tau_1$, the effect of τ_1 will be lost, and both the time dependence and phase shift methods will simply yield τ_2. This is the case with $^3F_2$ and $^3F_4$ in Pr^{3+} at 300°K in Table 3.3. The gaps below these levels are 491 cm^{-1} and 333 cm^{-1} respectively, so that, using Fig. 1.2, $\tau_1 < 0.1\ \mu$sec in both cases. As it should be,

the measured lifetime in each case is the same as τ_2, the lifetime of the level immediately below.

4.3 ION-ION INTERACTIONS

4.3.1 Ion Pair Decay

All of the levels whose lifetimes were followed to 100% concentration showed concentration quenching. Inspection of the energy level diagrams, however, shows that only five of these levels are capable of being de-excited by a single transfer to an ion of the same type, assisted by three or fewer phonons. (These five all require, in fact, absorption rather than emission of vibrational energy.) The remainder of the levels decay by migration to sinks, a process that will be discussed in Sec. 4.3.2. In this section, we examine the five examples of ion pair decay (Table 4.2).

Because of the large energy assistance required by the 5th decay in Table 4.2, it is probably effective only at 300°K and at moderately high concentrations. It may account for the weakness of the B signal in the 25% and 50% samples at 300°K (Table 3.3).

The first four decays in Table 4.2 have a property in common with the $^4F_{3/2} + {}^4I_{9/2} \rightarrow {}^4I_{15/2} + {}^4I_{15/2}$ decay in Nd^{3+}:LaF_3 studied by Asawa and Robinson:[35] each decay has a number of component transitions (Tables 4.3, 4.4) involving higher Stark

Table 4. 2. Examples of ion-pair decay from Table 3. 3. The activation energy is the final energy of the ion pair minus their initial energy, assuming population only of the lowest Stark components.

		Decay	Activation Energy
1.	$Pr^{3+}:LaCl_3$	$^3H_6 + {}^3H_4 \rightarrow {}^3H_5 + {}^3H_5$	43 cm^{-1}
2.	"	$^3F_3 + {}^3H_4 \rightarrow {}^3H_6 + {}^3H_5$	88
3.	$Nd^{3+}:LaCl_3$	$^4I_{13/2}(X) + {}^4I_{9/2}(Z) \rightarrow {}^4I_{11/2}(Y) + {}^4I_{11/2}(Y)$	16
4.	"	$^4I_{15/2}(W) + {}^4I_{9/2}(Z) \rightarrow {}^4I_{13/2}(X) + {}^4I_{11/2}(Y)$	37
5.	$Er^{3+}:YCl_3$	$^4I_{9/2}(B) + {}^4I_{15/2}(Z) \rightarrow {}^4I_{13/2}(Y) + {}^4I_{13/2}(Y)$	666

Table 4.3. Transition components in $Pr^{3+}:LaCl_3$ which produce energy matches within 3 cm^{-1}. Numbers in parentheses are the crystal quantum numbers, μ.

$^3H_6 + {}^3H_4 \rightarrow {}^3H_5 + {}^3H_5$ Decay

1. $^3H_6(2) + {}^3H_4(3) \rightarrow {}^3H_5(3) + {}^3H_5(1)$
2. $^3H_6(3) + {}^3H_4(2') \rightarrow {}^3H_5(3) + {}^3H_5(1)$
3. $^3H_6(2) + {}^3H_4(2') \rightarrow {}^3H_5(2) + {}^3H_5(2')$
4. $^3H_6(2) + {}^3H_4(2') \rightarrow {}^3H_5(1) + {}^3H_5(3')$
5. $^3H_6(3) + {}^3H_4(1) \rightarrow {}^3H_5(3) + {}^3H_5(2')$
6. $^3H_6(3) + {}^3H_4(1) \rightarrow {}^3H_5(2) + {}^3H_5(1)$
7. $^3H_6(2) + {}^3H_4(1) \rightarrow {}^3H_5(3') + {}^3H_5(2')$

$^3F_3 + {}^3H_4 \rightarrow {}^3H_6 + {}^3H_5$ Decay

1. $^3F_3(3') + {}^3H_4(2) \rightarrow {}^3H_6(3) + {}^3H_5(3)$
2. $^3F_3(3') + {}^3H_4(3) \rightarrow {}^3H_6(3) + {}^3H_5(2)$
3. $^3F_3(2) + {}^3H_4(2') \rightarrow {}^3H_6(3) + {}^3H_5(2)$
4. $^3F_3(2) + {}^3H_4(1) \rightarrow {}^3H_6(2) + {}^3H_5(3)$
5. $^3F_3(1) + {}^3H_4(1) \rightarrow {}^3H_6(2) + {}^3H_5(1)$
6. $^3F_3(3') + {}^3H_4(1) \rightarrow {}^3H_6(2) + {}^3H_5(3')$

Table 4.4. Transition components in $Nd^{3+}:LaCl_3$ which produce energy matches within 3 cm^{-1}. The notation is that of Varsanyi and Dieke.[5]

$^4I_{13/2}(X) + {}^4I_{9/2}(Z) \rightarrow {}^4I_{11/2}(Y) + {}^4I_{11/2}(Y)$ Decay

1. $X_3 + Z_1 \rightarrow Y_3 + Y_1$
2. $X_5 + Z_1 \rightarrow Y_6 + Y_1$
3. $X_6 + Z_1 \rightarrow Y_3 + Y_2$
4. $X_2 + Z_2 \rightarrow Y_4 + Y_4$

$^4I_{15/2}(W) + {}^4I_{9/2}(Z) \rightarrow {}^4I_{13/2}(X) + {}^4I_{11/2}(Y)$ Decay

1. $W_2 + Z_1 \rightarrow X_1 + Y_2$
2. $W_3 + Z_1 \rightarrow X_1 + Y_6$
3. $W_1 + Z_2 \rightarrow X_1 + Y_5$
4. $W_1 + Z_2 \rightarrow X_4 + Y_1$
5. $W_1 + Z_2 \rightarrow X_2 + Y_2$
6. $W_2 + Z_2 \rightarrow X_4 + Y_4$
7. $W_2 + Z_2 \rightarrow X_5 + Y_3$
8. $W_2 + Z_2 \rightarrow X_7 + Y_1$
9. $W_3 + Z_2 \rightarrow X_7 + Y_3$
10. $W_1 + Z_3 \rightarrow X_1 + Y_6$

components, which match in energy to within a linewidth.† At elevated temperatures, when the required activation energy is available, one would expect such a decay to occur by resonant transfer involving the matched Stark components listed in Tables 4.3 and 4.4. The alternative (phonon-assisted transfer involving Stark components unmatched in energy) is a higher order process, and therefore probably has a slower rate.

Further, the two types of transfer (which we will call "R" for resonant and "N" for non-resonant) have different temperature dependences, which make it possible to distinguish between them experimentally. Asawa and Robinson[35] formulated the R process temperature dependence for the $^4F_{3/2} + {}^4I_{9/2} \rightarrow {}^4I_{15/2} + {}^4I_{15/2}$ decay in Nd^{3+}:LaF_3, and found that it agreed adequately with experiment. By a similar formulation, we will now attempt to establish that decays 1-4 in Table 4.2 occur by the R process. Having established this, it will then be possible to use the measured transfer rates to draw conclusions about energy migration (Sec. 4.3.2).

It should be noted that under the weak excitations used here, the crystals will generally be optically thin for absorptions

†Linewidths will be assumed throughout to be 3 cm^{-1}, a number based on data in Ref. 51.

from excited states, and stimulated emission will be negligible. Then, assuming concentration-independent spontaneous emission rates, radiative energy transfer will be incapable of explaining a decrease in a level's lifetime with increasing concentration. It is such decreases that will be dealt with in this study, hence a non-radiative transfer mechanism must be invoked.

We make the simplifying assumption that the probability per unit time, W(c), for an excited ion in a crystal of concentration c transferring its energy to a nearby ion is the same for each combination of quantum states for which an R process is energetically possible.† This ignores differences in oscillator strengths which, by Eq. (1.7), are responsible for differences in W(c). This simplification should not alter, however, the feature of the R temperature dependence which distinguishes it from the N temperature dependence, namely, saturation when kT approaches the activation energy.

We denote energies measured relative to the lowest Stark components in the various manifolds by the notation of Fig. 4.1.

Let us first consider the simple case in which there is only one combination of Stark components, namely $i_0' + i_0 \rightarrow f_0 + f_0'$,

† For each concentration c, there is a typical ionic separation which serves as the R in Eq. (1.7).

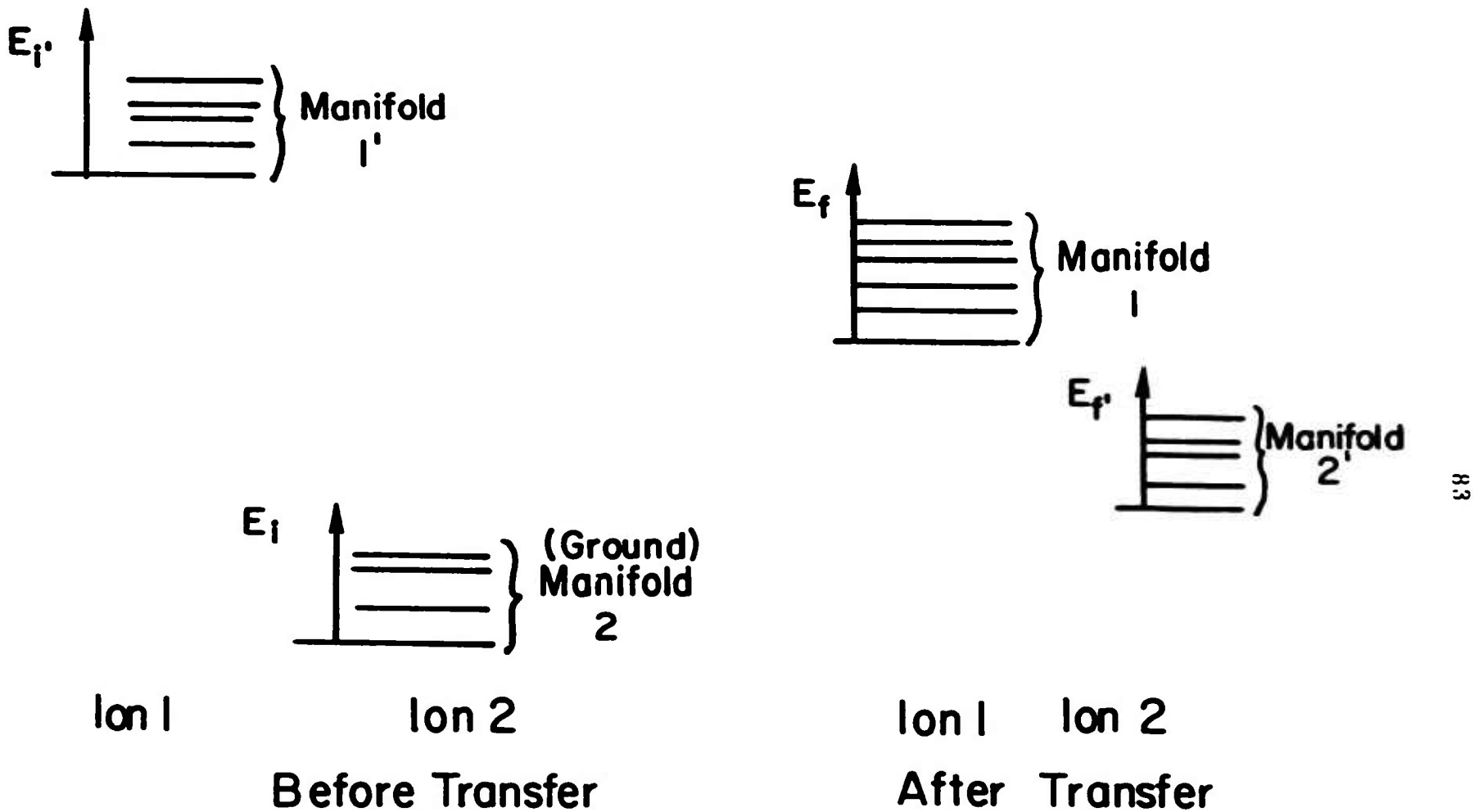

Fig. 4.1 Energy Level Notation

which match in energy for an R type transfer. Thermal equilibrium within a manifold is achieved in times $\sim 10^{-10}$ sec, which are short compared to energy transfer times. Hence the probability that an ion in manifold $1'$ will be in the Stark component i'_0 is†

$$\frac{g_{i'_0} \exp(-E_{i'_0}/kT)}{\sum_{\text{all } i'} g_{i'} \exp(-E_{i'}/kT)}$$

where $g_{i'}$ is the degeneracy of Stark component i'. We assume that the degree of excitation of the crystal is low enough that the probability of the near neighbors of ion 1 being in the ground manifold is essentially unity. Then the probability that a given near neighbor

†By summing only over the components of manifold $1'$ in the denominator, we are assuming negligible thermal population of higher J manifolds. The case in which this assumption is poorest, among the four cases to be dealt with, is $^3F_3$ in Pr^{3+}:$LaCl_3$. The center of gravity of the $^3F_4$ manifold is only about 470 cm^{-1} above the lowest component of $^3F_3$. Since the total degeneracies of the two manifolds are of the same order, at 300°K about exp(-470/200) $\sim$ 10% of the ions excited to $^3F_3$ will actually be in $^3F_4$ at any given moment. A 10% error is not significant in this calculation.

of ion 1 is in Stark component i_0 is

$$\frac{g_{i_0} \exp(-E_{i_0}/kT)}{\sum_{\text{all } i} g_i \exp(-E_i/kT)}$$

For a given initial quantum state of the ion pair involving Stark components i'_0 and i_0, there are $g_{f_0} g_{f'_0}$ final quantum states, so that the rate of transfer from the initial state will be $g_{f_0} g_{f'_0} W(c)$, by our previous assumption. Hence the rate of transfer from an arbitrarily selected ion in manifold i' will be

$$\left[\frac{g_{i'_0} \exp(-E_{i'_0}/kT)}{\sum_{\text{all } i'} g_{i'} \exp(-E_{i'}/kT)}\right]\left[\frac{g_{i_0} \exp(-E_{i_0}/kT)}{\sum_{\text{all } i} g_i \exp(-E_k/kT)}\right]\left[g_{f_0} g_{f'_0} W(c)\right]$$

If we now allow energy matches for other combinations besides $i'_0 + i_0 \rightarrow f_0 + f'_0$, we must form a term of the above type for each such combination, and sum the terms to obtain the observed transfer rate $W_{obs}(c, T)$:

$$W_{obs}(c,T) = \frac{\sum_{\substack{\text{resonant} \\ \text{combinations}}} g_{i'} g_i g_{f'} g_f \exp[-(E_{i'} + E_i)/kT]}{\left[\sum_{\text{all } i'} g_{i'} \exp(-E_{i'}/kT)\right]\left[\sum_{\text{all } i} g_i \exp(-E_i/kT)\right]} W(c)$$

$$= \xi(T)\, W(c) \quad , \qquad \text{(R process)} \qquad (4.1)$$

Since ion-pair decays are non-exponential, the observed transfer rate $W_{obs}(c,T)$ will be determined from the "1/e" lifetime, τ_e, defined in Sec. 3.1. The reason[65] for the non-exponentiality will be described in Sec. 4.3.2.

The temperature dependence of the N process is somewhat simpler. We assume that the transfer in this case occurs between ions in the heavily populated ground components of the 1' and 2 manifolds, with the absorption of a single phonon whose energy equals the activation energy (E_a). If we neglect thermal depopulation of the ground components, the transfer rate will be proportional to the occupation number of a phonon mode of energy E_a:

$$W_{obs}(T) \propto \left[\exp(E_a/kT) - 1\right]^{-1} . \qquad \text{(N process)} \qquad (4.2)$$

Table 4.5. Temperature Dependence Factors. [See Eqs. (4.1), (4.2)]

Decaying Level	ξ (T)		$\exp(E_a/kT) - 1$	
	77^oK	300^oK	77^oK	300^oK
Pr $^3H_6$	1.5	3.6	1.2	.23
Pr $^3F_3$	.42	1.1	4.1	.52
Nd $^4I_{13/2}(X)$	1.6	1.3	.34	.079
Nd $^4I_{15/2}(W)$	4.3	5.2	.98	.192

Table 4.6. Theoretical and experimental transfer rate ratios. The middle columns are computed from Table 4.5. The experimental values of W_{obs} were obtained from lifetimes measured in the 2% Pr^{3+}:$LaCl_3$ and 1% Nd^{3+}:$LaCl_3$ samples. Radiative and phonon decay rates are negligible in each case, hence W_{obs} is simply the reciprocal of the observed lifetime.

Decaying Level	Theoretical, R Process $\frac{\xi\ (300^oK)}{\xi\ (77^oK)}$	Theoretical, N Process $\frac{\left[\exp[E_a/k(300^o)] - 1\right]^{-1}}{\left[\exp[E_a/k(77^o)] - 1\right]^{-1}}$	Experimental $\frac{W_{obs}(300^oK)}{W_{obs}(77^oK)}$
Pr $^3H_6$	2.4	5.2	1.0 ± 0.5
Pr $^3F_3$	2.6	7.9	1.2 (>0.4, <3.0)
Nd $^4I_{13/2}(X)$	.81	4.3	0.6 ± 0.3
Nd $^4I_{15/2}(W)$	1.2	5.1	1.7 ± 0.8

Using the known energies and degeneracies of the Stark components (see References in Sec. 1.1), the quantity $\xi(T)$ in Eq. (4.1) can be calculated for the cases in question. These values are listed in Table 4.5, along with the values of the N process factor from Eq. (4.2).

The Table 4.5 values are then used to compute theoretical rate ratios for the R and N processes. The experimental ratios are seen in Table 4.6 to be in reasonable agreement with the R process ratios, but in definite disagreement with the N process ratios. This is not surprising, in view of the fact that the N process, involving a phonon, is a higher order process. Based on evidence in Table 4.6, we henceforth assume that these four examples of energy transfer occur by the R process.

4.3.2 Migration to Sinks

As pointed out in Sec. 4.3.1, concentration quenching was observed even for levels whose energy could not be degraded by the interaction of the dopant ions alone. (The lowest excited level is always such an example.) Such concentration quenching can be explained[23] by a succession of transfers of the energy, from one dopant ion to another, until a sink is reached which is capable of dissipating the energy. A quantum of excitation which is not localized at a single site throughout its lifetime is called an "exciton." If, as

is the case here, the excited electron itself remains tightly bound to a single ion, the exciton is of the Frenkel (as opposed to the Wannier) variety.

If, despite the tightly bound electrons, the excitation energy is spread uniformly through the crystal, the exciton is characterized by a $\vec{K}$ (momentum) vector. In the case of rare earth salts, both the electron and the electronic excitation are localized on one ion for times long compared to vibrational periods. The excitation executes a random walk as it is transferred from one ion to another. Each step of the walk requires a time long compared to a vibrational period, but, in many cases, short compared to the radiative lifetime. The $\vec{K}$ vector of such an exciton undergoes random changes in direction as the exciton is elastically "scattered" during each step of the migration.[66]

On the basis of rate calculations and fluorescence measurements, Imbusch[50] concluded that the enhancement of the N lines at the expense of the R lines in ~ 1% Cr^{3+}:Al_2O_3 resulted from non-radiative migration of excitation to coupled ion pairs, which in this case served as the sinks.

Van Uitert and co-workers[39] have presented the concentration dependence of the quenching of fluorescence from certain levels in doubly-doped tungstates as evidence of migration,

with a known RE^{3+} ion serving as the sink in each case.

Pearson and Peterson[67] gave a very direct and convincing demonstration of this decay mode when they excited fluorescence of a Eu^{3+} impurity (believed to be present at a level of 50 to 300 ppm in the dopant starting material) by pumping Gd^{3+} in Calibo-1 glass doped with 10% Gd_2O_3. The disappearance of Eu^{3+} fluorescence at 2.5% Gd_2O_3 concentration correlated with an increase in the lifetime of the metastable $^6P_{7/2}$ level of Gd^{3+}. At 10% concentration, the $^6P_{7/2}$ lifetime was found to be longer when higher purity Gd_2O_3 was used.† The quenched $^6P_{7/2}$ Gd^{3+} level was found to decay exponentially, a feature characteristic of migration (the reason for this will be discussed later in this section). All of these observations pointed conclusively to the decay of the Gd^{3+} $^6P_{7/2}$ level by migration of the excitation to a Eu^{3+} impurity sink.

Weller, Gandy, and Ginther[46] found that the presence of .05% Fe^{2+} in glass reduced the lifetimes of fluorescing levels of Nd^{3+}, Yb^{3+}, Ho^{3+}, Er^{3+}, and Tm^{3+} (in 3×10^{20} cm^{-3} conc.) of the order of a factor of two, an effect attributed to migration of the energy to Fe^{2+} ions. Since iron is a common impurity in rare earth salts (see Table 2.1), Fe^{2+} may be an important sink for migration quenching.

†The actual Eu^{3+} content of the Gd_2O_3 batches was not determined.

Since a single transfer in the migration process produces no change that can be observed with laboratory instruments, no attempts at measuring the time required for this single transfer have been reported. One possible method that comes to mind is to measure the distance r_0 between the initial and final positions of the excitation during its lifetime. The difficulty of such a measurement can be seen by making a liberal estimate of the magnitude of r_0. If a single transfer, covering a distance of 5 Å, occurs in 10^{-10} sec, a random walk during a 10 msec lifetime will produce a most probable displacement of[†]

$$r_0 = \sqrt{\frac{8}{3\pi}}\,(5\ \text{Å})\,\sqrt{(10^{10}\ \text{sec}^{-1})\,(10^{-2}\ \text{sec})} \cong .005\ \text{mm} .$$

However, an order of magnitude estimate of the time for a single transfer in the migration process can be made by measuring the time required for a process which, although similar in other respects, <u>does</u> produce an observable effect. It was demonstrated

[†]Eq. (87) in Ref. 68 gives the probability, W(r), that the displacement will fall between r and r + dr. The most probable displacement is then

$$r_o = \int_0^\infty rW(r)\,(4\,\pi\,r^2\,dr) = \ell\sqrt{\frac{8N}{3\pi}}$$

in Sec. 4.3.1 that at temperatures $\lesssim 77^{0}$K, decays 1-4 in Table 4.2 are just such processes, i.e., they involve resonant transfer (no phonon assistance) between like ions, and produce an observable effect by depopulating a level whose lifetime can be measured. Hence the measured decay rates for levels $^{3}H_{6}$ (Pr), $^{3}F_{3}$ (Pr), X(Nd), and W(Nd), when modified to account for the degree of thermal population, should be of the same order of magnitude as the single transfer time in the migration process.

In Sec. 4.3.1, we assumed that each combination of quantum states with an energy match for transfer has a transfer rate W(c). The result (Eq. 4.1) was that the observed transfer rate, $W_{obs}(c,T)$, was the product of W(c) and a quantity $\xi(T)$ which represented the effective number of resonant combinations which were active at temperature T.

For the single transfer in the migration process, all of the energy of one ion is transferred to an identical[69] ion, raising it to the Stark component that the first ion initially occupied. This basic step of the migration process occurs resonantly regardless of which Stark component is initially occupied, hence the transfer rate should be roughly independent of temperature. That is to say, the factor $\xi(T)$ (Eq. 4.1) for the single transfer of the migration process, unlike the single-transfer decay, should have little variation

with temperature. It should, in fact, equal the number of final states, $g_{f'}$ g_f, which is typically ~ 4, since two is the most commonly encountered degeneracy in C_{3h} symmetry (always encountered for Kramers ions). Thus if an excitation makes n transfers before being dissipated at a sink, we expect that order of magnitude accuracy may be maintained by writing the rate of quenching by migration as

$$W_M(c) \cong \frac{4\ W\ (c)}{n} \qquad (4.3)$$

As pointed out in connection with Eq. 4.1, W(c) varies from one transition to another because of differences in oscillator strengths. In fact, the rms deviation of log f about the median value, for 18 f numbers randomly picked from Varsanyi and Dieke's tables,[14] was 0.8, implying a factor of 6 variation in f itself. Since W(c) is proportional to the product of two f numbers, it should have a greater variation; on the other hand, there are usually a number of combinations (see, e.g., Tables 4.3, 4.4) capable of producing transfer, and this tends to reduce fluctuations of observed rates from case to case. Thus we might anticipate order of magnitude accuracy if we take W(c) to be the same for all

resonant combinations in all RE^{3+} ions in $LaCl_3$ and YCl_3.† Dividing Eq. (4.1) by Eq. (4.3) then gives the ratio of the observed single ion pair decay rate to the decay rate for migration to a sink:

$$\frac{W_{obs}(c,T)}{W_M(c)} = \frac{n\,\xi\,(T)}{4} \quad . \tag{4.4}$$

If we now define a temperature-independent single transfer rate by

$$W_S(c) \equiv \frac{4}{\xi\,(T)}\, W_{obs}(c,T) \quad , \tag{4.5}$$

then Eq. (4.4) becomes

$$W_S(c) = nW_M(c) \quad . \tag{4.6}$$

To obtain experimental values of W_S and W_M, it is necessary to ascertain which levels are quenched by which mechanisms. Inspection of the energy level diagram will tell whether a single ion can take up a portion of the level's energy, thus de-exciting it (S process). If one or two dopant ions cannot de-excite the level, then any

†Since Er^{3+} does not enter $LaCl_3$ in amounts $\gtrsim$ 5%, YCl_3 was used as a host for this ion. Er^{3+}:YCl_3 energy levels are given in Ref. 64. It should be remembered (Sec. 4.1) that oscillator strengths in YCl_3 are generally about a factor of 5 smaller than in $LaCl_3$.

observed concentration quenching must be due to migration to sinks (M process).

Multiphonon relaxation is known from Figs. 1.2 and 1.3 and the accompanying discussion to be negligible (below 100°K) for all levels used in obtaining W_S and W_M data. Radiative rates generally are not negligible, but were obtained by taking the reciprocal of the lifetime extrapolated to zero concentration. This radiative rate was assumed to be independent of concentration, and subtracted from the reciprocal of the measured lifetime at the higher concentrations to obtain the quantities $W_M(c)$ (for M decays) and $W_{obs}(c, T)$ (for S decays). For the S decays, $\xi(T)$ was computed (Table 4.5), and $W_S(c)$ then obtained from $W_{obs}(c, T)$ using Eq. (4.5). The quantities W_S and W_M are plotted as a function of concentration in Fig. 4.2. The fact that the slopes of (a) and (b) in Fig. 4.2 are the same indicates that n (Eq. 4.6) is independent of concentration. This is probably a result of the fact that all samples used in obtaining the Fig. 4.2(b) data were grown from 99.9% pure dopant oxide and 99.999% pure host oxide. Thus in concentrations greater than 1%, most of the impurities should come from the dopant oxide, in which case the ratio of dopant ions to impurity ions (sinks) should be independent of concentration. It is this ratio which determines n. The value of n can be obtained by dividing W_S by W_M at any given

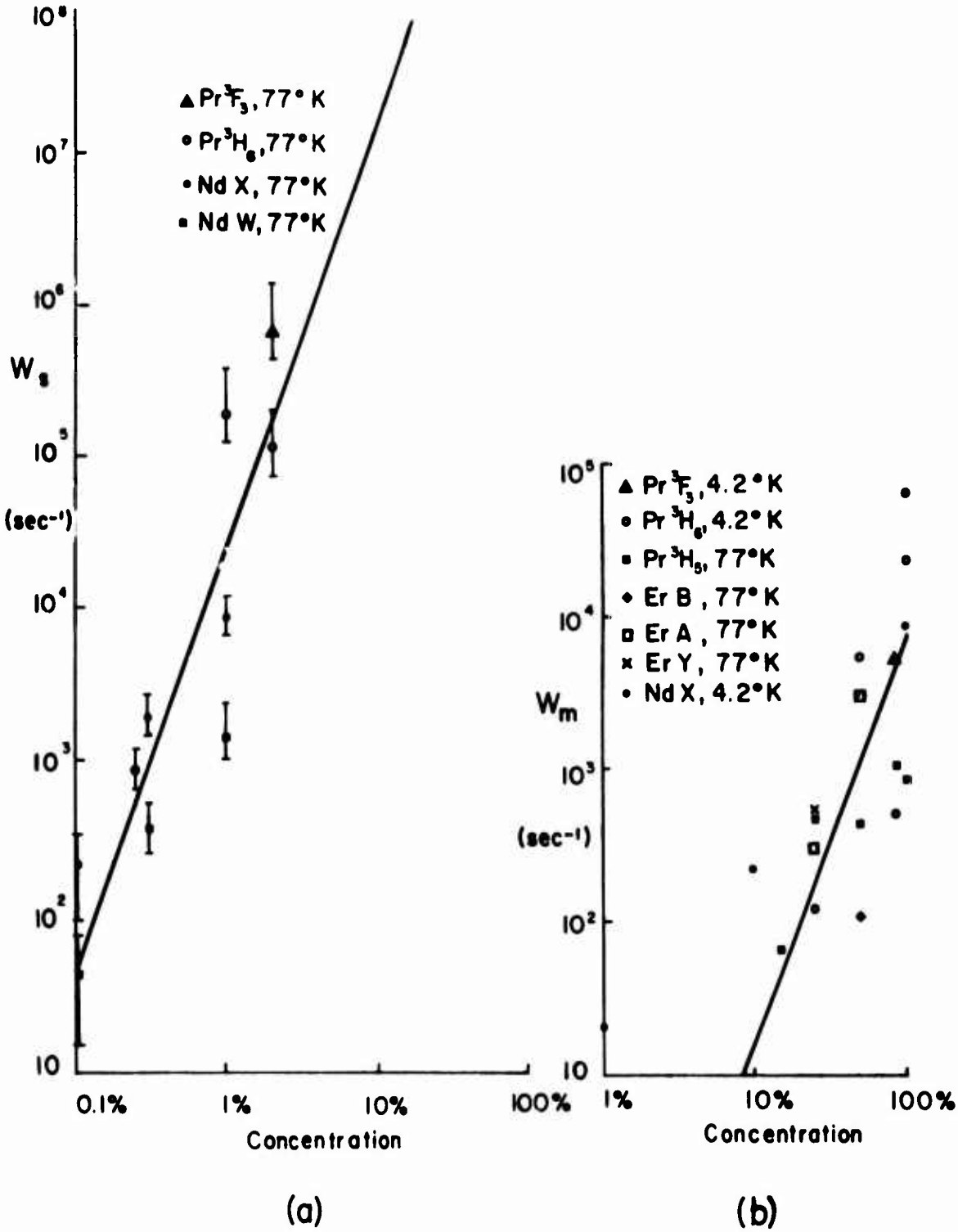

Fig. 4.2 Quenching rates for (a) single transfer and (b) migration decay. Experimental error is indicated in (a).

concentration in Fig. 4.2. The result is:

$$n \sim 4 \times 10^5 \quad . \tag{4.7}$$

Without knowing how the ion-ion transfer rate compares to the ion-sink transfer rate, no conclusions regarding the ratio of the number of sinks to the number of dopant ions in the sample can be drawn from the fact that $n \sim 4 \times 10^5$. The ion-sink transfer rate depends on which impurity serves as a sink, and it may be a different one for each of the seven levels listed in Fig. 4.2(b).

In addition to the possibility of Fe^{2+} serving as a sink (as mentioned earlier in this Section), unwanted lanthanide rare earths are common impurities in these crystals (see Table 2.1). Any rare earth ion with energy levels below 4000 cm^{-1} which are sufficiently closely spaced to be rapidly depopulated by multiphonon relaxation is a likely candidate for a sink. Sm^{2+}, Sm^{3+}, and Eu^{3+} are such ions, and with the absorption or emission of one phonon, most rare earth levels could be depopulated by energy transfer to one of the Sm^{2+}, Sm^{3+}, or Eu^{3+} levels.

If the sinks responsible for the quenching in Fig. 4.2(b) are really impurities, one would expect that this quenching rate, W_M, would be lower for samples grown with higher purity starting materials. This is indeed the case, as is seen from Fig. 4.3, which is a plot of the $^3H_6$ data from Table 3.4. Although all of the samples were grown by the same person, the scatter in the points may result from the fact that they were grown at different times over a period of five years.

It is interesting to note that for concentrations $\gtrsim$ 50%, migration quenched levels will have lifetimes which are no longer determined simply by concentration and temperature. Crystal purity, a parameter which is more difficult to specify, must also be given. This situation has been encountered in molecular crystals, where lifetimes of some of the long-lived triplet states have been found to depend on purity.[70]

Taking $W_S(c)$ from Fig. 4.2(a) to be the rate at concentration c for a single transfer in the migration process, then the number of transfers that will occur during the lifetime τ of an excited level will be $\tau W_S(c)$. This result is used to construct Fig. 4.4, which attempts to provide an answer to how extensive, on the average, energy migration is in these crystals.

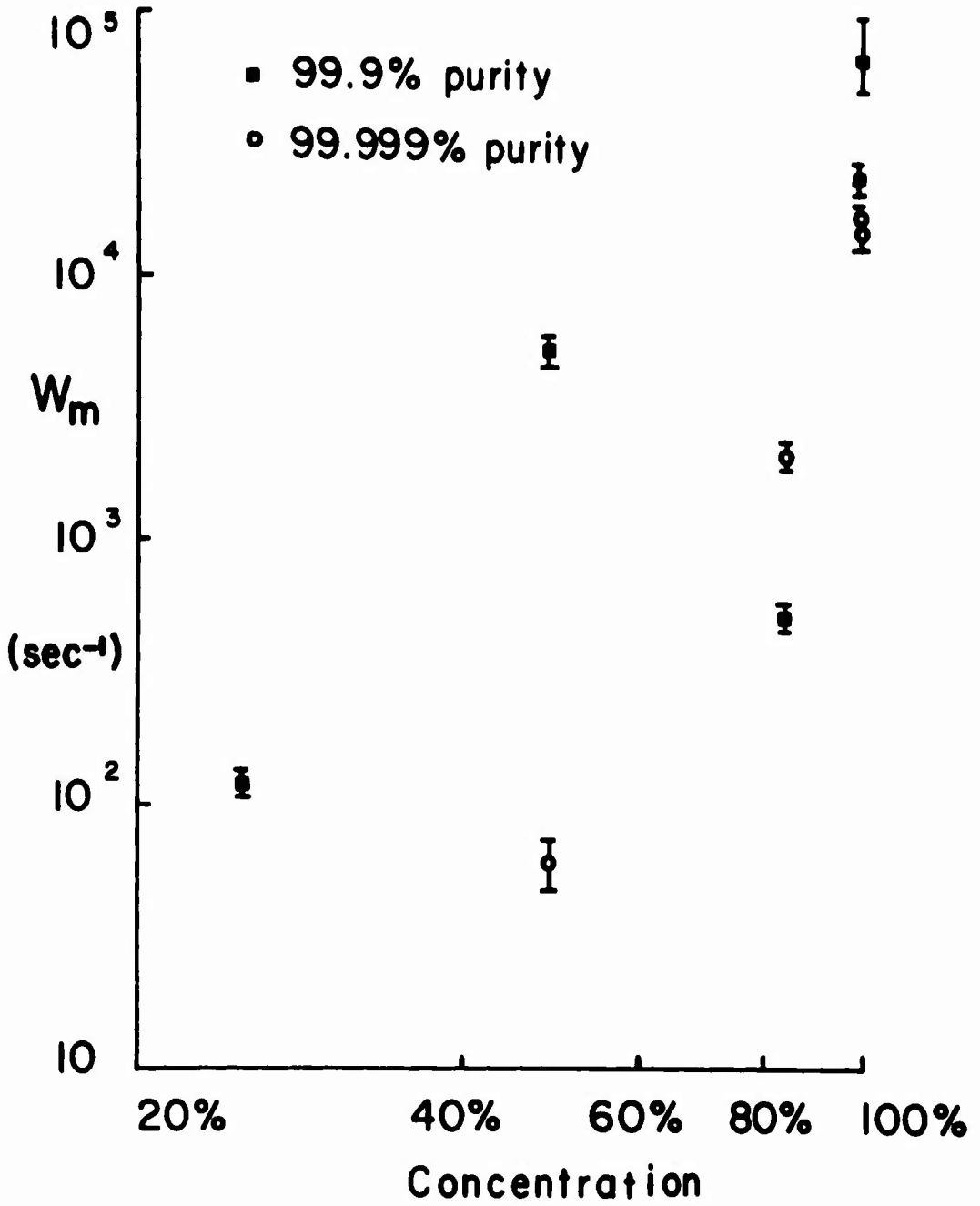

Fig. 4.3 Correlation between sink-terminated quenching rate (W_M) and starting material purity. All points are for the decay of $^3H_6$ in Pr^{3+}:$LaCl_3$ at 4.2 K. Host oxide purity was always 99.999%; dopant oxide purity was as indicated.

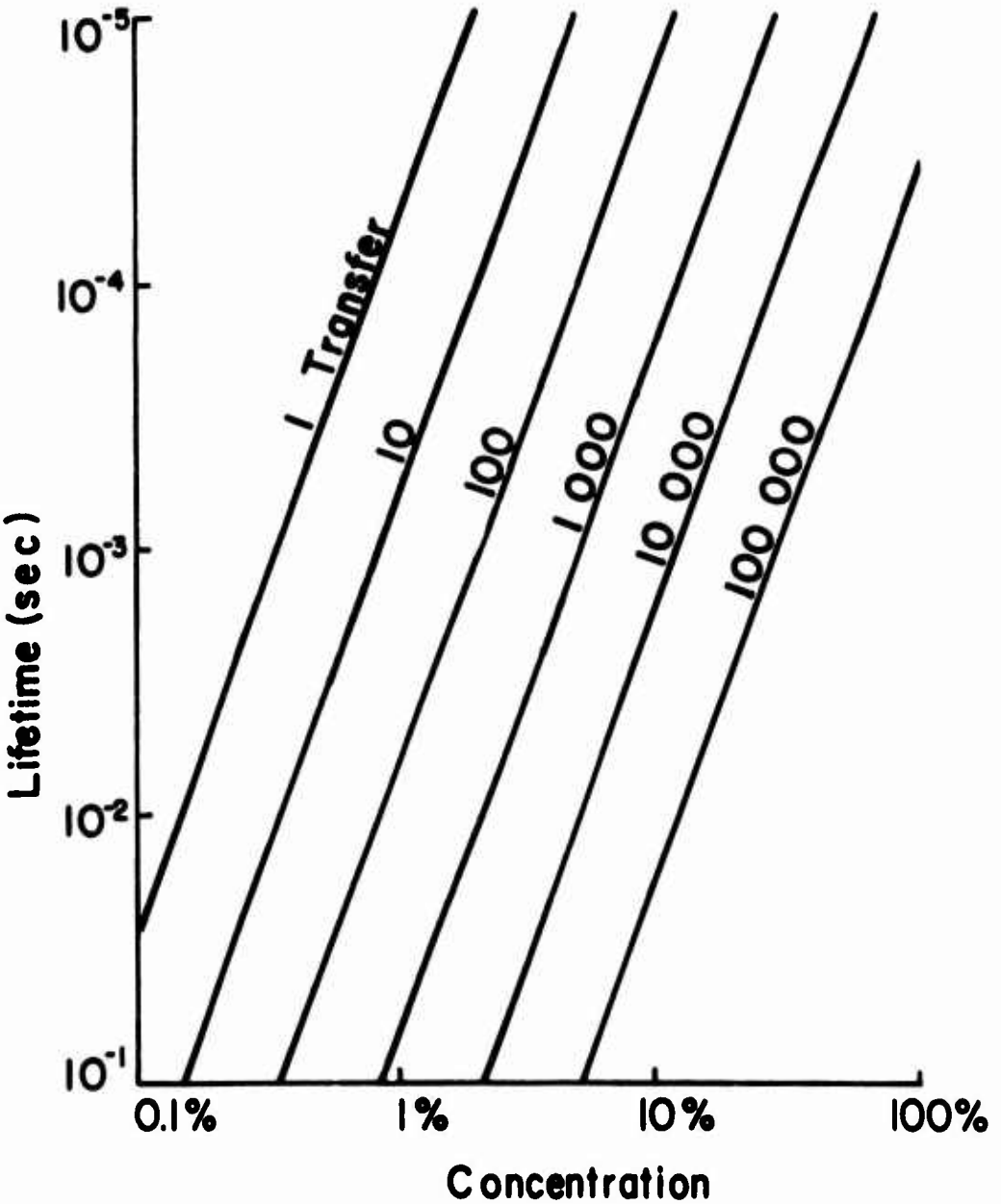

Fig. 4.4 Approximate number of transfers to be expected in the migration process in RE^{3+}:$LaCl_3$. The lifetime may be determined by any decay mode.[3] The figure is constructed by assuming that the rate for a single transfer is given by the solid line in Fig. 4.2(a).

S process decays are known to be non-exponential.[39,50] The theoretical time-dependence has been worked out for several types of ion-ion interaction by Inokuti and Hirayama.[65] The random placing of dopant ions in the available cation sites means that ion-ion spacings will vary, resulting in the observed decay being a sum of many exponentials with different time constants. This non-exponentiality was found in the S processes in this study whose decay waveforms were obtained (Table 3.1 and Fig. 3.1).

For an M process, however, the excitation resides on a large number of sites during its lifetime, and variations in transfer time from site to site are averaged out. The result, as found by others[39,67] and confirmed here (Table 3.2), is that levels quenched by the M process decay exponentially. This provides a convenient means of checking one's conjecture as to whether a given concentration quenching is due to the S or M process.

It was pointed out earlier in this section that the dopant ion-to-dopant ion transfer in the migration process should have very little temperature dependence. Thus, if the dopant ion-to-sink transfer occupies only a small fraction of the quenched level's lifetime (as is the case when $\sim 10^5$ transfers occur before the energy is quenched), one would expect that the quenched level's lifetime itself would be almost independent of temperature. This has been

found generally to be the case in this study.† Lifetimes of migration-quenched $Er^{3+}:YCl_3$ levels Y and A, for example, vary relatively little from 4.2°K to 300°K. Temperature-dependent migration rates have been observed by others,[69,71] and the reason for the thermal dependence is not clear.

4.3.3 Exciton-Exciton Annihilation

In Sections 1.2.3 and 4.3.1, the theory and observation of energy degradation by the interaction of ion pairs was presented. In the reverse process, two excited ions combine their energy to populate an electronic level which could not be reached simply by the absorption of exciting light. Under normal CW excitation conditions, the vast majority of ions in a crystal will be in the ground state, and hence migrating excitation (excitons) will enhance the rate for interaction between excited ions. We call this energy summation process "exciton-exciton annihilation," a name sometimes used to describe the analogous process in molecular crystals whereby two triplet excitons combine their energy to populate a higher (singlet) state, or generate a free charge carrier.[72]

†In some cases (e.g., Pr $^3H_6$), migration quenches the level at 4.2°K, but gives way to the temperature dependent S decay mechanism at higher temperatures.

Three examples of exciton-exciton annihilation have been reported for rare earth ions, to which we add a fourth (Table 4.7).

Table 4.7. Rare earth exciton-exciton annihilation observed to date.

	Ion	Host(s)	Process	Reference
(1)	Er^{3+}	Alkaline Earth Fluorides	$^4I_{11/2} + {}^4I_{11/2} \rightarrow {}^4F_{7/2} + {}^4I_{15/2}$	Ovsyankin and Feofilov[73,74]
(2)	Er^{3+}	Silicate Glass	$^4I_{13/2} + {}^4I_{11/2} \rightarrow {}^4F_{9/2} + {}^4I_{15/2}$	Woodward, Williams, and Brown[75]
(3)	Er^{3+}	SrF_2	$^4I_{13/2} + {}^4I_{13/2} \rightarrow {}^4I_{9/2} + {}^4I_{15/2}$	Brown and Shand[76]
(4)	Nd^{3+}	100% $NdCl_3$	$^4I_{15/2}(W) + {}^4I_{15/2}(W) \rightarrow {}^4F_{3/2}(R) + {}^4I_{9/2}(Z)$	Present Study

Process (4) in Table 4.7 was observed at 4.2°K by populating the Nd^{3+} level $^4I_{15/2}(W)$ with a tungsten-iodine lamp and .25m monochromator, and observing $^4F_{3/2}(R) \rightarrow {}^4I_{11/2}(Y)$ fluorescence with an S-1 photomultiplier. In 100% $NdCl_3$, the low temperature lifetime[15] of level R is $\sim 200\ \mu$sec, whereas τ_W at 4.2°K is 4.7 msec (Table 3.3). Since $\tau_W >> \tau_R$, observing the decay of the R fluorescence when the $Z \rightarrow W$ pump is suddenly blocked (by a chopper) determines whether R is populated by the two-step $Z \rightarrow W \rightarrow R$ absorption or $Z \rightarrow W$ absorption only, followed by exciton-exciton annihilation. In the former case, the time constant of the R decay would be $\sim \tau_R$, whereas in the latter case it would be $\sim \tau_W$. It was found to be $\sim \tau_W$, indicating that the annihilation was the dominant means of populating the R level. Ovsyankin and Feofilov[73] applied this same test to process (1) in Table 4.7, with the same result.

Using a quantum efficiency measurement procedure which was identical in principle to that described by Partlow and Moos,[15] it was found that the fraction of ions in level W which reached level R in process (4), Table 4.7, was 6×10^{-4}. This procedure consisted of measuring with a PbS cell with calibrated spectral response the relative amount of excitation energy absorbed under the $Z \rightarrow W$ and $Z \rightarrow R$ pumps, then measuring the relative $R \rightarrow Y$ fluorescence intensities under the $Z \rightarrow W$ and $Z \rightarrow R$ pumps.

The fact that the W → R quantum efficiency is only 6×10^{-4}, despite the 100% concentration, is undoubtedly due in part to the fact that twice the energy of the lowest Stark component of W is 284 cm^{-1} greater than the energy of the highest Stark component of R. This means that at 4.2°K, at least two phonons must be emitted to conserve energy in the W + W → R + Z annihilation., thus reducing the process's probability.

Since $6 \times 10^{-4} << 1$, the annihilation process is not a major factor in determining the lifetime of level W, at the Z → W pump strength used here. The reduction of the W lifetime in 100% concentration from the radiative value (Table 3.3) is probably due to migration to sinks. In any case, the extrapolated value of $W_S \sim 7 \times 10^9$ sec^{-1} at 100% concentration in Fig. 4.2(a) indicates that extensive migration of the W excitation should occur during the 4.7 msec lifetime, hence the appropriateness of the term "exciton-exciton annihilation".

The R → Y fluorescence intensity was found to be proportional to the power 3.2±0.2 of the Z → W pump intensity. Hence the W → R quantum efficiency could undoubtedly be made much greater than 6×10^{-4} by more efficient pumping (replacing the .25m monochromator with an interference filter, for example).

Ovsyankin and Feofilov[73] suggest that many of the IRQC schemes reported to date may actually involve ground state absorptions by two ions, followed by exciton-exciton annihilation, rather than two-step absorption by ions acting independently. To guard against the possibility of misinterpreting the process, the visible excitation for each scheme used in this study for lifetime measurement was examined by scanning in wavelength the monochromator in the visible beam, and observing the IRQC signal with the IR source on. For every scheme examined (~25 in all) in every crystal used (~40 in all), the output peaked sharply at a wavelength of the visible beam corresponding to absorption from an excited state, and not from the ground state. It thus appears unlikely that a large percentage of presently known IRQC schemes have been misinterpreted in this respect.

5. THE IRQC AS AN INFRARED DETECTOR

5.1 REVIEW OF IRQC DEVELOPMENT

In Sec. 2.1, the device (IRQC) which was used to obtain most of the lifetimes in this study was described. The IRQC was originally proposed, not for the measurement of lifetimes, but for the detection of infrared radiation. The reasoning behind the proposal[77] can be understood by referring to Fig. 2.2(a). If the crystal is cooled to an arbitrarily low temperature, the thermal population of level 1 can be made arbitrarily low. Thus the population of level 2 induced in the absence of an infrared signal by the intense visible pump at ν_{12} can be made arbitrarily small. Hence it should be possible to reduce the background fluorescence at ν_{20} to an arbitrarily low intensity, without adversely affecting the internal quantum efficiency of the device, simply by reducing the crystal's temperature to an arbitrarily low value.

This argument will be examined more carefully in Sec. 5.3. For the present, we simply note that no IRQC has yet been devised which is competitive in signal-to-noise with existing broadband semiconductor detectors in the same wavelength range. The measure of the smallest signal whose detection is permitted by noise is the Noise Equivalent Power (NEP), defined as the signal power incident on the detector which gives an output equal to the rms noise in a bandwidth

Table 5.1. IRQC NEP's Reported to Date

	Crystal	Scheme	Xtal Temp	NEP [watts(c/s)$^{-1/2}$]	Reference
(1)	1% Pr^{3+}:$LaCl_3$	Fig. 5.1(a)	4.2°K	2×10^{-5}	Porter[78]
(2)	1% Er^{3+}:SrF_2	Z-Y-D-Z	300°	3×10^{-8}	Brown et al[79]
(3)	15% Pr^{3+}:$LaCl_3$	Fig. 5.1(a)	4.2°	3×10^{-9}	Gandrud and Moos[80]
(4)	2% Tm^{3+}:$LaCl_3$	Fig. 5.1(b)	4.2°	2×10^{-7}	"
(5)	2% Tm^{3+}:$LaCl_3$	Fig. 5.1(b)	300°	3×10^{-7}	"

$\Delta\nu$, divided by $(\Delta\nu)^{1/2}$. Table 5.1 lists NEP's that have been obtained to date by IRQC's. For comparison purposes, a typical PbS detector of 5 mm^2 area, operated at $-56^{o}C$, has an NEP at 2.0 μ of $\sim 5 \times 10^{-12}$ watts$(c/s)^{-1/2}$.

Although investigation of IRQC device characteristics was not the purpose of this work, RE^{3+}:$LaCl_3$ has good potential as an IRQC material by virtue of its shallow phonon spectrum (260 cm^{-1} cutoff) and bright fluorescences, and it became apparent while measuring lifetimes for Table 3.3 that the strongest RE^{3+}:$LaCl_3$ schemes were giving NEP's which were low enough to warrant measuring. These measurements are described in the next section.

Reference to other experimental IRQC papers not mentioned here are given by Esterowitz et al.[81]

5.2 MEASUREMENT OF DEVICE CHARACTERISTICS

The best NEP in Table 5.1 [3×10^{-9} watts$(c/s)^{-1/2}$] was obtained with the scheme of Fig. 5.1(a), using the experimental arrangement shown in Fig. 5.2. Both IR and visible sources were 625 watt $3400^{o}K$ tungsten-iodine filament lamps. An EMI 9558 photomultiplier, cooled to dry ice temperature, viewed the crystal through four Corning 4-96 filters and a 4900 Å interference filter.

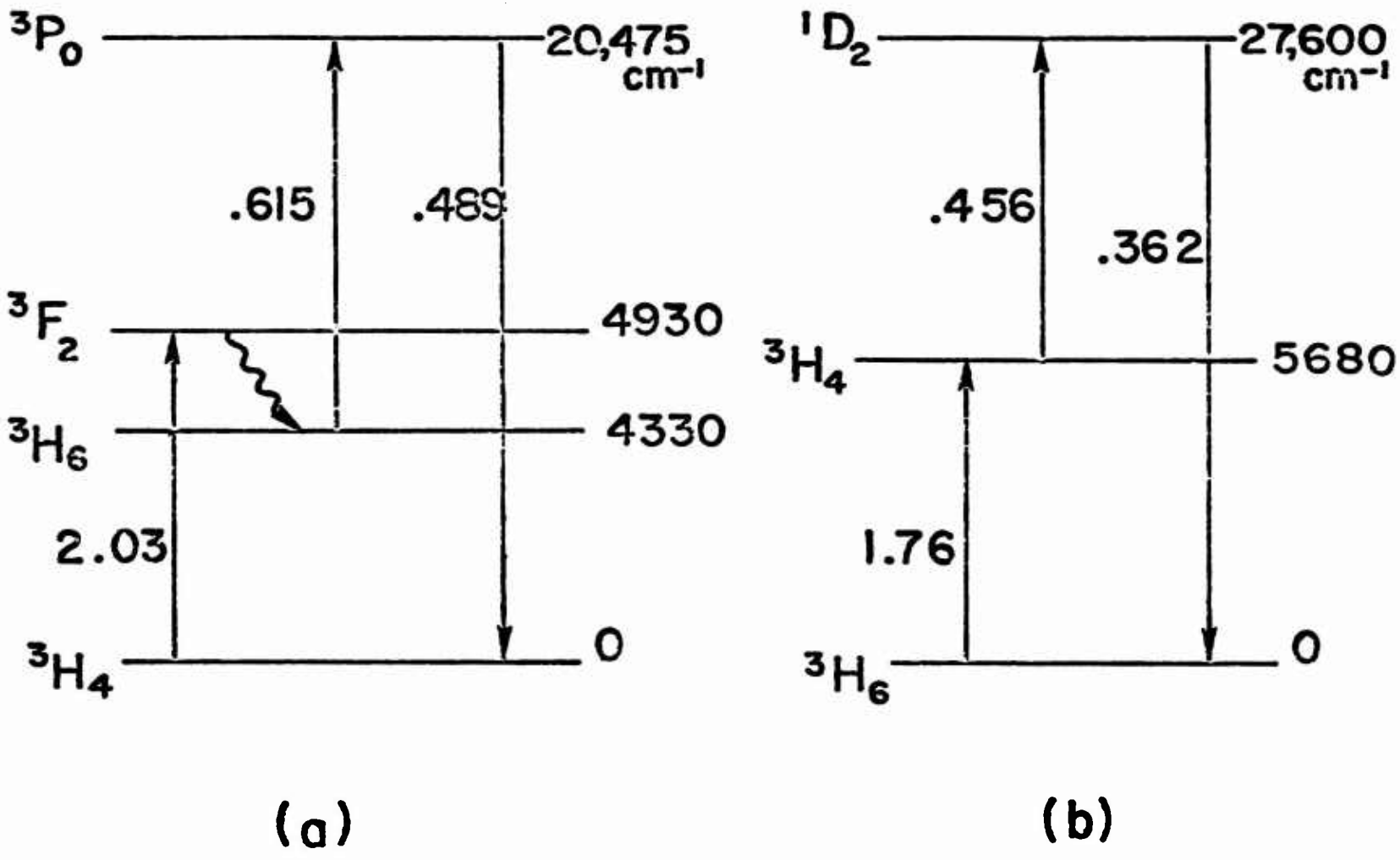

Fig. 5.1 IRQC Schemes for NEP Measurements in Table 5.1. Wavelengths in μ.

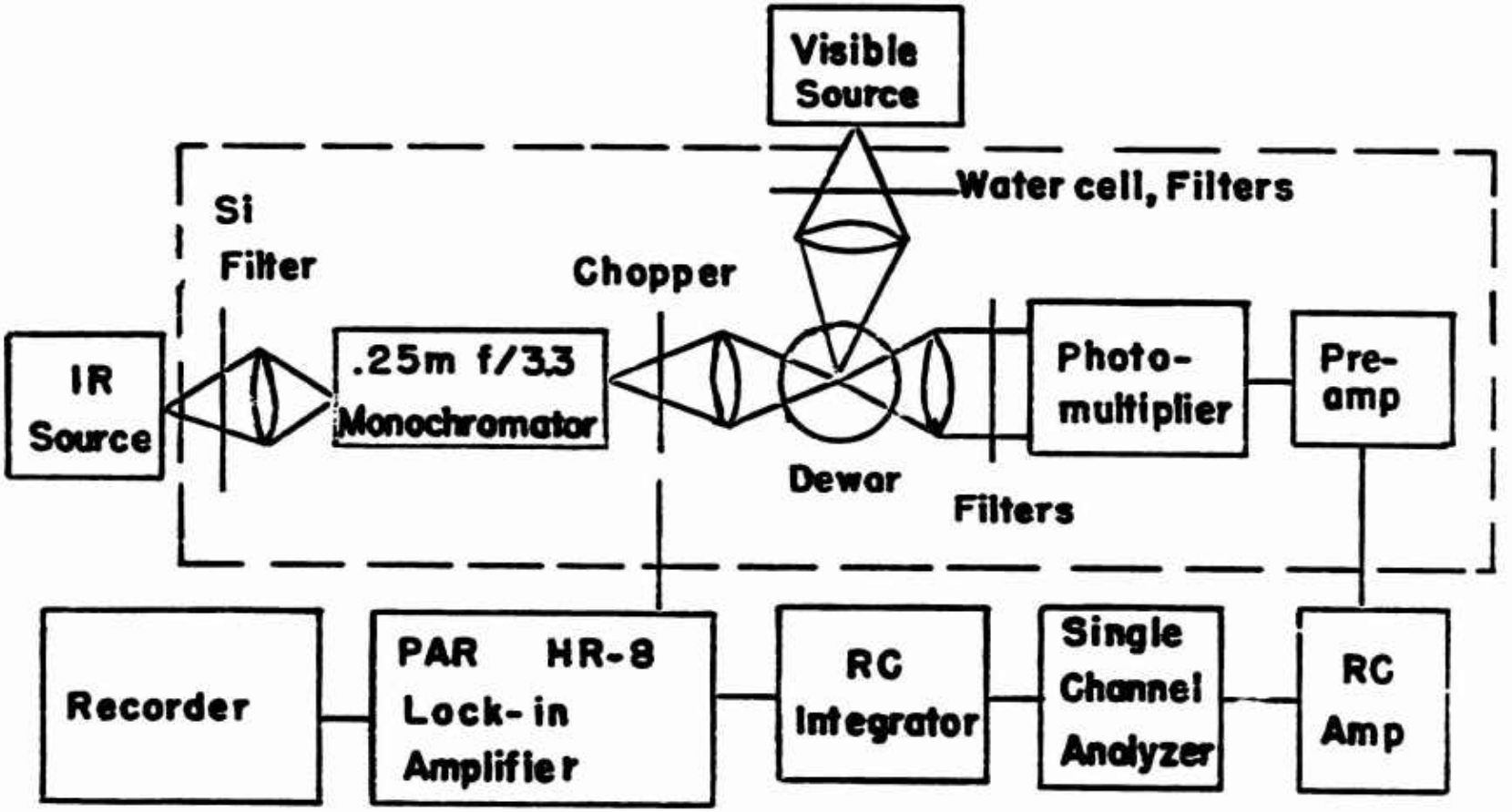

Fig. 5.2 Experimental Arrangement for NEP Measurement. Items Within the Dashed Rectangle Were Enclosed in a Light-tight Box.

A Corning 2-62 and a 6150 Å interference filter in the visible beam prevented any excitation from the ground state by this beam. Additional attenuation of wavelengths greater than 1.3 μ (some of which would be capable of populating the $^3H_6$ level) was provided by a 2 cm thick cell of circulating water. This cell was also found to be necessary to prevent breakage of the glass filters from excessive heating. The filters were situated between the water cell and the crystal, hence the 6150 Å filter had to be oriented so that the dielectric coating was facing the crystal, thus blocking infrared filter fluorescence,[60,61] which would also be capable of populating the $^3H_6$ level. The mechanical chopper (Sec. 2.4) was operated at 10 cps.

The power from the IR beam incident on the crystal was measured by replacing the crystal and dewar with a Reeder RBL 500 thermopile. The thermopile was calibrated both before and after the NEP measurements, using a tungsten ribbon standard lamp that had been calibrated by the National Bureau of Standards in 1965. The NEP measurements were found to be repeatable to within the estimated probable error of a factor of two.

For the Tm^{3+}:$LaCl_3$ measurements in Table 5.1, an A-H6 mercury lamp served as the visible source, with the water cell and filters replaced by a 0.5 m f/4.4 monochromator with a 100 Å

bandpass, and a Corning 3-73 at the exit slit. Two 7-60's and a 4-97 were used before the photomultiplier.

The factor of 7×10^3 improvement of value (3) over value (1) in Table 5.1 stems mostly from the replacement of monochromators by filters in the visible beam and before the photomultiplier. Additional small improvements resulted from the increased concentration† of Pr^{3+}, cooling the photomultiplier, and the use of pulse shaping and discrimination. In addition, a factor ~ 25 improvement in the NEP value resulted from using an 18 cm^{-1} bandpass monochromator in the IR beam instead of the 500 cm^{-1} bandpass interference filter used in obtaining (1) in Table 5.1. Most of the radiation seen by the thermopile when looking through the interference filter is not in the 10 cm^{-1} absorption linewidth of the IRQC crystal, hence the measured NEP becomes more indicative of the IRQC performance as the bandpass in the IR beam is narrowed down to 10 cm^{-1}.

With the visible source on and the IR source off in Fig. 5.2, the photomultiplier registered a count rate for 15% $Pr^{3+}:LaCl_3$ of 4000 photoelectrons/sec, which is 300 times greater than the dark current. By inserting test filters, this background was found to be

†15% was found to be optimum; at higher concentration, the reduction in the $^3H_6$ lifetime by migration to sinks offset the advantage of greater infrared absorption.

induced in the crystal by .615 μ pump light, and appeared at the photocathode as .489 μ light. The intensity of the background light was found to be linearly proportional to the .615 μ pump intensity and to the Pr^{3+} concentration. These observations suggest thermal population of the $^3H_6$ level as the cause of the background. $\sim 10^{-9}$ of the Pr^{3+} ions in the crystal would have to be in the $^3H_6$ level to account for the observed 4000 counts/sec. Assuming a Boltzmann population distribution, this would require a temperature $\sim 300^{\circ}K$. At first sight, this seems to be inconsistent with the fact that the crystal is immersed in liquid helium. However the spontaneous multiphonon emission rate for the $^3H_6$-$^3H_5$ gap in Pr^{3+}:$LaCl_3$ is expected from Fig. 1.2 to be $\sim .02\ sec^{-1}$, whereas the spontaneous radiative rate is known to be $50\ sec^{-1}$. Because the latter rate greatly exceeds the former, the $^3H_6$ population will come to equilibrium with the radiation field (whose temperature is $\sim 300^{\circ}K$ because of the windows in the dewar) rather than with the $4.2^{\circ}K$ phonon spectrum. The consequences of this will be discussed in the next section.

Since the lifetime of the visible level involved in IRQC action is usually short compared to that of the IR level, the response time of the device as an IR detector usually just equals the lifetime of the IR level. Thus the response time for (1) and (3) in Table 5.1 is $\sim$ 20 msec, whereas it is $\sim$ 2.5 msec for (4) and (5).

5.3 SIGNAL-TO-NOISE CONSIDERATIONS

In the event that radiative rates exceed multiphonon relaxation rates (as with Pr^{3+}:$LaCl_3$ in Sec. 5.2), the claim that cooling the crystal to an arbitrarily low temperature will make the IRQC an arbitrarily noiseless detector becomes invalid. In such a case, the population distribution between manifolds is determined by the temperature of the radiation field, and not by the lattice vibrations. This type of thermal population cannot be reduced by the use of dewars, if the dewars are to have windows of reasonable size which are transparent at the absorption wavelengths for the various levels.

To determine the effect of this thermal population on the IRQC signal-to-noise ratio, consider the IRQC scheme of Fig. 2.2(a). In the absence of radiation, the equilibrium populations N_0 and N_1 of levels 0 and 1 would be determined by the $0 \rightarrow 1$ and $1 \rightarrow 0$ transition rates per ion (W_L' and W_L, say) due solely to interaction with the lattice.

For simplicity, we assume that there are no levels between 0 and 1, that thermal population of the levels above level 1 is negligible, and that 0 and 1 have equal degeneracies.

Then
$$W_L' N_0 - W_L N_1 = 0 \qquad (5.1)$$

W_L is the total multiphonon relaxation rate, and hence will be temperature dependent if the temperature is high enough for stimulated multiphonon emission to be important (see Sec. 1.2.2).

Since N_0 and N_1 are equilibrium populations,

$$N_1/N_0 = \exp(-E_1/kT_L) \quad , \tag{5.2}$$

where E_1 is the energy of level 1 relative to the ground (0) level, and T_L is the lattice temperature.

Eliminating N_0 and N_1 between (5.1) and (5.2),

$$W_L' = W_L \exp(-E_1/kT_L) \quad . \tag{5.3}$$

An analogous situation arises if equilibrium is reached with a radiation field of temperature T_R, with no lattice interaction. If the radiative absorption and emission rates are W_R' and W_R, the equilibrium populations N_0 and N_1 will now be related by

$$W_R' N_0 - W_R N_1 = 0$$

$$\text{and} \quad N_1/N_0 = \exp(-E_1/kT_R)$$

$$\text{so that} \quad W_R' = W_R \exp(-E_1/kT_R) \quad . \tag{5.4}$$

If we now allow the ions to simultaneously interact with both the lattice and the radiation, the rate equation is

$$(W_L' + W_R')\, N_0 - (W_L + W_R)\, N_1 = 0$$

Then
$$\frac{N_1}{N_0} = \frac{W_L' + W_R'}{W_L + W_R} \tag{5.5}$$

Substituting (5.3) and (5.4) into (5.5),

$$\frac{N_1}{N_0} = \frac{W_L \exp(-E_1/kT_L) + W_R \exp(-E_1/kT_R)}{W_L + W_R} \tag{5.6}$$

For $T_L = T_R \equiv T$, (5.6) reduces to $\exp(-E_1/kT)$, as it should.

The IRQC fluorescence intensity from level 2 in Fig. 2.2(a) is given by (Eq. 6a, Ref. 79):

$$I_f = (N_0 B_{01} \rho_{01})(B_{12} \rho_{12} \tau_1)\, \eta \tag{5.7}$$

where the B's are the Einstein coefficients, the ρ's are the energy densities in the two beams, τ_1 is the lifetime of level 1, and η is the fluorescence quantum efficiency from level 2. τ_1 appears here because the number of fluorescence quanta per sec is determined by the competition of the $B_{12}\rho_{12}$ absorption with the τ_1 decay.

Now B_{01} and W_R are both proportional to the radiative oscillator strength of the $0 \leftrightarrow 1$ transition. (We have already assumed that no levels exist between 0 and 1.) Thus $B_{01} \ll W_R$. Also,

$\tau_1 = (W_L + W_R)^{-1}$. Then (5.7) gives

$$I_f \propto \frac{W_R}{W_L + W_R} \tag{5.8}$$

It was seen in Sec. 5.2 that for the IRQC scheme giving the best NEP, by far the dominant source of noise was fluorescence from level 2 resulting from $1 \rightarrow 2$ transitions induced by the visible beam in ions which were thermally excited to level 1. Since this background fluorescence is unchopped, it will show up in the lock-in amplifier output as noise whose rms value is proportional to the square root of the background fluorescence intensity. This intensity is proportional to N_1, hence the IRQC signal to noise will be

$$S{:}N \propto I_f/\sqrt{N_1} \tag{5.9}$$

Assuming $N_1 << N_0$, N_0 will be approximately constant, and putting (5.6) and (5.8) into (5.9) will give

$$S{:}N \propto \frac{\dfrac{W_R}{W_L + W_R}}{\sqrt{\dfrac{W_L \exp(-E_1/kT_L) + W_R \exp(-E_1/kT_R)}{W_L + W_R}}} \tag{5.10}$$

$$= \frac{1}{\sqrt{\left[1 + \dfrac{W_L}{W_R}\right]\left[\exp(-E_1/kT_R) + \dfrac{W_L}{W_R}\exp(-E_1/kT_L)\right]}}$$

For any temperature $\lesssim 100^{\circ}K$[†] (where stimulated phonon emission is negligible in $LaCl_3$), it was shown in Sec. 5.2 that $\frac{W_L}{W_R}$ for $^3H_6$ in Pr^{3+}:$LaCl_3$ is probably about .02/50 = .0004. Hence the T_R term dominates in Eq. (5.10), since $T_R \sim 300^{\circ}K$. Thus cooling the crystal any further, once $\sim 100^{\circ}K$ is reached, will not change the signal-to-noise ratio (or, hence, the NEP) in this case.

This being true, one might wonder whether it would be advantageous to place the ion in a lattice such as LaF_3, for which $W_L >> W_R$ for $^3H_6$ and $^3H_5$ in Pr^{3+}.[80] Eq. (5.10) indicates, however, that the overall effect of a large W_L/W_R on S:N is detrimental, and that S:N is maximized by choosing a lattice for which $W_L/W_R << 1$. accounts for the superiority of NEP's obtained in Pr^{3+}:$LaCl_3$ over those obtained in Pr^{3+}:LaF_3.[80]

[†]See Fig. 1.3.

Let us characterize the population N_1 by an effective temperature, T_e, defined by

$$\frac{N_1}{N_o} = \exp(-E_1/kT_e) \quad . \tag{5.11}$$

For $T_L \lesssim 30^oK$ in $^3H_6$, Pr^{3+}:LaF_3, the following relationships are satisfied:

$$\left.\begin{aligned} T_L &<< T_R \\ \exp(+E_1/kT_L) &>> \frac{W_L}{W_R} >> 1 \end{aligned}\right\} \tag{5.12}$$

Equating (5.6) and (5.11), and solving for T_e under the conditions (5.12),

$$T_e \cong \frac{T_R}{1 + \frac{kT_R}{E_1} \ln\left(\frac{W_L}{W_R}\right)} \tag{5.13}$$

W_L/W_R is probably $\sim 10^3$ for $^3H_6$ in Pr^{3+}:LaF_3, so that

$$T_e \cong \frac{300^oK}{1 + .34} = 220^oK \quad .$$

Thus LaF_3, even with its strong ion-lattice interaction, is not able to lower T_e to the bath temperature, which was assumed to be $T_L \lesssim 30^oK$. It should be noted that Eq. (5.13) is independent of T_L, so that reducing T_L further (once $\sim 30^oK$ is reached) will not

result in a reduction of T_e. Thus the presence of a 300°K radiation field has eliminated the IRQC's "arbitrarily noiseless" property (described on p. 107) for both $LaCl_3$ and LaF_3. The only way to restore this property in the presence of the radiation field is to find a lattice for which conditions (5.12) are replaced by

$$\frac{W_L}{W_R} \gg \exp(+E_1/kT_L) \quad . \tag{5.14}$$

Instead of (5.13), we would then have $T_e \sim T_L$, so that lowering T_L would indeed lower T_e. Condition (5.14) becomes more stringent as T_L is lowered, and at $T_L = 4.2°K$ and $E_1 = 4000\ cm^{-1}$, it becomes

$$\frac{W_L}{W_R} \gg 10^{600} \quad ,$$

a condition satisfied by no lattice.

Thus, in the presence of a 300°K radiation field, the argument on p. 107 is valid only for W_L/W_R and T_L sufficiently large that condition (5.14) is satisfied. Eq. (5.10) shows, however, that with the radiation field present, the condition for maximizing the IRQC's sensitivity is $W_L/W_R \ll 1$, and not condition (5.14).

Reducing T_R to below 300°K would require cooling lenses, choppers, etc., to cryogenic temperatures, and hence is to be avoided if possible.

If T_R is allowed to remain at 300°K, a basic limitation is imposed on the sensitivity of any infrared detector. If n photons/sec from a 300°K blackbody background are incident on the detector, and have a wavelength within the passband, then the detector will not be able to detect a modulated signal of $\sqrt{n}$ photons/sec with a signal-to-noise of better than 1 for a 1 sec integration time. The IRQC is still far from reaching this limiting sensitivity, even though the 300°K background radiation was the dominant source of noise in the best NEP measurement in Sec. 5.2. The reason is that the sensitivity limit will not be reached until the IRQC's overall quantum efficiency (defined as the number of photomultiplier pulses divided by the number of infrared quanta incident on the crystal) is ~1. In the Sec. 5.2 measurement, it was probably ~ 10^{-7}. Since the signal and noise are proportional to the one and one-half powers of the overall quantum efficiency, respectively, the signal-to-noise ratio will be proportional to the square root of the overall quantum efficiency. Thus S:N can be increased by increasing the quantum efficiency. Possible ways of doing this include increasing (1) the visible pump intensity, (2) the oscillator strength of the visible transition, and (3) the efficiency of collection of the fluorescence from level 2.

6. SUMMARY AND CONCLUSIONS

A lifetime survey of the lower levels of RE^{3+} ions in trichloride lattices has revealed a number of cases of concentration quenching. From the energy level diagrams, it is known that only four of these levels can be de-excited by a resonant transfer of a portion of the ion's energy to a neighboring ion. The temperature dependences of the decay rates for these four levels indicate that the transfer is indeed resonant (i.e., without phonon assistance) in each case. The observed transfer rate for these levels at concentration c and temperature T, $W_{obs}(c, T)$, is divided by a thermal population factor, ξ (T), to obtain the mean transfer rate, W(c), between two ions which are initially in Stark components matched for resonant transfer.

The concentration quenching of the other levels is assumed to be due to n successive transfers of the total energy from one ion to another ("migration"), until a sink is reached which is capable of dissipating the energy. Because the ions involved have identical energy levels, these transfers will also be resonant. Because of degeneracies, there are typically four final states for each resonant transfer in the migration process. An order of magnitude estimate for the rate for this single transfer is then $W_S(c) = 4W(c)$. If n transfers occur before a sink is reached, the observed quenching rate for the migration process, $W_M(c)$, will be $W_S(c,/n$.

From the measured decay rates, $W_{obs}(c, T)$, for the four levels quenched by a single transfer, the expected rate for the single transfer in the migration process, $W_S(c)$, is calculated. This quantity is then compared with the observed quenching rate, $W_M(c)$, for levels decaying by migration to sinks. It is found that $W_S(c)$ and $W_M(c)$ have approximately the same slope, indicating that n is independent of the concentration, and is of the order of 4×10^5.

$W_M(c)$ was found to depend on the purity of the starting materials from which the samples were grown, indicating that impurities, rather than structural defects or ion pairs, served as sinks in the cases investigated.

A quantum of electronic excitation which is mobile is called an "exciton". A typical time for one hop of an exciton in rare earth trichlorides is $\left[W_S(c)\right]^{-1}$. For c = 100%, this time is $\sim$ 0.2 nanoseconds. With $\sim 4 \times 10^5$ hops occurring before a sink is reached, the observed lifetime of a level quenched by migration will be $\sim$ 80 microseconds for c = 100%.

It was found empirically that the phase shift method yields 1/e lifetimes of non-exponential ion pair decays with an accuracy $\sim$ 25%, providing the modulation frequency is chosen to produce a phase shift of about 45^o. Decays of levels quenched by migration to sinks were found, in every case studied, to be exponential.

The roles that radiative, multiphonon, and migration quenching of the $^3H_6$ level of Pr^{3+} at 4.2°K play in the performance of the IRQC as an infrared detector have been considered. Because of migration quenching, the optimum concentration of Pr^{3+} in $LaCl_3$ with currently available purities is about 15%. A large multiphonon relaxation rate provides good coupling of the electronic levels to the lattice, and hence to the cryogenic bath, thus making low thermal populations of the $^3H_6$ level possible. Because increasing the multiphonon relaxation rate reduces the signal faster than the thermal noise, however, it was found necessary to minimize this rate to achieve optimum signal-to-noise. This results in a decoupling of the electronic levels from the cryogenic bath, so that the equilibrium population of the $^3H_6$ level will then be determined by the temperature of the radiation field, which is normally ~ 300°K. Despite this thermal population, the signal-to-noise was found both theoretically and experimentally to be best in a lattice which caused negligible multiphonon de-excitation of the $^3H_6$ level.

BIBLIOGRAPHY

1. B. R. Judd, Operator Techniques in Atomic Spectroscopy (McGraw-Hill Book Co., Inc., New York, 1963).
2. B. G. Wybourne, Spectroscopic Properties of Rare Earths (Interscience Publishers, New York, 1965).
3. R. Sarup and M. H. Crozier, J. Chem. Phys. 42, 371 (1965).
4. E. H. Carlson and G. H. Dieke, J. Chem. Phys. 34, 1602 (1961).
5. F. Varsanyi and G. H. Dieke, J. Chem. Phys. 33, 1616 (1960).
6. K. S. Thomas, S. Singh, and G. H. Dieke, J. Chem. Phys. 38, 2180 (1963).
7. H. M. Crosswhite and G. H. Dieke, J. Chem. Phys. 35, 1535 (1961).
8. K. Rajnak and W. F. Krupke, J. Chem. Phys. 46, 3532 (1967).
9. G. H. Dieke and S. Singh, J. Chem. Phys. 35, 555 (1961).
10. F. Varsanyi and G. H. Dieke, J. Chem. Phys. 36, 2951 (1962).
11. J. B. Gruber and J. G. Conway, J. Chem. Phys. 32, 1178 (1960).
12. B. R. Judd, Phys. Rev. 127, 750 (1962).
13. G. S. Ofelt, J. Chem. Phys. 37, 511 (1962).
14. F. Varsanyi and G. H. Dieke, J. Chem. Phys. 36, 835 (1962).
15. W. D. Partlow and H. W. Moos, Phys. Rev. 157, 252 (1967).

16. L. A. Riseberg, W. P. Gandrud, and H. W. Moos, Phys. Rev. 159, 262 (1967).

17. L. A. Riseberg and H. W. Moos, Phys. Rev. Letters 19, 1423 (1967).

18. M. J. Weber, Phys. Rev. 157, 262 (1967).

19. L. A. Riseberg and H. W. Moos (to be published).

20. Th. P. J. Botden, Philips Research Reports 6, 425 (1951); 7, 197 (1952).

21. C. C. Klick and J. H. Schulman, Sol. St. Phys. 5, 97 (1957).

22. D. L. Dexter, J. Chem. Phys. 21, 836 (1953).

23. D. L. Dexter and J. H. Schulman, J. Chem. Phys. 22, 1063 (1954).

24. F. Varsanyi and G. H. Dieke, Phys. Rev. Letters 7, 442 (1961).

25. G. H. Dieke and E. Dorman, Phys. Rev. Letters 11, 17 (1963).

26. J. S. Margolis, O. Stafsudd, and E. Y. Wong, J. Chem. Phys. 38, 2045 (1963).

27. D. L. Dexter, Phys. Rev. 126, 1962 (1962).

28. G. E. Peterson and P. M. Bridenbaugh, J. Opt. Soc. Am. 53, 301 (1963).

29. F. Varsanyi, Phys. Rev. Letters 11, 314 (1963).

30. J. F. Porter and H. W. Moos, Phys. Rev. 152, 300 (1966).

31. C. K. Asawa, Phys. Rev. 155, 188 (1967).

32. J. D. Axe and P. F. Weller, J. Chem. Phys. 40, 3066 (1964).

33. M. R. Brown, J. S. S. Whiting, and W. A. Shand, J. Chem. Phys. 43, 1 (1965).

34. W. W. Holloway and M. Kestigian, J. Chem. Phys. 43, 147 (1965).

35. C. K. Asawa and M. Robinson, Phys. Rev. 141, 251 (1966).

36. E. Snitzer, IEEE J. Quantum Electronics QE-2, 562 (1966).

37. R. V. Bakradze, G. M. Zverev, G. Ya. Kolodnyi, G. P. Kuznetsova, and A. M. Onishchenko, Soviet Phys. --Solid State 9, 733 (1967).

38. M. Robinson and D. P. Devor, Appl. Phys. Letters 10, 167 (1967).

39. L. G. Van Uitert, E. F. Dearborn, and J. J. Rubin, J. Chem. Phys. 47, 3653 (1967). This paper also contains references to other papers on this subject by these authors.

40. T. F. Ewanizky, J. Appl. Phys. 38, 4338 (1967).

41. Z. J. Kiss and R. C. Duncan, Appl. Phys. Letters 5, 200 (1964).

42. Z. J. Kiss, Phys. Rev. Letters 13, 654 (1964).

43. M. J. Taylor, Proc. Phys. Soc. (London) 90, 487 (1967).

44. G. Blasse and A. Bril, Phys. Letters 25A, 29 (1967).

45. A. J. Varga, B. Birang, and B. DiBartolo, Bull. Am. Phys. Soc. 12, 1068 (1967).

46. J. F. Weller, H. W. Gandy, and R. J. Ginther, Bull. Am. Phys. Soc. 12, 1069 (1967).

47. A. Lempicki, H. Samelson, and C. Brecher, Appl. Opt. Supplement #2, 205 (1965).

48. M. L. Bhaumik and M. A. El-Sayed, Appl. Opt. Supplement #2, 214 (1965).

49. V. L. Ermolaev, E. A. Saenko, G. A. Domrachev, Yu. K. Khudenskii, and V. G. Aleshin, Opt. Spectry. (USSR) 22, 466 (1967).

50. G. F. Imbusch, Phys. Rev. 153, 326 (1967).

51. E. Dorman, J. Chem. Phys. 44, 2910 (1966).

52. J. M. Blatt and V. F. Weisskopf, Theoretical Nuclear Physics (John Wiley and Sons, Inc., New York, 1952), Chap. XII, Sec. 3C.

53. L. J. F. Broer, G. J. Gorter, and J. Hoogschagen, Physica 11, 231 (1945).

54. W. P. Wolf and R. J. Birgeneau, Phys. Rev. (to be published).

55. G. E. Barasch and G. H. Dieke, J. Chem. Phys. 43, 988 (1965).

56 J. F. Porter, Jr., Phys. Rev. Letters 7, 414 (1961).

57 J. F. Porter, Jr., Bull. Am. Phys. Soc. 11, 811 (1966).

58. M. R. Brown and R. J. Strain, J. Appl. Phys. 37, 4806 (1966).

59. E. A. Bailey and G. K. Rollefson, J. Chem. Phys. 21, 1315 (1953).

60. L. N. Pfeiffer and J. F. Porter, Jr., Appl. Opt. 3, 317 (1964).

61. C. S. French, Appl. Opt. 4, 514 (1965).

62. C. A. Hutchison and E. Wong, J. Chem. Phys. 29, 754 (1958).

63. C. Opal and W. B. Gandrud, Rev. Sci. Instr. 38, 838 (1967).

64. J. W. Rakestraw and G. H. Dieke, J. Chem. Phys. 42, 873 (1965).

65. M. Inokuti and F. Hirayama, J. Chem. Phys. 43, 1978 (1965).

66. D. L. Dexter and R. S. Knox, Excitons (Interscience Publishers, New York, 1965), Sec. 5.4.

67. A. D. Pearson and G. E. Peterson, Appl. Phys. Letters 8, 210 (1966).

68. S. Chandrasekhar, Rev. Mod. Phys. 15, 1 (1943).

69. A. D. Pearson, G. E. Peterson, and W. R. Northover, J. Appl. Phys. 37, 729 (1966), point out that shifts ~1 cm^{-1} of energy levels from one ion to another because of site inequivalence may retard energy transfer in some cases. They report an increase in migration rate with temperature in a glass host, which they suggest may be due to the over-coming of such an energy mis-match by thermal line-broadening.

70. D. F. Williams and W. G. Schneider, J. Chem. Phys. 45, 4756 (1966).

71. L. G. Van Uitert, E. F. Dearborn, and H. M. Marcos, Appl. Phys. Letters 9, 255 (1966).

72. R. G. Kepler, J. C. Caris, P. Avakian, and E. Abramsen, Phys. Rev. Letters 10, 400 (1963); M. Silver, D. Olness, M. Swicord, and R. C. Jarnagin, Phys. Rev. Letters 10, 12 (1963).

73. V. V. Ovsyankin and P. P. Feofilov, Soviet Phys. --JETP Letters 3, 322 (1966).

74. P. P. Feofilov and V. V. Ovsyankin, Appl. Opt. 6, 1828 (1967).

75. R. J. Woodward, J. M. Williams, and M. R. Brown, Phys. Letters 22, 435 (1966).

76. M. R. Brown and W. A. Shand, Phys. Letters 18, 95 (1965).

77. N. Bloembergen, Phys. Rev. Letters 2, 84 (1959).

78. J. F. Porter, IEEE J. Quantum Electronics QE-1, 113 (1965).

79. M. R. Brown, W. A. Shand, and J. S. S. Whiting, Brit. J. Appl. Phys. 16, 619 (1965).

80. W. B. Gandrud and H. W. Moos, IEEE J. Quantum Electronics (to be published).

81. L. Esterowitz, J. Noonan, and J. Bahler, Appl. Phys. Letters 10, 126 (1967).

Unclassified

DOCUMENT CONTROL DATA R & D

Department of Physics
The Johns Hopkins University
Baltimore, Maryland 21218

Unclassified

RARE EARTH INFRARED LIFETIMES AND EXCITON MIGRATION RATES IN TRICHLORIDE CRYSTALS

Interim Technical

William B. Gandrud

January, 1968 | 131 | 81

DA-31-124-ARO-D-339

2001450181IB

Technical Report No. 1

This document has been approved for public release and sale; its distribution is unlimited.

U. S. Army Research Office--Durham
Box CM, Duke Station
Durham, North Carolina 27706

Lifetimes of trivalent rare earth ion levels below 14,000 cm^{-1} have been measured in the $LaCl_3$, $GdCl_3$, and YCl_3 hosts, using the Infrared Quantum Counter and infrared fluorescence techniques. Because of their low radiative and multi-phonon relaxation rates, these levels are well suited to concentration-quenching studies. Temperature dependences provide evidence that the ion pair decays of four levels in Pr^{3+} and Nd^{3+} occur resonantly (i.e., without phonon assistance) between excited Stark components. This enables the measured decay rates for these four levels to be used in estimating the rate for a single resonant transfer of all of the ion's energy to a neighboring ion. This latter process is the basic step of the excitation migration process. From the lifetimes of a number of levels which are quenched by migration of the excitation to "sinks," an estimate of 4×10^5 is obtained for the number of transfers that occur before a sink is reached. Levels quenched by migration to sinks are found to decay exponentially, with a lifetime which increases with increasing crystal purity. The roles of the various relaxation processes in determining the performance of the Infrared Quantum Counter as an infrared detector are discussed.

DD FORM 1473

Unclassified
Security Classification

14 KEY WORDS	LINK A		LINK B		LINK C	
	ROLE	WT	ROLE	WT	ROLE	WT
Rare Earth Lifetimes						
Infrared Quantum Counter						
Energy Migration						
Ion-Ion Interactions						
Time-Resolved Spectroscopy						